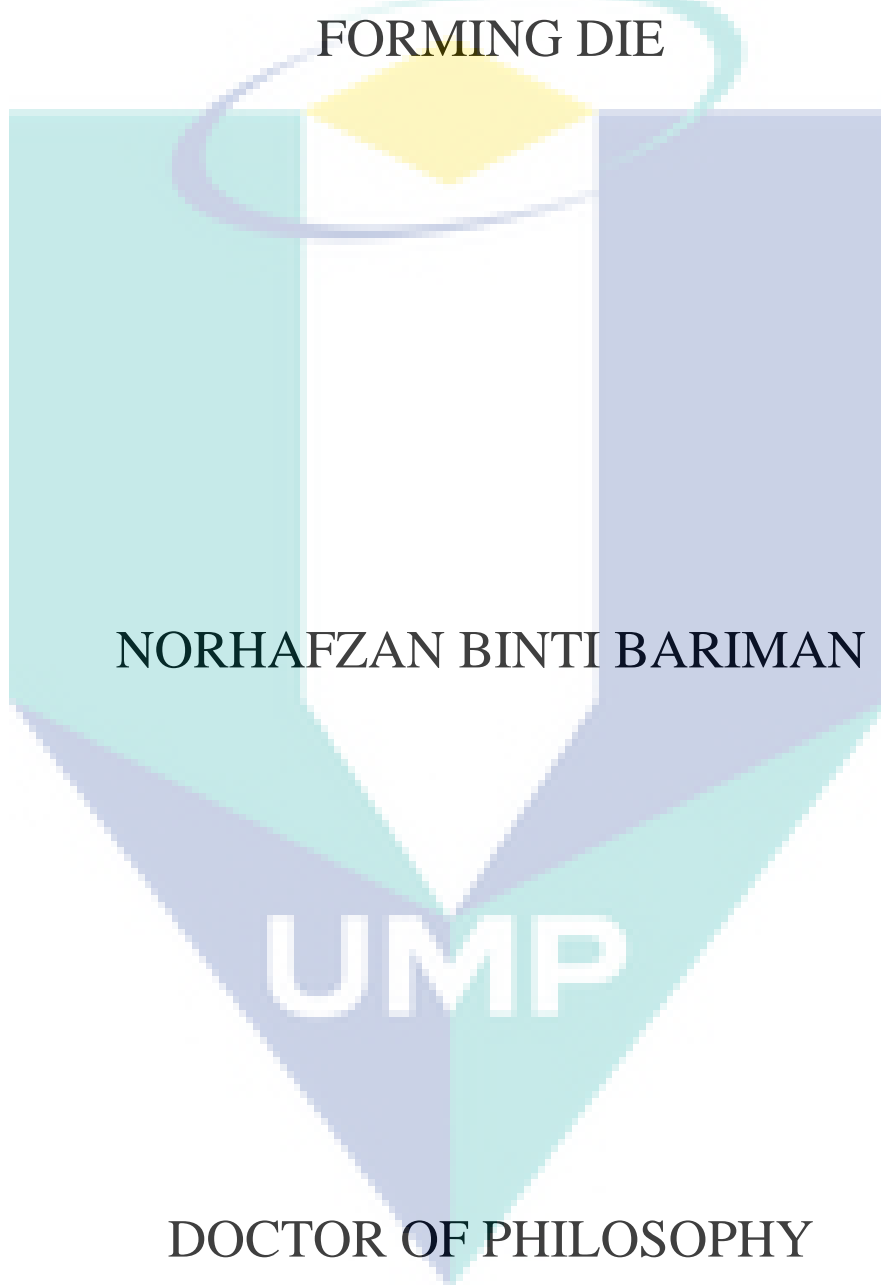


LASER SURFACE MELTING TO ENHANCE  
SURFACE PROPERTIES IN HOT PRESS  
FORMING DIE



NORHAFZAN BINTI BARIMAN

UMP

DOCTOR OF PHILOSOPHY

UNIVERSITI MALAYSIA PAHANG

## UNIVERSITI MALAYSIA PAHANG

### DECLARATION OF THESIS AND COPYRIGHT

Author's Full Name : NORHAFZAN BINTI BARIMAN

Date of Birth : 23 APRIL 1979

Title : LASER SURFACE MELTING TO ENHANCE  
SURFACE PROPERTIES IN HOT PRESS FORMING  
DIE

Academic Session : SEM 2 2019/2020

I declare that this thesis is classified as:

- CONFIDENTIAL (Contains confidential information under the Official Secret Act 1997)\*
- RESTRICTED (Contains restricted information as specified by the organization where research was done)\*
- OPEN ACCESS I agree that my thesis to be published as online open access (Full Text)

I acknowledge that Universiti Malaysia Pahang reserves the following rights:

1. The Thesis is the Property of Universiti Malaysia Pahang
2. The Library of Universiti Malaysia Pahang has the right to make copies of the thesis for the purpose of research only.
3. The Library has the right to make copies of the thesis for academic exchange.

Certified by:

\_\_\_\_\_  
(Student's Signature)

790423-01-5132

\_\_\_\_\_  
New IC/ Passport Number

Date:

\_\_\_\_\_  
(Supervisor's Signature)

AP. DR. Syarifah Nur Aqida binti  
Syed Ahmad

\_\_\_\_\_  
Name of Supervisor

Date:

NOTE : \* If the thesis is CONFIDENTIAL or RESTRICTED, please attach a thesis declaration letter.

### **SUPERVISOR'S DECLARATION**

I hereby declare that I have checked this thesis and in my opinion, this thesis is adequate in terms of scope and quality for the award of the degree of Doctor of Philosophy.

---

(Supervisor's Signature)

Full Name : AP. DR SYARIFAH NUR AQIDA BINTI SYED AHMAD

Position : ASSOCIATE PROFESSOR

Date :



UMP

### **STUDENT'S DECLARATION**

I hereby declare that the work in this thesis is based on my original work except for quotations and citations which have been duly acknowledged. I also declare that it has not been previously or concurrently submitted for any other degree at Universiti Malaysia Pahang or any other institutions.

---

(Student's Signature)

Full Name : NORHAFZAN BINTI BARIMAN

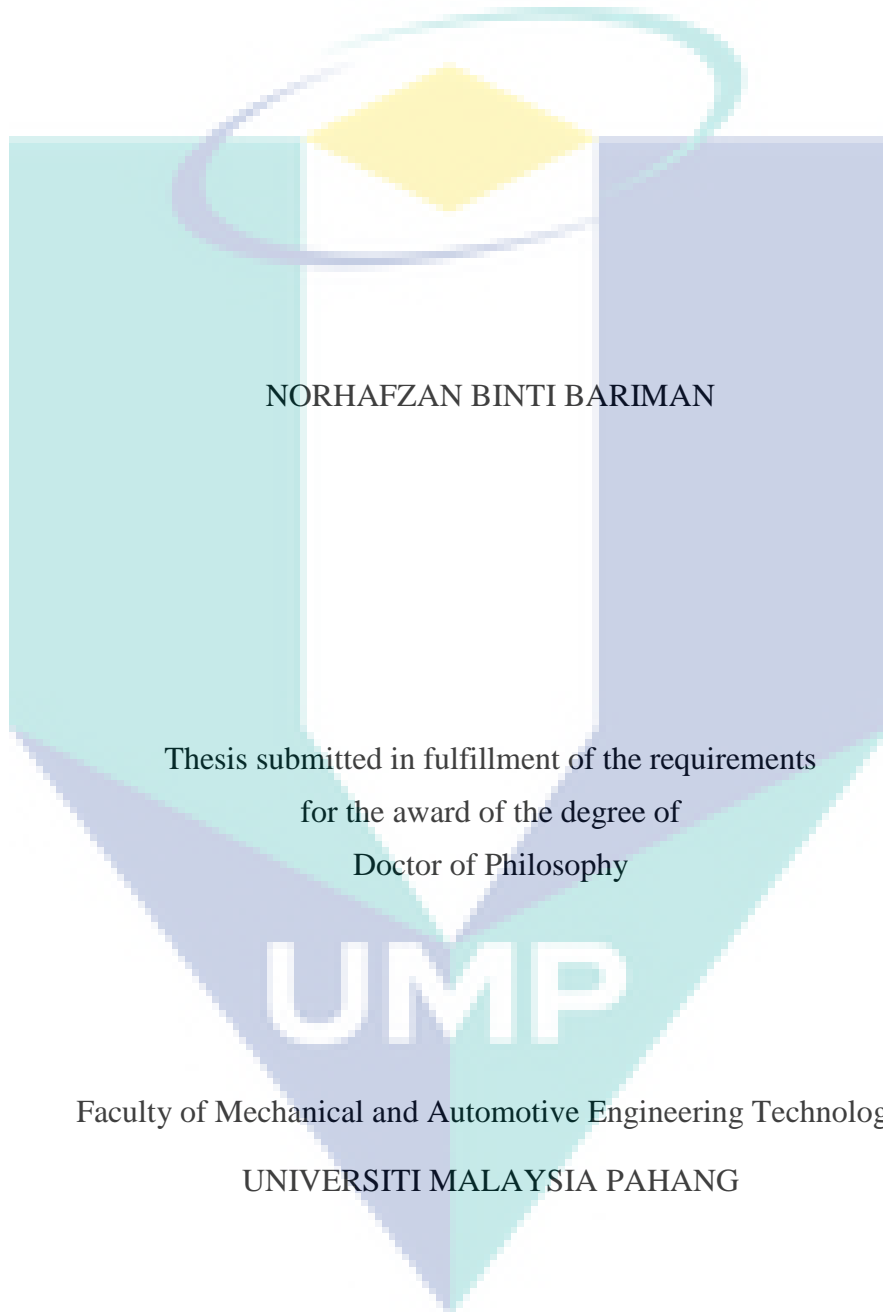
ID Number : PMM14009

Date :



UMP

LASER SURFACE MELTING TO ENHANCE SURFACE PROPERTIES IN HOT  
PRESS FORMING DIE



FEBRUARY 2020

## ACKNOWLEDGEMENTS

Praise be to Allah SWT, finally I completed this study. My express and gratitude especially to my Supervisor, AP. Dr. Syarifah Nur Aqida binti Syed Ahmad who have given me hope and accepted me under his supervision. Thanks also for kindly spend her time, patient and encouragement from the start and until this study is completed.

I would like to express my deepest gratitude to my beloved husband (Khairil) also to my children (Ikmal Hilmy, Irdina Dania, Irfan Zikry, Insyirah Humaira and my new baby Irsa Ayra) for your patience also prayers and endless devotions that always keep lifting me up to give my very best along my studies.

A special appreciation to my mother (Katijah binti Selamat), mother in-law, brothers, sisters and in-laws for all their never endings support.

I gratefully acknowledge the financial support from the Ministry of Education Malaysia and Jabatan Pengajian Politeknik.

Special thanks to all staff in laser processing lab UTHM (Mr. Faizal and AP. Dr Erween), and staff in CNC Lab Politeknik Sultan Mizan Zainal Abidin, also staff in materials lab and Foundry Lab UMP for their valuable advice, guidance, supports, motivation and encouragement in successfully finish this study.

And last but not least, many thanks to all my team members for this study Fazliana, Zulhishamuddin, Reeza and Hassan for their advice and support. Last but not least, may Allah bless with acceptance the sincere efforts and helps from all of them and from all of those associated directly or indirectly in the completion of this thesis.



UMP

## ABSTRAK

Proses pembentukan tekanan panas (HPF) digunakan bagi menghasilkan komponen kenderaan yang berkekuatan tinggi sehingga 1500 MPa. Semasa proses HPF, die akan beroperasi pada suhu 600 hingga 850°C untuk membentuk keluli boron. Semasa proses HPF, suhu tinggi dan beban yang berulang menyebabkan permukaan die kehilangan kekuatan, kekerasan dan menyebabkan kegagalan seterusnya mengurangkan kualiti produk. Objektif utama penyelidikan ini adalah untuk menghasilkan komponen berkekuatan tinggi melalui proses HPF menggunakan die yang diubahsuai menggunakan proses lasik peleburan. Sistem lasik Nd:YAG digunakan untuk memproses permukaan die. Permukaan die dianalisis bagi mendapatkan morfologi, kekasaran, kekerasan, struktur metalogografi, analisis fasa, dan komposisi kimia. Hasil kajian menunjukkan parameter lasik yang digunakan memberikan kesan kepada sifat permukaan die yang diproses menggunakan lasik peleburan. Kadar peratus pertindihan yang tinggi pada 70% menghasilkan permukaan die yang lebih rata dengan kekasaran permukaan sebanyak 1.886 $\mu\text{m}$  dan kedalaman kolam leburan sebanyak 0.33 mm. Seterusnya nilai kekerasan permukaan die yang telah diubahsuai meningkat tiga kali ganda daripada kekerasan asalnya kepada 793.7 HV<sub>0.1</sub>, kerana struktur bijian menjadi semakin halus (1.02  $\mu\text{m}$ ). Sementara itu, keamatan puncak, menunjukkan bahawa tahap kekristalan yang tinggi meningkatkan kekerasan permukaan die yang dikenakan lasik peleburan. Proses HPF bagi membentuk keluli 22MnB5 dijalankan menggunakan mesin "Hydraulik press" sebanyak 40 kitaran bagi setiap permukaan die. Pemindahan haba yang pantas daripada permukaan die yang diubahsuai semasa proses HPF meningkatkan kekerasan permukaan keluli 22MnB5 sehingga 508.1 HV<sub>0.1</sub>. Pemindahan haba yang pantas menyumbang kepada peningkatan kadar penyejukan dan menghasilkan komponen berkekuatan tinggi. Kajian ini juga bertujuan untuk menentukan sifat terma semasa proses HPF. Analisis taburan suhu pada permukaan die yang diubahsuai semasa proses lindapkejut menunjukkan pemindahan haba daripada keluli 22MnB5 kepada permukaan die yang diubahsuai adalah sebanyak 40.4°C, manakala pemindahan haba pada die tanpa lasik peleburan adalah 60.9°C. Ini menunjukkan kadar penyejukan adalah lebih pantas pada die yang dikenakan lasik peleburan. Dapatan kajian ini juga membuktikan pentingnya lasik peleburan dalam meningkatkan sifat terma permukaan die seterusnya meningkatkan kualiti keluli 22MnB5 selepas proses HPF.

## ABSTRACT

Hot press forming (HPF) used to produced ultra-high strength component of automobile structure up to 1500 MPa. During HPF processes die works at temperatures between 600 and 850°C to form boron steel blank. During hot working processes the high temperatures and cyclic loading caused the HPF dies surface to lose strength and hardness and lead to failure and reduce quality product produced from HPF process. The main objective of this research is to produce high strength component via hot press forming with laser modified die inserts. The Nd:YAG laser system was used to process AISI H13 tool steel as die insert to formed 22MnB5 blank. The melted die surface was analysed for surface morphology, roughness, hardness, metallographic study, phase analysis, and chemical composition. The resultant outcomes of this study revealed the effect of laser processing parameters on the properties of the melted layer. The minimum surface roughness was 1.886  $\mu\text{m}$  and maximum melted depth was 0.33 mm respectively when process at 70% overlapping rate due to slow solidification rate. Additionally, the surface hardness value of melted layer increased three time from its substrate up to 793.7  $\text{HV}_{0.1}$ , due to the grain structure of melted layer refined with an average grain size of 1.02  $\mu\text{m}$ . Meanwhile, the peak intensity showed that high crystallite increased surface hardness of the melted layer. The HPF process to form 22MnB5 steel blank was conducted using 60-tonne hydraulic press machine with various die insert for 40 cycle per die insert. Rapid heat transfer across melted die surface during HPF processed produced high surface hardness of 22MnB5 blank up to 508.1  $\text{HV}_{0.1}$  when formed using melted die insert. Fast heat transfer contributed to increased cooling rate and produce high strength component. The study was also aimed to determine the thermal properties of the die insert surface subjected to melting during the HPF process. Thermal distribution analysis of die insert surface indicates heat transfer from high temperature blank surface to the melted die insert during quenching process was up to 40.4°C. While the temperature for the as-received die recorded 60.9°C. Its shows that the cooling rate of laser melted die surface was higher than the cooling rate of as-received die insert. This study proved the significance of laser melted surface in enhancing the thermal properties of die surface and improving the quality of 22MnB5 after HPF process.

The logo for UMP (Universiti Malaysia Perlis) is a large, stylized letter 'U' composed of several overlapping triangles in shades of blue and teal. The letters 'UMP' are printed in a bold, white, sans-serif font across the center of the 'U'.



## TABLE OF CONTENT

<b>DECLARATION</b>	
<b>TITLE PAGE</b>	
<b>ACKNOWLEDGEMENTS</b>	<b>ii</b>
<b>ABSTRAK</b>	<b>iii</b>
<b>ABSTRACT</b>	<b>iv</b>
<b>TABLE OF CONTENT</b>	<b>v</b>
<b>LIST OF TABLES</b>	<b>ix</b>
<b>LIST OF FIGURES</b>	<b>x</b>
<b>LIST OF SYMBOLS</b>	<b>xiii</b>
<b>LIST OF ABBREVIATIONS</b>	<b>xiv</b>
<b>LIST OF APPENDICES</b>	<b>xv</b>
<b>CHAPTER 1 INTRODUCTION</b>	<b>1</b>
1.1 Introduction	1
1.2 Problem Statement	3
1.3 Research Objective	4
1.4 Scope of Research	4
<b>CHAPTER 2 LITERATURE REVIEW</b>	<b>6</b>
2.1 Introduction	6
2.2 Hot Press Forming	6
2.3 Die Failure in Hot Forming	7
2.4 Surface Properties of Hot Forming Die	8
2.5 Problem in Various Laser Surface Modification	11
2.6 Surface Modification	12
2.7 Laser Surface Modification	13

2.7.1	Nd:YAG Laser Technology	14
2.7.2	Laser Melting	16
2.7.3	Effect of Laser Processing Parameter	17
2.7.4	Overlapping Rate	19
2.8	Hardness Properties	21
2.9	Grain Properties	22
2.10	Thermal Properties	24
2.10.1	Thermal Cycle	25
2.11	Thermal Conductivity on Die Surface	27
2.11.1	Cooling Channel	27
2.11.2	Quenching Process	28
2.12	Summary	29
<b>CHAPTER 3 METHODOLOGY</b>		<b>30</b>
3.1	Introduction	30
3.2	Research Flow Chart	30
3.3	AISI H13 Tool Steel Die	32
3.4	Development of Hot Press Forming Die	33
3.5	Laser Surface Melting	38
3.6	Design of Experiment (DOE) for AISI H13 Tool Steel Sample and Optimisation	43
3.6.1	DOE Optimisation	44
3.7	Characterization of Laser Modification Surface	45
3.7.1	Sample Preparation	45
3.7.2	Surface Roughness Measurement	45
3.7.3	Surface Morphology Analysis	45
3.7.4	Microhardness Test	45

3.7.5	X-ray diffraction (XRD) analysis	46
3.7.6	Metallographic study	46
3.7.7	Chemical Composition and Element Mapping	46
3.8	Hot Press Forming Process	46
3.9	Image Analysis	49
3.10	Thermal Analysis	50
<b>CHAPTER 4 RESULTS AND DISCUSSION</b>		<b>51</b>
4.1	Introduction	51
4.2	Surface Morphology	51
4.3	Metallographic Study	53
4.3.1	As-received AISI H13 Steel	53
4.3.2	Laser Melted AISI H13 Surface	54
4.3.2.1	Melted Depth	54
4.3.2.2	Grain Size and Structure	57
4.4	Chemical Composition	62
4.5	Surface Roughness Properties	65
4.6	Hardness Properties	67
4.7	X-ray Diffraction (XRD) Analysis	70
4.8	Respond Surface Method (RSM) Analysis	74
4.8.1	Hardness Properties	74
4.8.2	Melt Depth	76
4.8.3	Surface Roughness	78
4.9	Design Optimization	80
4.10	Validation process	84
4.11	Analysis of Hot Press Forming Process	84

4.11.1	Metallographic Study	85
4.11.2	Martensite Percentage	88
4.11.3	Hardness Properties of 22MnB5 after HPF	90
4.12	Hardness Properties of Die insert after HPF	92
4.13	Thermal Analysis of Die Insert After HPF Processes	94
4.13.1	Thermal Stability and Performance of Hot Press Forming Die Insert	98
4.13.2	Thermal Distribution of Die Insert	99
4.14	Summary	101
<b>CHAPTER 5 CONCLUSION</b>		<b>103</b>
5.1	Conclusion	103
5.2	Recommendation	105
<b>REFERENCES</b>		<b>106</b>



UMP

## LIST OF TABLES

Table 2.1	Thermal properties of high thermal conductive steel	9
Table 2.2	Physical and mechanical properties of high thermal conductive steel	10
Table 3.1	Chemical composition of ASSAB 8407/ AISI H13 steel	32
Table 3.2	Physical and mechanical properties of ASSAB 8407/ AISI H13 steel	33
Table 3.3	Chemical composition of 22MnB5	33
Table 3.4	Parameter setting for laser melting process.	39
Table 3.5	Parameter for laser surface melting of AISI H13 steel	41
Table 3.6	Laser spot patterns at different overlap percentages.	42
Table 3.7	Laser melting parameter produce by Design of Experiment (DOE)	43
Table 3.8	Hot Press Forming Processing Parameter	47
Table 4.1	Average grain size of melted layer at various parameter settings	61
Table 4.2	Chemical composition of AISI H13 tool steel in melted zone, heat affected zone and substrate material	64
Table 4.3	Element distribution of melted surface at line spectrum 1	65
Table 4.4	Surface roughness of melted layer at various parameter settings	66
Table 4.5	Laser parameters for process optimisation	74
Table 4.6	ANOVA result for melted surface hardness response using quadratic model with stepwise elimination	75
Table 4.7	ANOVA result for melted surface melted depth response using quadratic model with stepwise elimination	77
Table 4.8	ANOVA result for melted surface roughness response using quadratic model with stepwise elimination	79
Table 4.9	Constrain selected in design optimization of laser melted processes	81
Table 4.10	Design solution for maximised surface hardness and melted depth	82

## LIST OF FIGURES

Figure 2.1	Schematic diagram for laser surface melting for flat plate workpiece	16
Figure 2.2	Laser power density as a function of interaction time for different examples of laser material processing	18
Figure 2.3	Schematic diagram of (a) a rectangular laser power pulse trains and (b) its corresponding partially overlapping spots	20
Figure 2.4	Symmetry cells for simulation of different overlapping rates; (a) $\eta=50\%$ , (b) $\eta=70\%$ , (c) $\eta=90\%$	21
Figure 2.5	Schematic drawing of columnar and equiaxed grain growth during solidification	23
Figure 2.6	Schematic of an equiaxed solidification system	24
Figure 2.7	Estimated hardness loss for the thermal cycling experiments	26
Figure 2.8	Effect of thermal fatigue on hardness of aluminium at temperature; $T_h=100, 300$ and $500^\circ\text{C}$	26
Figure 2.9	Cooling holes parameter; a-hole diameter, b-distance between cooling holes, c-distance to tool contour	28
Figure 3.1	Research methodology outline.	31
Figure 3.2	Hot press forming die design.	34
Figure 3.3	Upper die insert holder with dimension	34
Figure 3.4	Lower die insert holder with dimension	35
Figure 3.5	Die insert with dimension	35
Figure 3.6	Cooling channel design in die insert holder	36
Figure 3.7	As-machined geometry of (a) upper and (b) lower die	37
Figure 3.8	Assembly of (a) upper die with holder and (d) lower die with holder	37
Figure 3.9	Die inserts after machining into $70 \times 33 \times 8$ mm	37
Figure 3.10	Schematic diagram of laser surface melting process setup	38
Figure 3.11	Die insert condition after laser melting at (a) 70%, (b) 50% and (c) 30% overlapping rate.	40
Figure 3.12	Optimisation of parameter setting	44
Figure 3.13	Schematic diagram of hot press forming process setup	48
Figure 3.14	Hot press forming processes setup	48
Figure 3.15	Hot press formed of 22MnB5 sample	49
Figure 3.16	Thermocouple attach at lower die insert	50

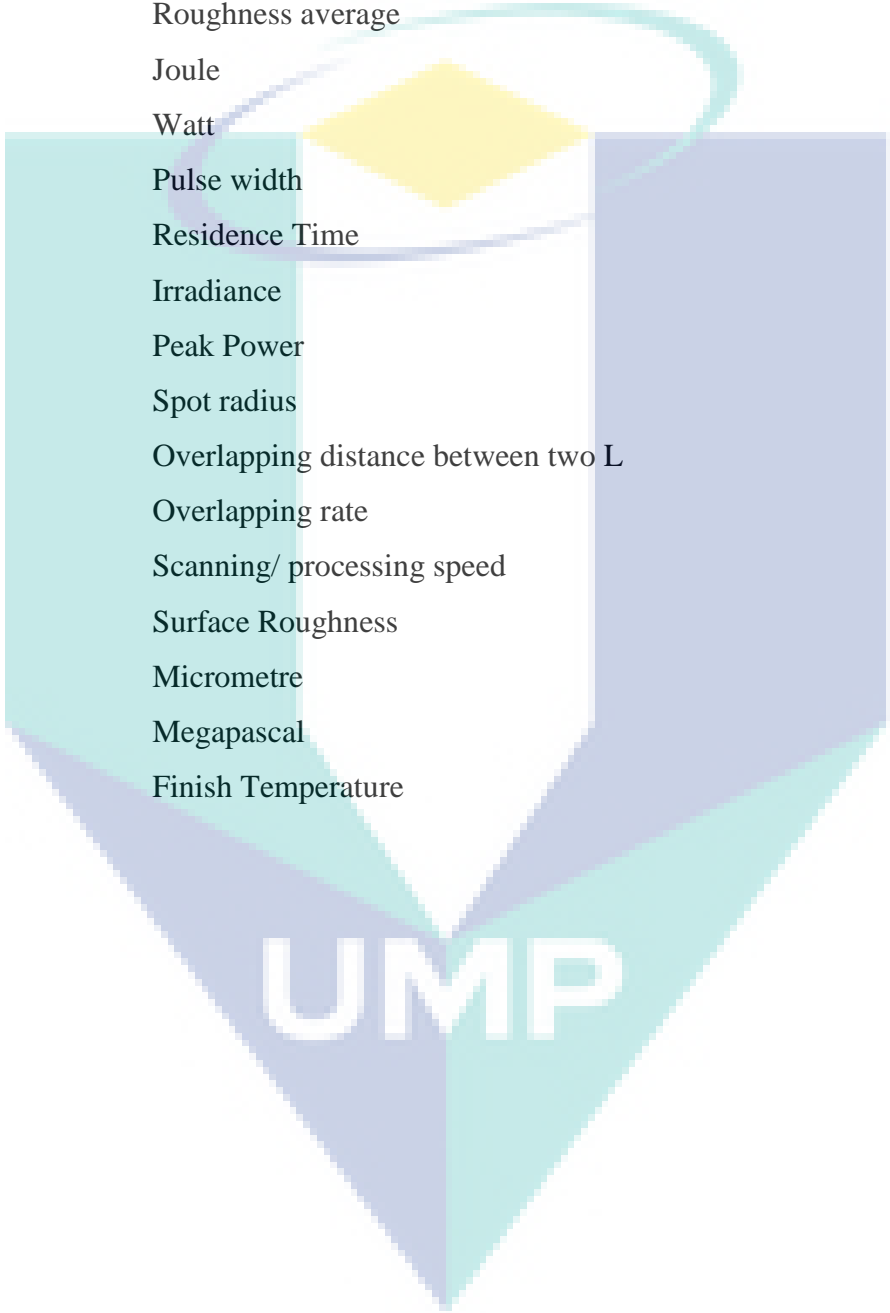
Figure 4.1	Overlapping laser spots of melting sample processed with different overlapping percentage of (a) 30%, (b) 50% and, (c) 70% overlapping rate	52
Figure 4.2	(a) Micrograph of as-received H13 steel before laser melting at 15000× magnification and (b) threshold analysis of grain boundary percentage.	53
Figure 4.3	Micrographs of varying molten pool and melted depth at 30, 50 and 70% overlap with different pulse repetition frequency.	55
Figure 4.4	SEM micrographs of (a) laser melted AISI H13 tool steel cross section with presence of melted zone (MZ), heat affected zone (HAZ) and substrate material, (b) fine equiaxed grain structure in the MZ, (c) Columnar grain structure in the HAZ, and (d) large equiaxed grain structure at 6000x magnification for sample 10.	58
Figure 4.5	Area observed for SEM micrograph of grain structure evolution laser melted zone of AISI H13 at sample 5.	59
Figure 4.6	SEM Micrographs of grain structure evolution laser melted zone of AISI H13 samples which were processed at (a) 30%, (b) 50% and 70% overlapping rate at 15000x magnification.	60
Figure 4.7	(a) EDX Spectrum analysis of melted layer for sample 6 and (b) line spectrum along the depth at modify layer	63
Figure 4.8	Cross-section surface of melted zone (MZ), heat affected zone (HAZ) and substrate with Vickers hardness indentation	68
Figure 4.9	Microhardness as a function of distance from surface of laser melting H13 steel cross section	69
Figure 4.10	Grain of AISI H113 surface (a) before and (b) after melting processed	70
Figure 4.11	X-ray diffraction pattern of die insert surface with the corresponding micrograph of laser melted surface of overlapping rate (a) 30%, (b) 50%, (c) 70% and (d) As-received H13 steel	72
Figure 4.12	Contour plot of hardness properties responding to various peak power and PRF at 50% overlapping rate	76
Figure 4.13	Contour plot of melt depths at various overlapping rate and peak power at 60Hz PRF	78
Figure 4.14	Contour plot of surface roughness at different overlapping rate and PRF at 2100 W peak power	80
Figure 4.15	Desirability Contour plot of melted surface with highest desirability factor of 0.847	83
Figure 4.16	As-received 22MnB5 boron steel (a) microstructure of cross section before HPF process, (b) shape after HPF processes	85
Figure 4.17	Micrograph of 22MnB5 blank after HPF process using as-received H13 die	86

Figure 4.18	Die insert cross section micrograph of (a) as-received AISI H13, (b) laser melted of overlapping rate at (b) 30%, (c) 50%, and; (d) 70% with corresponding of 22MnB5 steel blank structure (e)-(h) after HPF processes	87
Figure 4.19	Micrograph of martensite formation in 22MnB5 steel blank after HPF process responding to the parameters of laser melted die insert	88
Figure 4.20	Micrograph of martensitic structure in hot press formed 22MnB5 steel with red threshold formed using die insert of (a) 30% overlap, (b) 50% overlap, (c) 70% overlap and (d) as-received die.	89
Figure 4.21	Average hardness properties of 22MnB5 steel blank before and after HPF using different die insert	90
Figure 4.22	Hardness properties of melted surface before and after HPF of 22MnB5 steel blank as a function of distance from surface	94
Figure 4.23	Maximum and minimum thermal distribution in die inserts with (a) melted surface of 30% overlap, (b) melted surface of 50% overlap, (c) laser melted surface of 70% overlap and; (d) as-received AISI H13 condition during 40 cycles of HPF	96
Figure 4.24	Temperature history of as-received and laser melted HPF die inserts from experimental measurement	100

UMP



## LIST OF SYMBOLS



$^{\circ}\text{C}$	Degree Celsius
%	Percentage
ZSI	Z source inverter
$R_a$	Roughness average
J	Joule
W	Watt
$\tau$	Pulse width
$T_R$	Residence Time
I	Irradiance
$P_p$	Peak Power
L	Spot radius
$L_o$	Overlapping distance between two L
$\eta$	Overlapping rate
v	Scanning/ processing speed
$R_a$	Surface Roughness
$\mu\text{m}$	Micrometre
MPa	Megapascal
$M_f$	Finish Temperature

## LIST OF ABBREVIATIONS

HPF	Hot Press Forming
Nd:YAG	Neodymium doped yttrium aluminium garnet
DOE	Design of Experiment
HTCS	High Thermal Conductivity Steel
LSR	Laser Surface Remelting
EPPD	Effective Peak Power density
APPD	Average Peak Power Density
HV	Hardness Vickers
CNC	Computer Numerical Control
RSM	Response Surface Method
XRD	X-Ray Diffractometer
EDXS	Energy Dispersive X-ray Spectroscopy
BSD	Back Scatter Detector
MZ	Melted Zone
HAZ	Heat Affected Zone



UMP

## LIST OF APPENDICES

Appendix A	List of Publication	117
Appendix B	Contour Plot of PRF, Peak Power and Hardness at 30% overlapping rate.	118
Appendix C	Contour Plot of PRF, Peak Power and Melt Depth at 30% overlapping rate.	119
Appendix D	Contour Plot of PRF, Peak Power and Roughness at 30% overlapping rate.	120
Appendix E	Relative Error for Hardness	121
Appendix F	Relative Error for Roughness	122
Appendix G	Laser Processing Parameter	123
Appendix H	Upper Die Insert Holder Drawing	125
Appendix I	Lower Die Insert Drawing	126
Appendix J	Die Insert Drawing	127
Appendix K	Die Insert with Curve Drawing	128
Appendix L	Die Insert with Curve Drawing: Die Insert with Curve Drawing (a) Micrograph of laser melted layer of sample 9, and the corresponding EDXs mapping of, (b) silicon, (c) sulfur, (d) titanium, (e) vanadium, (f) chromium, (g) manganese, (h) iron, (i) nickel, (j) molybdenum and (k) carbon distribution.	129

UMP

## CHAPTER 1

### INTRODUCTION

#### 1.1 Introduction

The rapidly developed metal forming technologies in recent years have become highly imperative in the tooling industry. In metal forming, the blank material deforms to take shape according to the die geometry. Hot press forming (HPF) is recognised as the top technology in the automotive manufacturing sector for the production of automobile structural component with the strength of 1500 MPa or more (Naderi, Uthaisangsuk et al. 2008). The HPF technique produces ultra-high strength with complex and excellent shape accuracy of the steel components without the case of spring back (Li, Ying et al. 2013). Prior studies on HPF were rather extensive, which reported findings on blank steel behaviour and formability at high temperature (Bariani, Bruschi et al. 2008), microstructural evolution (Aziz and Aqida 2013), numerical modelling for hot forming process (Tekkaya, Karbasian et al. 2007), HPF optimisation (Aziz and Aqida 2013), friction at blank and die boundary conditions (Azushima, Uda et al. 2012), and heat transfer coefficients (Wieland and Merklein 2010).

Despite that, the findings on the behaviour of HPF die, especially its wear resistance and remain scarce. A novel approach was reported on blank coating wear at high temperature that simulated the industrial practice of HPF (Ghiotti, Sgarabotto et al. 2013). The die surface in HPF process requires enhanced hardness properties at elevated temperatures. Changes in surface topography of tool steel material due to high temperature may result in large variations in friction and wear of HPF tool steel materials. Adding to that, repeated heating leads to changes in the quenching time of HPF tool steel material. Due to this cyclic thermal exercise, the die would easily wear and crack and its surface would experience heat checks.

Essentially, thermal properties are important factors that influence the stabilisation of molecules of a material at high temperature. Higher thermal conductivity of material during the HPF process would increase the lifetime of the die. The thermal conductivity of a material depends on its crystallinity or grain size. For instance, a material with high thermal conductivity has smaller grain size, which then affects its hardness properties. The thermal conductivity of particles as well as the crystal size increase since there are fewer grain boundaries in the material. A study on thermal properties for various materials demonstrated that the hardness of materials decreased when the operating temperature increased (Aqida, Maurel et al. 2009).

Evidently, thermal stability is an important factor for material where used at high temperature. Basically, thermal stability reflects the tendency of a modified surface to retain its properties at high operating temperature. The thermal stability of Ti-6Al-4V was found improved after the cladding process with TiVCrAlSi (Huang, Zhang et al. 2011). Alloying elements, such as molybdenum and chromium, improve the strength, hardness, toughness, and hardenability of materials, which also improve the thermal stability of materials (Zulhishamuddin and Aqida 2015). In addition, another study on thermal stability found that increased annealing temperature reduced microhardness and increased grain size in Ni-based alloy (Sun, Fu et al. 2017).

Laser technology today, widely used for medicine, dentistry, manufacturing, biophysics, automotive and military. In manufacturing sector, laser surface modification such as laser melting, cladding and welding used as a remanufacturing process. The implementation of laser melting was found to deliver excellent bonding, improve hardness, have no flaws, and produce new mechanical properties and high temperature stability of surface layer, which improved the lifetime of die. The heating and cooling processes in laser melting depend on the processing parameter, which affects the chemical composition, microstructures, and properties of materials (Montealegre, Castro et al. 2010). Besides that, laser melting of cracked surface on hot work tool steel SKD6 die casting was deemed as an effective means to expand the lifetime of the damaged tool (SUN, HANAKI et al. 2004). Accordingly, a series of laser surface melting experiment was performed to examine the microstructure evolution of material. When the sample was thoroughly laser melted with low scanning velocity of 0.1 mm/s, the anomalous eutectic was found at the bottom of the molten pool or sample (Wang, Lin et al. 2013).

The assessment of microstructural evolution and thermal fatigue behaviour of H21 die steel revealed that the effective treatment depth was 650  $\mu\text{m}$  and reduced microhardness of laser treated surface, but its reduction was still higher than that of the original surface (Zhang, Lin et al. 2013). On the other hand, biomimetic laser melting process was adopted to repair thermal fatigue cracks on an annealed hot work die AISI H13 steel, which revealed that both crack density and crack length were reduced due to the blocking effect of strengthening unit (Cong, Zhou et al. 2014). In view of the above, the effect of laser melting on AISI H13 tool steel was specifically examined in this study to improve the lifetime of die in the HPF process.

## **1.2 Problem Statement**

Hot press forming (HPF) become one of most important technology in automotive manufacturing sector. It produced ultra-high strength component of automobile structure up to 1500 MPa (Naderi, Uthaisangasuk et al. 2008). During HPF processes die works at temperatures between 600 and 850°C to form boron steel blank (Merklein and Lechler 2006, Gui, Wang et al. 2014). The cyclic heating and tension during cooling impose on die surface during production process cause die easily wear on its surface (Chen, Wang et al. 2014). Major causes of die failures during operations are high thermal shock, mechanical strain, cyclic loading and corrosion which resulting in heat checking, wear, plastic deformation and fatigue (Altan and Deshpande 2011, Jhavar, Paul et al. 2013, Jia, Liu et al. 2015). Besides, during hot working processes the prolonged contact period between die surfaces and the working material leads to plastic deformation of the die along with the high pressure and temperature (Papageorgiou, Medrea et al. 2013). The high temperatures and cyclic loading caused the HPF dies surface to lose strength, hardness and lead to failure and reduce quality product produced from HPF process (Jhavar, Paul et al. 2013). From the problem stated, need more study to be done on die surface to improved die life. Die life is an important factor in automotive industry due to high cost involvement in production lost, maintenance and fabrication die block. To obtained optimum production and reduce production cost, the properties on die surface such as hardness and thermal conductivity must be improved (Valls, Casas et al. 2010). Die material require for higher hardness caused the typical hardness for dies today is in the range of 44 to 50 HRC.

One of the techniques that overcome this problem is laser surface modification. Laser surface modification is widely used in remanufacturing process. It produces new properties on the surface of a substrate which improves toughness, hardness and corrosion thus reduce wear resistance and thermal stress (Aqida, Ahmad et al. 2012, Fauzun, Aqida et al. 2013) due to the homogenous and ultrafine structure (Kusinski, Kac et al. 2012, Telasang, Majumdar et al. 2014). Increase the surface hardness of AISI H13 die is significant to endure wear at elevated temperature during applications (Aqida, Maurel et al. 2009). In this research, surface of AISI H13 die insert modified using laser melting process to improve die properties in hot press forming environment. Development of a prototype HPF die was carried out to evaluate the modified surface die inserts. The die inserts were characterised for sub-surface hardness properties, roughness, chemical and phase properties due to thermal changes. These findings contribute to the analysis of HPF die insert surface integrity and properties of 22MnB5 steel after HPF processes.

### **1.3 Research Objective**

The main objective of this research is to produce high strength component via hot press forming with laser modified die inserts. In order to fulfil the main objective, this study addresses three sub-objectives:

- i. To develop a modified layer on die steel substrate using laser processing for enhanced surface properties.
- ii. To characterise properties of 22MnB5 steel after hot press forming using laser melted die surface.
- iii. To determine thermal behaviour on laser modified surface in hot press forming environment.

### **1.4 Scope of Research**

To achieve the objectives of this research, this research was conducted through experiment. The first step is to machine a prototype HPF die with a lower and upper die holder size of  $140 \times 70 \times 38$  mm. The prototype was machined using CNC milling machine, EDM wire cut, EDM die sinking and drilling. Then, 18 pieces of die insert of  $70 \times 33 \times 8$  mm dimension were cut using EDM wire cut with finishing surface by CNC milling. Modification or melting process was conducted on 17 pieces of die insert surface

using JK300HP Nd:YAG twin laser source with 1064 nm wavelength and pulse processing mode. The controlled parameters are peak power ( $P_p$ ) at a range of 1700 to 2500 W, pulse repetition frequency (PRF) at a range of 50 to 70 Hz and spot overlap percentage ( $\eta$ ) range of 30 to 70%. While the average power was constant at 100 W and argon gas flow at 30 kPa pressure was used to protect the sample surface from oxidation during laser melting. Process optimisation of melted die insert surface was carried out using Design Expert software with 17 laser parameter settings. The effect of laser parameters on hardness, melt depth and roughness of melted surface was analysed using Box-Behnken design. The last stage for objective one is the surface and sub surface characterisation of melted layer for surface morphology, roughness, melt depth, hardness test, metallographic test, chemical composition and phase analysis.

The next step is to fulfil the second objective which is hot press forming of 22MnB5 boron steel blanks ( $70 \times 140 \times 1.8$  mm) using prototype dies. Four thermocouples were attached inside the lower die holder. The HPF process was conducted using a 60-tonne hydraulic press machine. During HPF process, the laser melted die inserts surface and the as-received die insert were used to form 40 pieces of 22MnB5 blank sample. The cooling medium of HPF process was cool water at temperature of  $5^\circ\text{C}$ . After HPF process, surface characterisation was carried out on laser melted die surface for hardness properties. The 22MnB5 blank surface was characterised for hardness properties and martensite percentage analysis. The last step was to determine thermal distribution in die insert during quenching process at 1 mm from top surface of melted die insert and as-received die insert. A data logger was used to collect temperature data from the four thermocouples to fulfil the third objective.



## CHAPTER 2

### LITERATURE REVIEW

#### 2.1 Introduction

This chapter discusses previous works of modified surface using laser processing and effect of modified surface on hot press forming (HPF) processes on 22MnB5 steel. The aims of this chapter to using past finding and knowledge with current study in this research area to provide guidelines and direction for this research. It consists of hot press forming processes include thermal properties on die surface and various problem in die surface. Other topic discusses was surface modification using laser processing technique and effect of parameter on laser melting process. The grain, hardness and thermal properties of various material surface were discussed.

#### 2.2 Hot Press Forming

In manufacturing industry, hot press forming become the top technology in automotive manufacturing sector (Naderi, Uthaisangsuk et al. 2008). Die element are most important factor in hot press forming process. Hot press forming technique used to produce ultra-high strength with complex and excellent shape accuracy of steel components without any spring back (Li, Ying et al. 2013). High strength steel are being increasingly used in the manufacturing industry and hot press forming of high strength steel plays an important role of light weighting without affecting the structural permormance of final project (Guler and Ozcan 2014).

Hot press forming is a process by plastic deformation of a thin metal sheet called blank. The process converts low-tensile strength metal to a very high-strength steel. Therefore, friction force has much effect on forming drawability (Jeong-Hwan, Jae-Ho et

al. 2009). This forming technique consists in heating blanks towards 900°C to 950°C, during 5 to 10 minutes, in a furnace until complete austenitisation. Afterwards the hot sheet is transferred, as fast as possible, from the furnace to the press and immediately stamped in order to take advantage of the excellent formability at high temperature between 600°C to 800°C. In the last stage, the tool is held closed for 20s for quenching the sheet below the martensite finish temperature  $M_f$ . The cooling velocity must be high enough exceed 27°C/s to obtain a final martensitic structure giving the desired mechanical properties to the part.

### **2.3 Die Failure in Hot Forming**

In hot forming process, the dies are subjected to high contact pressures and temperature. Selection of the die materials, hardness and coating is critical for increasing die life in precision stamping. The most important criteria for selection of die steel material are its resistance to wear, plastic deformation and fatigue (Jhavar, Paul et al. 2013). When the temperature at elevated temperature during hot forming, the dies soften and lose their hardness quickly, and to provide resistance to wear and plastic deformation, the die hardness should be as high as possible (Altan and Deshpande 2011). Several study have been conduct about hot stamping process and defect encountered after forming.

The defect on die surface will be produce some defect of end product such as wrinkle, crack, springback and distrotion (Naderi 2007) of product if the die and process are not planned reasonably (Guler and Ozcan 2014). From several previous works on die failure, cracking on or in die-casting dies for aluminum alloys is caused by a number of different and simultaneously operating factors. Some of them that affect die failures may be controlled to some extent by the die-casting experts (Kosec, Sokovic et al. 2005). Machining the dies may produce cracks on the surface of the forging dies. Once the dies are in service, these machining cracks act as stress concentrators and cause catastrophic failure of the die. The mode of failure has shown low cycle, high stress fatigue behavior, with the fracture propagating to complete failure in very few cycles (Bergeron, Burns et al. 2004). Study on gray cast iron shown, when the temperature is above 600°C, the die surface is easy to wear and collapse due to brittleness, thermal wear and fatigue, so the grey cast iron life at high temperature is not long enough.

Another previous studied are on failure analysis of fractured tool steel die plate, the die plate cracked as a result of a brittle nitride case and an insufficient cross-sectional area of the narrow ligament between the cap screw hole and the heater cartridge hole on the inlet face. Cracking initiated at the cap screw hole and propagated to the heater hole and beyond in a rapid manner. The heating of the inserted heater cartridge caused thermal stress on the adjoining thin ligament (cap screw wall) resulting in cracking of the extremely hard and brittle nitride case. Nitriding also reduces the corrosion resistance and hardness of the die plate (Go 2014).

#### **2.4 Surface Properties of Hot Forming Die**

For many engineering applications especially tooling industry, enhanced surface properties are significant to better endure high temperature, wear and friction. Although various advanced materials with significant properties have been developed, nevertheless when it concerns a particular surface engineering application, a materials' physical properties are among other factors that need to be considered, which include practicality, cost and time consumption. Implementation of surface treatments, coatings and plating are increasingly important to increase tool life and reduce the lubricant requirements.

In automotive manufacturing industry today, HPF process seen as one of the best solutions to produce a vehicle frame that is durable (impact-less) and at the same time lightweight. Current die material used is produced by Rovalma company which is commercially known as high thermal conductive steel (HTCS) 150. Table 2.1 and 2.2 show the thermal, physical and mechanical properties of HTCS material. Rovalma HTCS-150 is a hot work tool steel with very high thermal conductivity of 66 W/mK and high wear resistance (T. Wu 2013). It's known for their high precision, mechanical properties and high manufacturing cost. It is specially designed for dies of hot stamping of coated sheet, plastic injection molding where the plastic material is reinforced with abrasive fiber materials and closed forging. Furthermore, HTCS from Rovalma is produced by powder metallurgy, which is known very expensive. However, high thermal conductivity steel (HTCS) from Rovalma have low hardness compared to the H13 tool steel. The hardness of the steel will change of differ when the composition in the steel is being modified in order to get high thermal conductivity (Peet, Hasan et al. 2011).

Table 2.1 Thermal properties of high thermal conductive steel

Test Temperature		300 K	373 K	473 K	673 K	723 K	Unit
Linear thermal expansion coefficient	42 HRC		10.9	12.5	13.9	14.3	$\times 10^{-6}/K$
	50 HRC		10.5	12.1	13.5		$\times 10^{-6}/K$
Thermal diffusivity	42 HRC	16		13.1	9.8	6.3	$mm^2/s$
	52 HRC	12.5		10.6	8.2		$mm^2/s$
Thermal conductivity	42 HRC	66		62.4	53.4		W/mK
	50 HRC	55		53	47		W/mK
Specific heat capacity	44 HRC	496		594	667		J/kgK
	50 HRC	496		564	646		J/kgK

Source: T. Wu (2013)

Table 2.2 Physical and mechanical properties of high thermal conductive steel

Test temperature	300 K	723 K	Unit
Density	7.97		x 103kg/m <sup>3</sup>
Elastic modulus	216		x 103 MPa
Mechanical resistance	42 HRC 1305	928	MPa
Yield strength 0.2 %	42 HRC 1233	858	MPa
V-Notched Charpy resilience	42 HRC 18		J
Unnotched Charpy resilience	42 HRC 331		J
Fracture toughness	42 HRC 65		MPa•m <sup>1/2</sup>
Abrasive Wear resistance	45 HRC 178		Roalma-coefficient 2
	50 HRC 350		Roalma-coefficient 2
Fracture toughness	42 HRC 65		MPa•m <sup>1/2</sup>

Source: T. Wu (2013)

Subsequently, repeat heating has resulted in changes in quenching time of HPF tool steel material (Altan 2007). Changes in surface topography of tool steel material due to high temperature have caused large variations in friction and wear of HPF tool steel materials (Zheng, Wu et al. 2016). Cyclic heating and cooling cause cracks on die surface which required repairs to prolong its service. The convenient and economical method without buying a new die were modified or remanufactured. Lack of knowledge about the repair behaviour of die materials, need to identify new repair processes. From the economic point of view, it is crucial to use high precision laser processing for HTCS die surface repair (Leunda, Navas et al. 2012). Thus, a complete exploration of laser surface melting of HTCS materials in the tooling field is significant for extension of die life (Šturm, Štefanikova et al. 2015).

## **2.5 Problem in Various Laser Surface Modification**

Some study of surface modification using laser technique such as melting, cladding, alloying, heat treatment and welding indicate some problem of this technique. Laser cladding process on H13 tool steel and turbine blade shown crack, porosity and decreased hardness at clad zone (Rottwinkel, Nölke et al. 2014, Telasang, Majumdar et al. 2014, Kattire, Paul et al. 2015). While, laser melting on H13 and AISI D2 tool steel show defects such as shrinkage cracking, hardness decreased with increased thermal cycle and coarse grain at melted zone (Pleterski, Tušek et al. 2010, Jia, Liu et al. 2015). Laser welding of AISI P20 steel require double layer and tempering processes after laser welding processed (Suarez, Suarez et al. 2015). Repaired method using laser welding still showed some weaknesses such as crack and cavities at melted zone (Cong, Zhou et al. 2013). Furthermore, similar defects occurred in powder metallurgy materials which laser modified (Leunda, Soriano et al. 2011, Leunda, Navas et al. 2012, Šturm, Štefanikova et al. 2015). From the problem on laser processing stated, there are need more studies to be done on laser processing, especially on modify surface of AISI H13 hot press forming die insert.

Another study shown laser welding, remelting and alloying on H13 die steel also shown problem after repairing processed include coarse microstructure, reduce hardness at alloying zone and crack propagated at laser surface remelting (LSR) (Cong, Zhou et al. 2014). After repaired using laser welding, some defect produce on die surface such as

crack and cavities at melted zone (Cong, Zhou et al. 2013). No major effect on crack initiation after repaired H13 die casting using laser heat treatment (Mellouli, Haddar et al. 2014). Repaired low carbon steel and ductile cast iron using laser alloying shown crack and porosity after repairing processed. Laser modification of powder metallurgy materials using laser cladding, laser tempering and laser melting also shows porosity, crack, decreased hardness at clad zone and coarser microstructure on the modified surface (Leunda, Soriano et al. 2011, Leunda, Navas et al. 2012, Šturm, Štefanikova et al. 2015).

## **2.6 Surface Modification**

Surface modification on die surface were conduct using laser processing technique such as laser melting, laser cladding, hardening and welding due to very versatile technique for enhance surface integrity of die surface. Surface integrity reflects the properties of a material after it has been subject to some type of manufacturing process or modification. After the material has been modified, these original properties may no longer apply, as many manufacturing processes create a permanent change in the material (Freiburg, Biermann et al. 2014). Also show how a material will change under certain conditions, and what are new properties are compared to its old ones.

The surface properties of any material were made up of two basic components. They include the topography and internal surface features of the product. Topography reflects changes on the exterior surface of a material, and includes things like smoothness, bumps or waves, pitting and cracks. Internal features address changes just below the outer surface, such as deformation and changes in strength or hardness. They do not include internal changes deep within the heart of a material, but rather in the layer just below the surface (Group 1970). Previous findings on laser modified surface integrity show laser offer a wide range of possibility to achieve desire surface properties. This is used to reduce wear and improve fatigue resistance of processing component especially where hard surface layer are required on tough and possibly cheap base materials and where no measurable thermal distortion is allowed (Treatment 2014).



## 2.7 Laser Surface Modification

Laser surface modification is widely used as a remanufacturing process, especially for repairing cracks in mold and dies surface. It's a unique tool for the high quality surface modification. It produces new properties on the surface of substrate which improves toughness, hardness and corrosion thus reduce wear resistance and thermal stress due to homogenous and ultrafine structure due to localized rapid heating and cooling (Aqida, Ahmad et al. 2012, Kusinski, Kac et al. 2012, Fauzun, Aqida et al. 2013, Telasang, Majumdar et al. 2014, Norhafzan, Aqida et al. 2016). Laser surface processing provides a unique tool for the high precision surface modification with micron size heat source. The positive effects of laser surface modification are based on a change of the microstructure or the material composition of the surface layer due to a thermal cycle which is induced by a moving laser source (Schneider 1998).

Laser surface modification offer a wide range possibilities to achive desire surface properties. This is used to improved properties of materials with reduce wear and improve fatigue resistance of materials. Generally, three class of laser surface treatment can be divided as follows;

- i. Laser surface with melting.  
Produces very rapid heating and cooling on melted surface to modify the surface properties, examples lazer remelting and lazer glazing.
- ii. Laser surface without melting.  
Surface of material not melt where the material surface in solid state transformation, examples laser heat treatment and hardening.
- iii. Laser surface melting with addition of material.  
Surface of material melt with added same or different material, examples laser cladding and alloying.

One of the laser surface modification technique is laser cladding. Laser cladding offers a good metallurgical bonding with the substrate with wear, corrosion and high-temperature oxidation resistance that guarantees the toughness of the base material (Wang, Zhang et al. 2013, Wu, Li et al. 2013). Coating layer between the substrate and the cladding material has a high bonding strength due to a good metallurgical bonding (Xu, Li et al. 2015). In laser cladding, parameters like laser power, processing speed and



powder feed rate have been optimized to achieve acceptable clad-substrate integrity with maximum clad geometry and dilution, and homogenous structure without any surface porosity and cracks (Sun and Hao 2012, Telasang, Majumdar et al. 2014, Sahoo and Masanta 2015).

Laser assisted process is preferable due to its high precision, localised surface melting and solidification. Laser modified surface have been shown to have enhanced surface properties of the substrate due to grain refinement, secondary carbides and hard non-equilibrium microstructure formation (Aqida, Brabazon et al. 2011, Fauzun, Aqida et al. 2013). To date, cracks on dies surface were repaired using welding process, laser melting, biomimetic laser surface re-melting and laser cladding (Cong, Zhou et al. 2014, Kattire, Paul et al. 2015). Laser melting deposition restore groove defect and increased tensile strength on TC17 forging plate (Liu, Wang et al. 2016). While laser cladding successfully repaired crack with notching on single-crystalline blades made of CMSX-4 (Rottwinkel, Nölke et al. 2014). Among the many surface modification processes that are available today, laser provides unique tool for the high quality surface modification. One of the techniques to enhance surface properties is a laser melting. Laser melting is an advanced technology for enhance surface properties of various components and appliances (Kusinski, Kac et al. 2012).

### **2.7.1 Nd:YAG Laser Technology**

Nd:YAG (neodymium-doped yttrium aluminium garnet) is a crystal that is used as a lasing medium for solid-state lasers. Nd:YAG lasers are optically pumped using a flashtube or laser diodes. These are one of the most common types of laser, and are used for many different applications. Nd:YAG lasers typically emit light with a wavelength of 1064 nm, in the infrared. However, there are also transitions near 946, 1120, 1320, and 1440 nm. Nd:YAG lasers operate in both pulsed and continuous mode. Pulsed Nd:YAG lasers are typically operated in the so-called Q-switching mode: An optical switch is inserted in the laser cavity waiting for a maximum population inversion in the neodymium ions before it opens. Then the light wave can run through the cavity, depopulating the excited laser medium at maximum population inversion. In this Q-switched mode, output powers of 250 megawatts and pulse durations of 10 to 25 nanoseconds have been achieved. The high-intensity pulses may be efficiently frequency doubled to generate laser light at 532 nm, or higher harmonics at 355, 266 and 213 nm.

Nd:YAG lasers usually used for medicine, dentistry, manufacturing, biophysics, automotive and military. Nd:YAG lasers are used in manufacturing for engraving, etching, or marking a variety of metals and plastics, or for metal surface enhancement processes like laser peening (Ganesh, Sundar et al. 2012). They are extensively used in manufacturing for cutting and welding steel, semiconductors and various alloys. For automotive applications (cutting and welding steel) the power levels are typically 1–5 kW. Super alloy drilling (for gas turbine parts) typically uses pulsed Nd:YAG lasers (millisecond pulses, not Q-switched). Nd:YAG lasers are also employed to make subsurface markings in transparent materials such as glass or acrylic glass. Lasers of up to 2 kW are used for selective laser melting of metals in additive layered manufacturing. In aerospace applications, they can be used to drill cooling holes for enhanced air flow/heat exhaust efficiency. Researchers from Japan's National Institutes of Natural Sciences are developing laser igniters that use YAG chips to ignite fuel in an engine, in place of a spark plug. The lasers use several 800 picosecond long pulses to ignite the fuel, producing faster and more uniform ignition (Pavel, Tsunekane et al. 2011). The researchers say that such igniters could yield better performance and fuel economy, with fewer harmful emissions.

In manufacturing industry, laser system is basically used for welding, metal cutting, heat treating, alloying, and coating or cladding. Various types of laser have been developed to meet industrial needs with three main process includes vaporising, heating and melting process. Some laser system used to harden die material are carbon dioxide (CO<sub>2</sub>) laser, (neodymium-doped yttrium aluminium garnet (Nd:YAG) laser, fibre laser and high power diode laser (HPDL). However, the laser processing performance and usage depends on laser technique and equipment specification (Ganeev 2002). The Nd:YAG laser system was used to harden surface at various parameters. The Nd:YAG laser produced shorter wavelength compared to CO<sub>2</sub> laser with a longer wavelength (Jae-Ho, Jeong-Hwan et al. 2009). The shorter wavelength laser beam easily penetrates deep into the base material as metals absorb shorter wavelength efficiently.

Nd:YAG laser is suitable for heat treating and is cheaper to operate. Besides that, the system comes in smaller size that applicable for most metals and work efficiently compare CO<sub>2</sub> lasers. Basically, the Nd:YAG laser has more advantages such as high energy absorption rate and high energy density (Jiang, Xue et al. 2011). Meanwhile, CO<sub>2</sub> laser is a traditional high power laser with moderate efficiency, high power density, reliable operation and excellent beam quality. To enhance laser absorption, pre-treatment

of sample surface is required prior to CO<sub>2</sub> laser processing (Dobrzański, Piec et al. 2007). HDPL laser is new generation of high power laser for material processing. However, HDPL laser produces poor beam quality and only suitable for laser hardening and coating. Overall, Nd:YAG, fibre and diode laser shows a high surface absorption compared to CO<sub>2</sub> laser..

### 2.7.2 Laser Melting

Laser melting is one of the technologies uses in surface modification. It's can improve surface properties such as hardness, wear resistance, toughness and corrosion due to homogenous and ultrafine structure (Kusinski, Kac et al. 2012, Telasang, Majumdar et al. 2014). Laser melting Process is one of the technique to modified surface in advanced manufacturing. Figure 2.1 shown schematic diagram for laser surface melting for flat plate workpiece. Three fundamental procedure involved in laser surface modification namely heat transfer, momentum transfer and mass transfer. Laser surface melting produce an increase of the hardness, toughness and wear resistance of the material surface in very short time (Steen and Watkins 1993). In the laser melting coating, distribution of chemical elements are uniforms, grain are fine dendrites and big blocky.

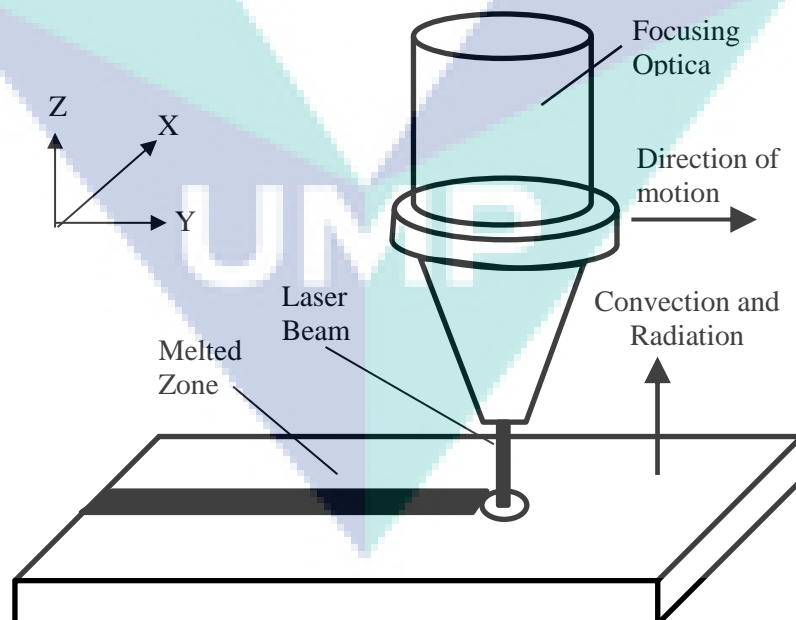


Figure 2.1 Schematic diagram for laser surface melting for flat plate workpiece  
Source: Li, Wang et al. (2010)

Laser melting was implemented to improve die life due to excellent bonding, improve hardness, absence of flaws, produce new mechanical properties and high temperature stability of surface layer. Heating and cooling during laser melting depend on processing parameter which affected chemical composition, microstructures and properties (Montealegre, Castro et al. 2010). Heating and cooling during laser melting process depend on processing parameter which affected chemical composition, microstructures and properties (Kusiński, Kaç et al. 2010, Montealegre, Castro et al. 2010). Laser melting of cracked surface on hot work tool steel SKD6 die casting resulted in an effective method to expand life of the damaged tool (SUN, HANAKI et al. 2004).

Series of laser surface melting experiment were performed to investigate the microstructure evolution of material. When the sample was laser melted thoroughly with the low scanning velocity of 0.1 mm/s, the anomalous eutetic can be found at the bottom of the molten pool/sample (Wang, Lin et al. 2013). Investigation for microstructural evolution and thermal fatigue behaviour of H21 die steel, show that the effective treatment depth is 650µm and thermal fatigue show the microhardness of laser treated area was considerably reduce, but it was still higher than that of the original surface (Zhang, Lin et al. 2013). Biomimetic laser melting process was adopted to repair thermal fatigue cracks on an annealed hot work die AISI H13 steel. Thermal fatigue result show that both crack density and crack length are reduced due to the blocking effect of strengthening unit (Cong, Zhou et al. 2014).

### **2.7.3 Effect of Laser Processing Parameter**

Laser process is preferable due to its high precision, localised surface melting and solidification. Laser modified surface have been shown to have enhanced hardness up to 4 times of the substrate due to grain refinement, secondary carbides and hard non-equilibrium microstructure formation (Aqida, Brabazon et al. 2011, Fauzun, Aqida et al. 2013). Control of laser parameter setting yields different effects on the modified surface properties. The laser power and scan speed or material-laser interaction time have previously been shown by the applicant to have a strong influence on the resultant temperature profile, modified microstructure, chemical composition, and modified layer depth (Aqida, Brabazon et al. 2011, Aqida, Brabazon et al. 2013, Aqida, Brabazon et al. 2013, Fauzun, Aqida et al. 2013).

Selection of proper processing parameter is necessary to prevent the high residual stress concentration (Farahmand and Kovacevic 2014). Laser parameter play a crucial role in determining the microstructures and surface topography of alloyed zone (Nath, Pityana et al. 2012). Effect of laser processing parameter on the geometric characteristics, microstructure and mechanical property of H13 steel shown there was an obvious increase in both depth and width of unit with effective peak power density (EPPD). The geometrical characteristic could be predict by the combination of average peak power density (APPD) and (EPPD) (Zhang, Lin et al. 2014). To decrease the production time, high processing speeds should be aimed. Furthermore, the surface quality of generated parts has to be improve (Meier and Haberland 2008). Figure 2.2 shows interaction time for different laser processing technique. Combination of interaction time and power density essential to improve surface properties. Surface properties improved due to short interaction time with high power density caused grain structure refined.

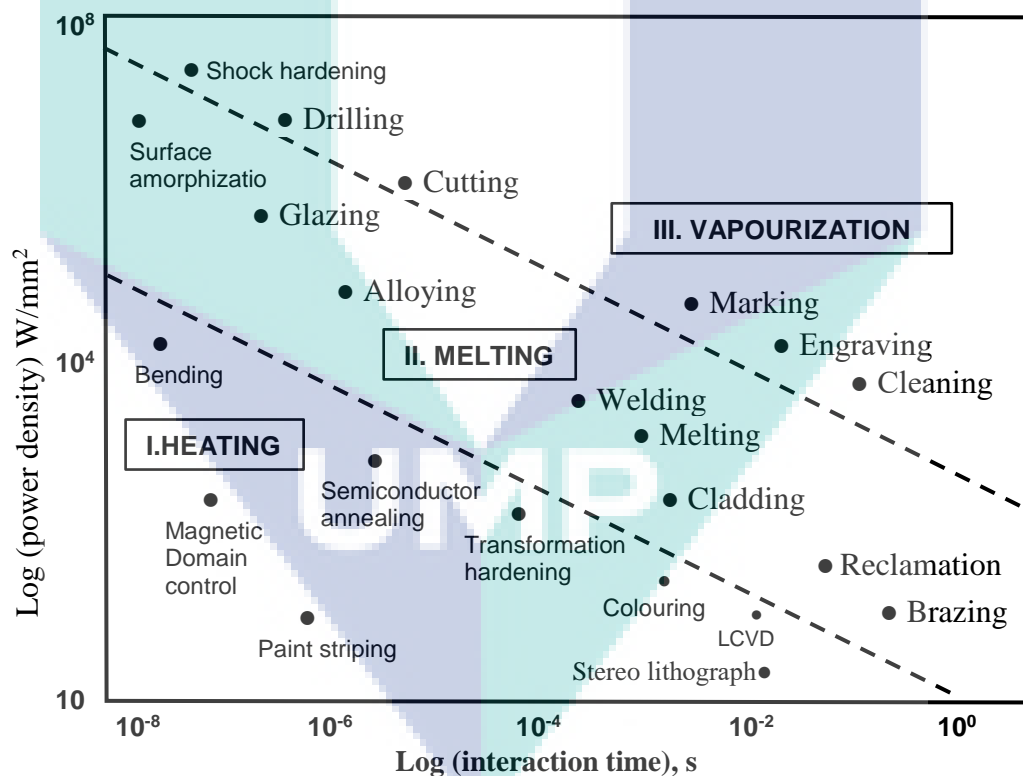


Figure 2.2 Laser power density as a function of interaction time for different examples of laser material processing  
Source: Majumdar and Manna (2003)

Optimization of laser parameter is a very important factor to enhanced surface properties in laser surface modification due to cracking tendency at laser modified layer during laser surface melting process (Petrovič and Šturm 2014). Control of overlapping laser spots yields different effects on the modified surface properties due to additional heating of melted layer . The laser power and scan speed or material-laser interaction time have previously been shown by the applicant to have a strong influence on the resultant temperature profile, modified microstructure, chemical composition, and modified layer depth (Aqida, Brabazon et al. 2011, Aqida, Brabazon et al. 2013, Aqida, Brabazon et al. 2013, Fauzun, Aqida et al. 2013). Varied processing parameter such as scanning speed and laser power in similar based material produce different microstructure and microhardness (Elhamali, Etmimi et al. 2013). Control of laser parameter setting yields different effects on the modified surface properties. Laser surface processing provides a unique tool for high precision surface modification using the heat source to enhance surface integrity of used die.

Laser modification on AISI H13 surface with various laser parameter enhanced surface properties such as hardness increased after laser procesed and various surface morphology achived (Aqida, Naher et al. 2011). During laser process, the peak power produced a deeper penetration due to higher absorption rate achived by changing the duty cycle. While, decreasing scan rate and increasing PRF caused overlapping area increased (Kumar 2006). Increasing pulsed width decreased depth of heat penetration (Sabbaghzadeh, Azizi et al. 2008). The melted zone depth decreased when the processing speed increased (Jae-Ho, Jeong-Hwan et al. 2009). A higher PRF caused faster cooling rate due to pulse energy was lower at higher PRF. While, increasing PRF caused the hardness properties of metal sample to increase. Laser parameter also influenced the surface roughness properties. During laser processing, the surface roughness of metal surface depends on pulse period and pulse width (Pinkerton and Li 2003). The higher overlapping rate with increased beam scanning speed produced a high surface roughness (Jiang and Molian 2001).

#### **2.7.4 Overlapping Rate**

The overlapping rate in laser processing effect of material properties such as hardness, roughness and residual stress after laser processed due to overlapping rate



influence of grain refinement during recrystallization processed (Cao, Liu et al. 2013). Overlapping rate can calculate from Equation 2.1.

$$\eta = \frac{L-L_0}{L} \times 100 \quad 2.1$$

where  $L$  is the spot radius plus scanning speed ( $v$ ) times with pulsed width ( $T_p$ ).  $L_0$  is overlapped distance between two  $L$  as shown in Figure 2.3.

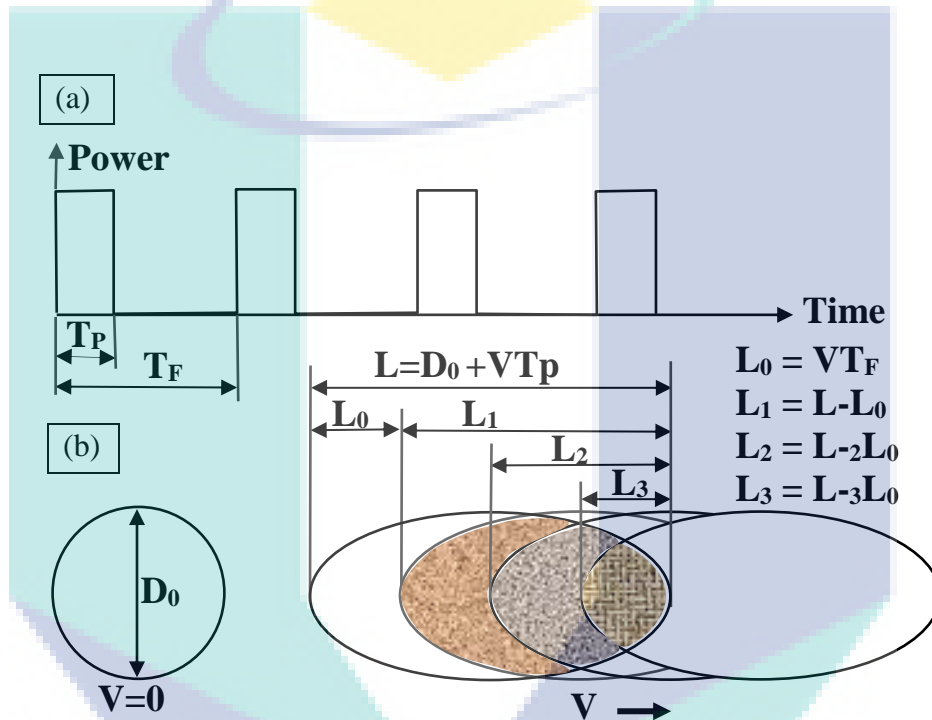


Figure 2.3 Schematic diagram of (a) a rectangular laser power pulse trains and (b) its corresponding partially overlapping spots  
Source: Zhang, Lin et al. (2014)

Higher overlapping rate produce more overlap and decreased scanning speed due to more pulsed reached (Zhang, Lin et al. 2014). Figure 2.4 (a) shown overlap rate of 50% with less overlap. Increased overlapping rate up to 90% in Figure 2.4 (c) show more overlap produce. Different overlap ratio effect on processing time, when overlap ratio increased more overlap produce on sample surface as shown in Figure 2.4 (c) and increased processing time. Increasing processing time will increase the processing cost. For cost and time consumption, the overlapping rate below 30% is suitable to used (Li, Wang et al. 2010, Karbalaian, Yousefi-Koma et al. 2015). Another study shown 70% overlapping rate produce homogeneous microstructure and eliminate porosity on Al-Si

alloy (Houndri, Polymenis et al. 1992). While, Laser surface melting on roller steel with 15, 30 and 50 % overlapping shown the surface hardness decreased with increased overlapping rate (Li, Wang et al. 2010).

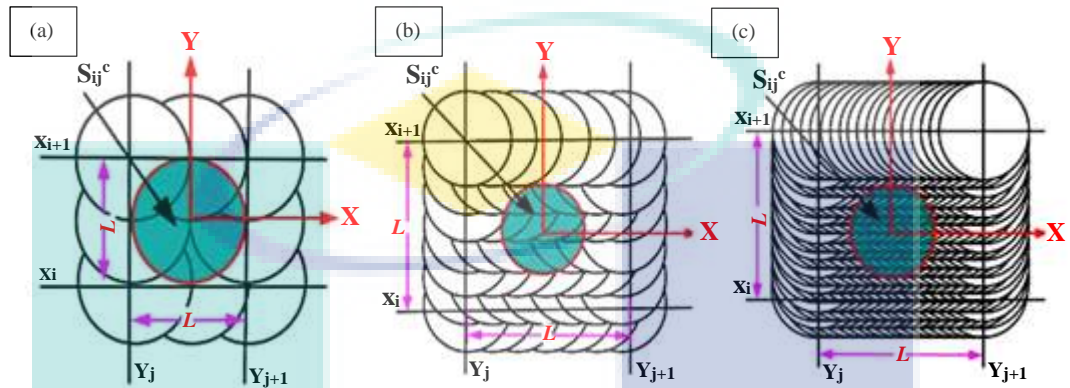


Figure 2.4 Symmetry cells for simulation of different overlapping rates; (a)  $\eta=50\%$ , (b)  $\eta=70\%$ , (c)  $\eta=90\%$   
Source: Hu and Yao (2008).

## 2.8 Hardness Properties

HPF die surface requires high hardness properties at elevated temperatures. Changes in surface topography of tool steel material due to high temperature have caused large variations in friction, and wear of HPF tool steel materials (Zheng, Wu et al. 2016). Subsequently, repeat heating has resulted in changes in quenching time of HPF tool steel material. The hardness properties of modified layer decreased directly proportional to heating period. Surface hardness in melted zone increase due to brittle martensite structure formation. Martensite structure acted as the strengthening to produce high strength material or component (Du, Hoefnagels et al. 2018). At cooling rate above  $30^{\circ}\text{C}/\text{s}$  the austenite transformed to martensite structure. The strength of material reduce when the austenitisation temperature decreased below  $775^{\circ}\text{C}$  (Mori, Bariani et al. 2017). Study of Thyrotherm E38K steel shown the thermal fatigue resistance increased when the toughness and hardness properties of Thyrotherm E38K increased (Fuchs 2002).

Study of gray cast iron shown, surface hardness properties of gray cast iron before laser surface cladding were approximately  $177 \text{ HV}_{0.1}$ . Surface hardness of gray cast iron



increased up to 1000 HV<sub>0.1</sub> after cladding process. The surface hardness of melted layer reported previously was increased up to 737 HV<sub>0.1</sub> (Zulhishamuddin, Aqida et al. 2016). Hardness of melted surface on gray cast iron increased up to four times of the substrate hardness due dissolved carbon content into melted zone. Hard phase of clad layer surface improve hardness properties and wear resistance of gray cast iron (Paczkowska 2012). These properties are important to increase thermal stability of gray cast iron for enhanced lifetime when used at cyclic heating and cooling condition.

Study of laser melting on HTCS-150 steel shown low surface hardness measured at the nearest distance from surface was due to repeated heating which caused a slower cooling rate. Hardness of melted zone increased along surface layer depth and start to decrease from the heat affected zone to substrate layer. Hardness decreased in melted zone possibly caused carbides are unable to be dissolved in austenite due to short interaction time between laser beam and substrate (Kusinski, Kac et al. 2012). Increased hardness in melted layer was due to higher irradiance with high scanning speed of the laser gun and laser power. High speed possibly reduced heating time and allowed faster solidification. At average power of 50 and 60 W, HTCS-150 sample produced subsurface hardness of 778.7 HV<sub>0.1</sub> which is approximately two times higher than its substrate of 311.6 HV<sub>0.1</sub>. Hardness for modified surface of HTCS-150 from previous paper were 610.9 HV<sub>0.1</sub> due to different parameter selection.

Various laser melting parameter were used to modified steel surface which resulted in changes of surface morphology, chemical element, groove depth and hardness properties. Another study shown the hardness properties of AISI H13 surface decreased directly propotional to the scanning speed. The hardness of modified surface increased up to approximately 2.9 times of the substrate hardness. High hardness properties in clad layer was due to grain refinement. A lower hardness was measured in the HAZ down to the substrate .

## **2.9 Grain Properties**

Laser melting processed improved properties on melted surface due to refined grain structure. Grain structure refined due to localized rapid heating and cooling with equiaxed grain at edge of melted pool during solidification processes. When grain saize refine, the properties of material such as ultimate tensile strength, yield strength, and

elongation was improved. Several study conduct for microalloyed with Ti and C and successfully refined the grain size with changed the grain shape from columnar to equiaxed (Liu, Laplanche et al. 2019). Another study shown equiaxed grain produced in aluminium alloy after arc welding are the prefferd structure (Kurz, Bezencon et al. 2001). Study of solidification behavior and grain morphology for laser additive manufacturing of titanium alloys shown equiaxed grain formation affacted of supercooling at melt pool (Zhu, Tang et al. 2019). The small equiaxied grain begin from the edge continue by columnar grain and finally large and homogenous equiaxied grain form at central zone of melted pool as shown in Figure 2.5 due to delay solidification with under cooling and lantent heat.

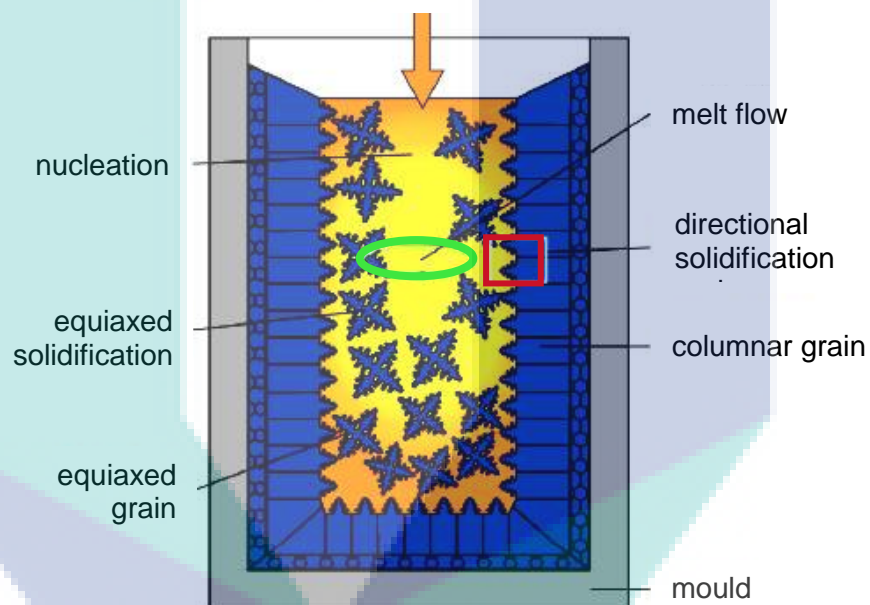


Figure 2.5 Schematic drawing of columnar and equiaxed grain growth during solidification

Source: Zimmermann, Sturz et al. (2011)

The solidification processes change liquid to solid material at lower melting point. Different temperature between melted pool and substrate during solidification processes caused cooling rate decreased and nucleation start growth to produce equiaxed grain in undercooling condition (Zimmermann, Sturz et al. 2011). The solidification processes transformed melt material during laser melting to new phase. The melt pool start solidify from edge between substrate and melted pool due to higher cooling rate at this area, then continue solidify into central zone of melted pool. Columnar oriented in one direction while equiaxed growing in random orientation to produced different mechanical

properties. Figure 2.6 shown an equiaxed solidification system where small grain start growth with heat flow direction.

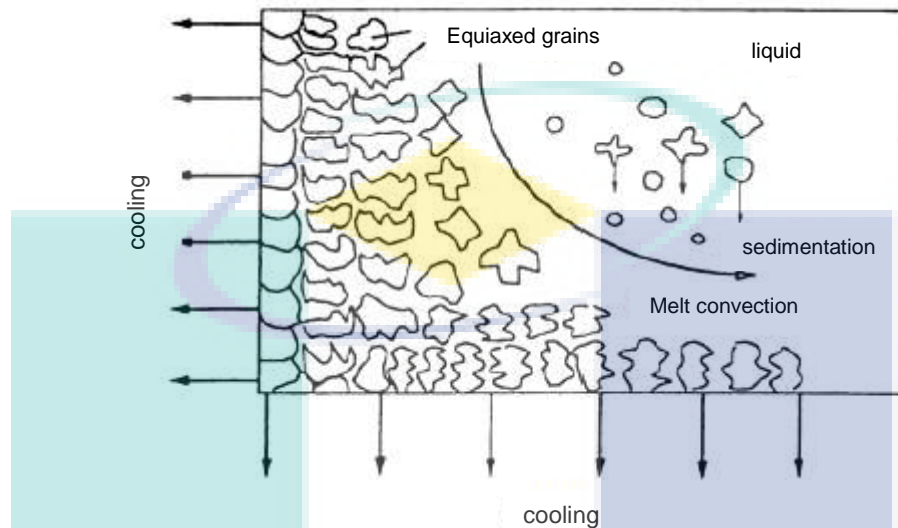


Figure 2.6 Schematic of an equiaxed solidification system  
Source: Beckermann (1997)

Material with strength and fatigue at high temperature required in industry, so the material with equiaxed structure required to improved material structure (Jung, Mangelinck-Noël et al. 2009). The distribution of grain size affect mechanical properties of the material such as strength, hardness, toughness, elasticity, plasticity, brittleness, ductility and malleability. The grain size depend of Hall-Petch relationship, where the yield strength improved when grain size decreased (Lehto, Remes et al. 2014). Heating and cooling rates are significant values in laser surface melting to control the size of the micro structurally altered region and comply with the Hall-Petch relation (Aqida, Brabazon et al. 2011).

## 2.10 Thermal Properties

Thermal properties were the important factor of material to stabilize its molecule at high temperature. Thermal conductivity is ability of a material to transport heat energy from high temperature region to low temperature region as fast as possible. Higher thermal conductivity of material during hot forming processes (HPF) required to increased die lifetime. The thermal conductivity of materials depends on crystallinity or grain size. High thermal conductivity material has smaller grain size. The decreased of

grain size affected on hardness properties. The thermal conductivity of particles increased because less grain boundaries in material exist due to crystal size increased.

Study of thermal properties for various material shown hardness of the sample decreased when the temperature increased (Aqida, Maurel et al. 2009). Thermal stability is the important factor to conduct material in high temperature. Thermal stability is a tendency for modified surface to retain its properties at high working temperature. Thermal stability on Ti-6Al-4V improve after cladding process with TiVCrAlSi (Huang, Zhang et al. 2011). Alloying element such as Molybdenum and chromium improve strength, hardness, toughness and hardenability also improve thermal stability (Zulhishamuddin and Aqida 2015). Another thermal stability study shown, increased annealing temperature caused decreased microhardness and enlarge grain in Ni-based alloy (Gordillo, de Castro et al. 2017, Sun, Fu et al. 2017). The thermal stability of die material at elevated temperature was investigated through micro hardness testing and metallographic study. The combination of wear resistance, high strength and thermal stability can increase significantly the lifetime.

### **2.10.1 Thermal Cycle**

Cyclic heating and cooling processes in HPF processed as known as thermal cyclic. Heating temperature in thermal cyclic processes given significant effect of die material and blank surface after HPF processed (Sadak 2015). At elevated temperature, grain structure are instable and restructure to formed new grain structure. Figure 2.7 shown estimated hardness loss for the thermal cycling experiments for hot work tool steel. The surface of hot work tool steel start softening at elevated temperature above 575°C and the surface hardness decreased after 100 cycle thermal loading (Caliskanoglu, Siller et al. 2002). Decreased surface hardness caused wear rate increased at elevated temperature above 400°C due to recrystallisation (Mori, Bariani et al. 2017). However, the previous study of aluminium for thermal cycle shown the surface hardness decreased when thermal cycle below 40 cycle (Sadak 2015). Figure 2.8 shown Effect of thermal fatigue on hardness of aluminium at temperature;  $T_h=100, 300$  and  $500^\circ\text{C}$ . The previous study shown heating temperature are important factors influence of material properties in thermal cyclic processes. While, the pressure applied during forming of blank is possible to retain and produced fine grain structure of melted surface (Ventura 2017).

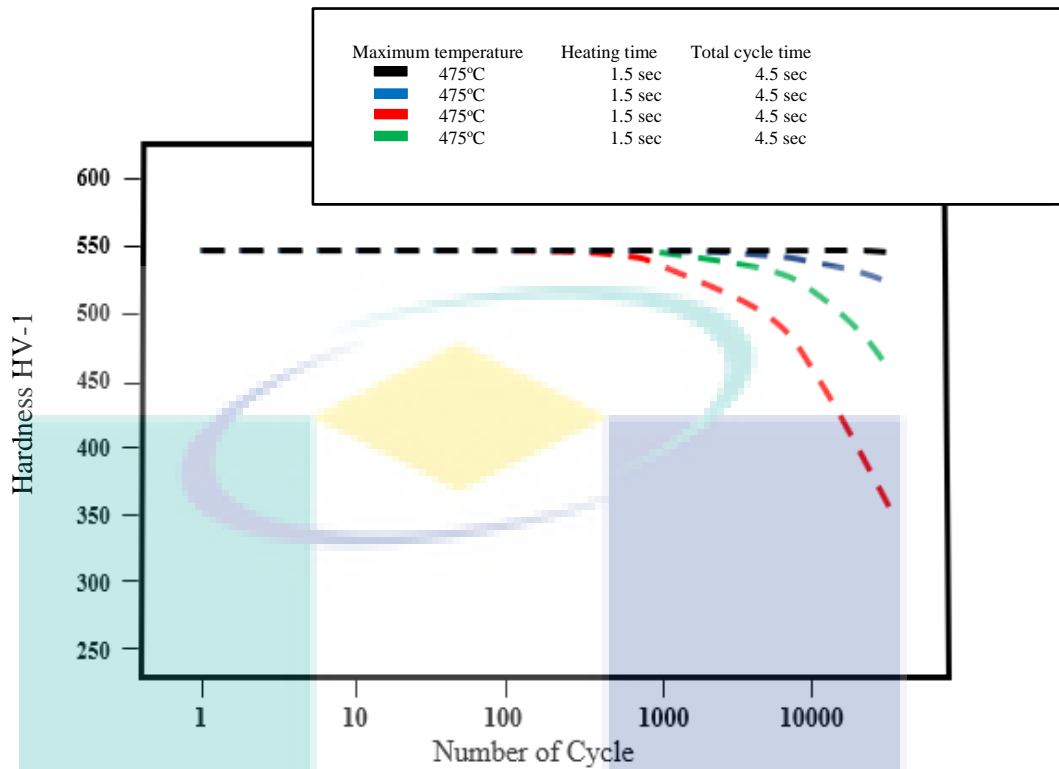


Figure 2.7 Estimated hardness loss for the thermal cycling experiments  
 Source: Caliskanoglu, Siller et al. (2002)

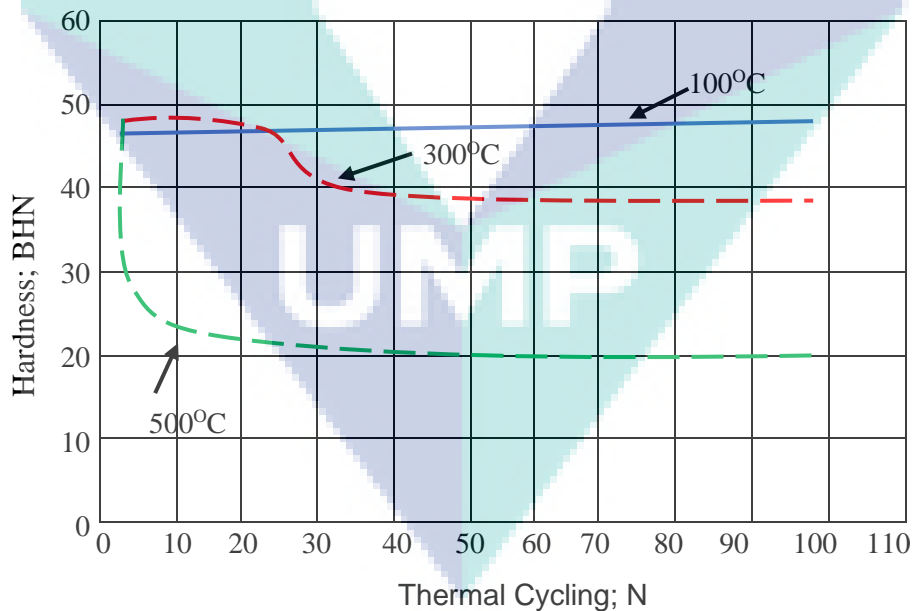


Figure 2.8 Effect of thermal fatigue on hardness of aluminium at temperature;  
 $T_h=100, 300$  and  $500^\circ\text{C}$   
 Source: Sadak (2015)

## 2.11 Thermal Conductivity on Die Surface

High strength component produced from hot press forming due to high quenching rate. High quenching rate require high thermal conductivity on die surface to increased cooling rate during HPF processed (Zulhishamuddin and Aqida 2015). Thermal conductivity can define as how fast the heat can diffuse from material. Thermal conductivity can prevent material from premature degradation due to substantial overheating caused heat from the material diffuse very fast (Burger, Laachachi et al. 2016). Thermal conductivity on die surface depends on grain structure or microstructure and heat transfer from blank material to die surface. Improved cooling rate gain martensite structure in pressed blank material to produced high strength component. To produce high strength product using HPF process, some parameter such as die cooling channel, quenching time, water flow rate and cooling temperature must be select correctly. While to get optimum production and reduce production cost, the cooling strategy must be optimize and thermal conductivity on die surface must be improve (Valls, Casas et al. 2010).

### 2.11.1 Cooling Channel

Cooling channel in HPF used to control cooling rate during quenching processed. Selected optimum cooling channel in die design can cool down die surface efficiently. The cooling channel diameter and depth from loading surface important to achive homogenous temperature distribution on HPF product. The Cooling channel distance from loading surface influence major effect on performance of HPF tool and forming product due to effect of cooling rate during HPF (Zamri and Yusoff 2015). Previous researchers have proven that high cooling rate during quenching processed in HPF was important factor in HPF process which required optimisation of cooling channel design in HPF die (Mohd Fawzi, AR et al. 2014). The usual cooling channel parameter used in HPF shown in Figure 2.9, where a is diameter hole, b is distance between cooling holes and c is distance from loading surface. The optimum cooling channel parameter to produce better performance of quenching processed during HPF from several study for a, b and c were (8, 10, 8) mm (Zamri and Yusoff 2015), the diameter range of cooling channel was between 8 and 12 mm, pitch distance was 10 mm while distance to loading surface was between 10 and 15 mm (Zamri and Yusoff 2015).



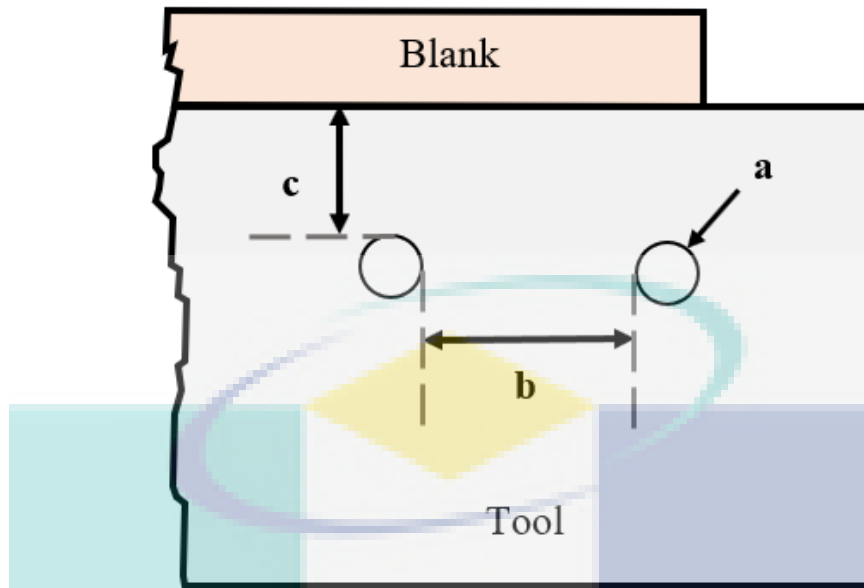


Figure 2.9 Cooling holes parameter; a-hole diameter, b-distance between cooling holes, c-distance to tool contour  
Source: Mohd Fawzi, AR et al. (2014)

### 2.11.2 Quenching Process

The quenching processes is the rapid cooling of blank during HPF processes. Cooling time and temperature during quenching process produce brittle or harder material compare substrate material due to various martensite formation. The cooling transfer in blank sample in HPF processes usually thru cooling channel in HPF die. Various quenching time and water temperature produce various hardness on HPF blank sample. Previous study shown quenching time of 5, 8 and 11 second with 30 l/min water flow rate at 27°C produce hardness between 477 to 551.4 HV<sub>0.1</sub> due to affect of water temperature and quenching time during HPF processed (Aziz and Aqida 2013). Surface hardness of an AlSiMg alloy increased from 34 HB to 99 HB when the quenching rates increased from 0.008 °C/s to 3 °C/s (Fracasso 2010). Higher quenching rate of 2000 °C/s, in 25 °C water increased hardness of material (Fan, Lei et al. 2018). However, slow cooling during quenching improved tensile strength up to 1096 Mpa (Li, Liu et al. 2018). Slow cooling improved toughness and reduce fracture but it's reduced hardness of material. Selected proper cooling time and temperature prevent material from brittle and produce hard and tough material.

## 2.12 Summary

This chapter discussed literature review on hot press forming, laser processing and thermal properties from previous researchers. The main review discussed about hot press forming, including die failure in HPF, surface properties resulted from HPF, factors that affect HPF product. The HPF die failure specifies the criteria for selection of die material, the effects of defect on die surface and mode of die failure. The surface properties of HPF topic discussed about die material properties including thermal, physical and mechanical properties.

The topic of laser processing includes the problems in various laser surface modification, surface modification techniques, laser surface modification process, Nd:YAG laser technology, laser melting mechanism, and the effects of laser processing parameters and overlapping rate on surface properties. This topic discussed about the defects on material after repaired using various type of laser processing method. While laser surface modification topic discussed about the types of laser processing and surface repair method using laser processing. Other than that, Nd:YAG laser technology is included with their advantages and applications, along with the effect of laser melting process on various surface conditions.

From the review the hardness and grain properties influenced the properties of die insert and 22MnB5 surface during HPF process. The grain structure was affected by heating and cooling, and solidification behaviour on sample surface. The temperature distribution on material surface and blank properties were due to thermal cycle, thermal conductivity of die surface, cooling channel dimension and quenching process. The optimum cooling channel in die design produced a better performance of quenching process during HPF apart from quenching time, water temperature and water flow rate on HPF blank sample. At different temperature conditions, the surface hardness was affected. Overall, the benefits of laser melted surface have not been applied at high temperature due to its stability issue. Thus, this study was carried out to characterise the laser melted die insert surface properties and martensitic phase transformation in 22MnB5 blanks after HPF process.



## CHAPTER 3

### METHODOLOGY

#### 3.1 Introduction

This chapter explains all the element of research methodology to fulfil the objective of this study. The research methodology include method, design, materials, laser parameter, equipment, optimisation, type of testing and analysis. The methodology and procedures planned are important to determine method, direction and flow of this study.

#### 3.2 Research Flow Chart

The study was conducted based on the flow chart of Figure 3.1. The first stage is to develop a design of HPF die for 60 tonne hydraulic press machine using UGNX 10 software. The design included cooling channel, thermocouple holder, upper and lower die holder, and die insert. The next stage is to machine HPF dies from AISI H13 tool steel block using CNC Milling, EDM wire cut, Die sinking and drilling.

The third stage is to develop a DOE for laser surface melting of HPF die inserts using Design Expert software. The laser melting parameter was predict using preliminary study before actual parameter developed using Box-Behnken design. Then laser melting conduct on HPF die inserts surface using Nd:YAG laser system with 17 laser parameters setting produced from Box-Behnken design. After laser melting process done on all die insert, the dies insert then characterise for surface morphology, surface roughness, melted depth, hardness, metallographic study, chemical composition and phase analysis.

**LASER SURFACE MELTING TO ENHANCE SURFACE PROPERTIES IN HOT PRESS FORMING DIE**

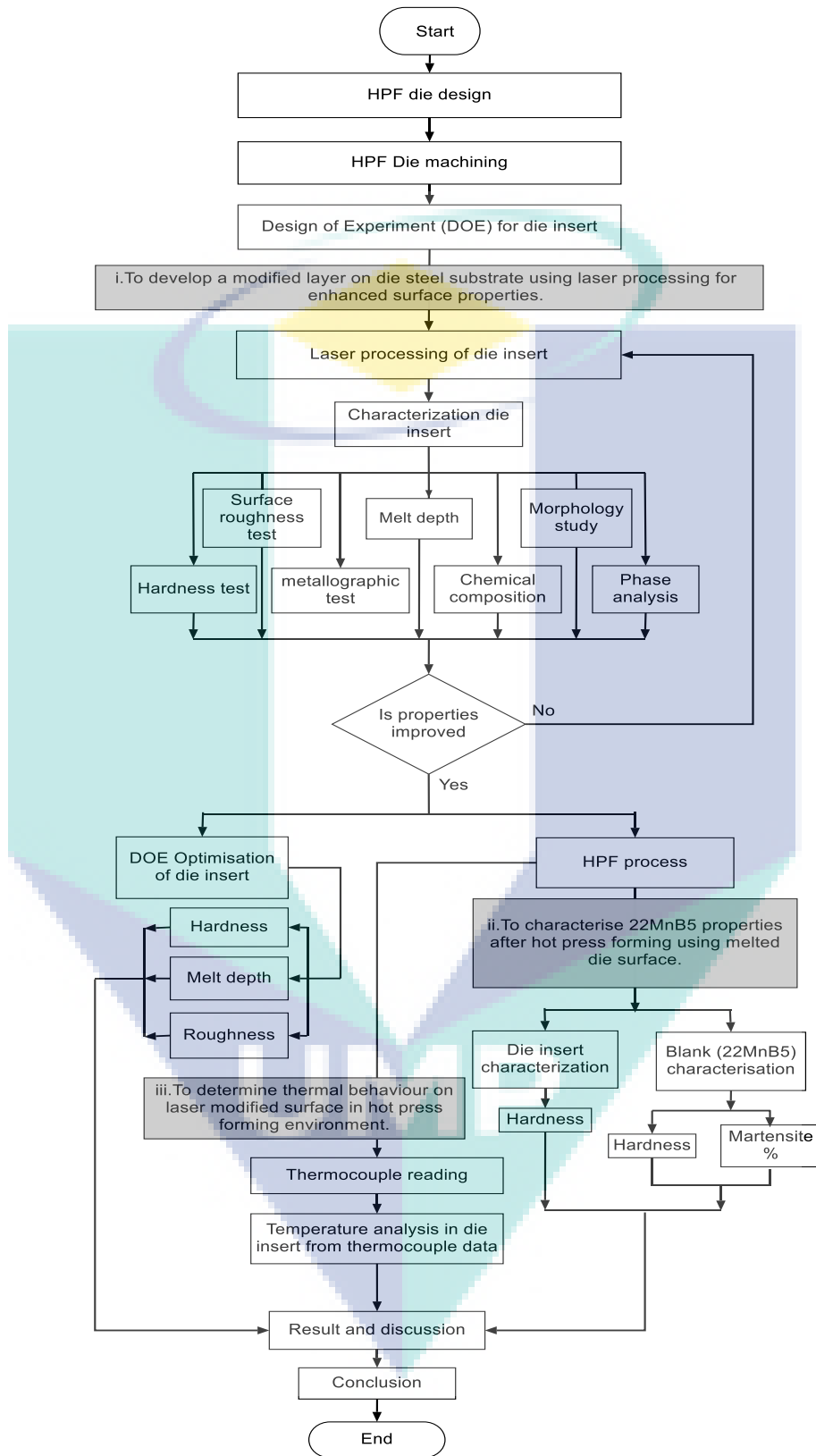


Figure 3.1 Research methodology outline.

In the next step, hot press forming of 22MnB5 blanks steel was conducted using melted dies insert. Every melted die inserted formed 40 pieces of 22MnB5 blank steel equivalent for 40 cycle cooling and heating applied on every die insert surface during HPF processes. The blank sample was heating up to 950°C for 5 minutes. Consequently, the hot press formed 22MnB5 boron steel blanks were characterised for hardness properties and martensitic percentage. The martensite percentage of 22MnB5 steel and grain of AISI H13 was analysed using ImageJ software. Surface hardness of die insert after HPF process for 40 cycle was characterized for surface hardness. After that, optimisation of dies insert was conduct to get optimum parameter and finding. Validation process conduct to prove that parameter used is valid. Four thermocouples reader with data logger was used to characterise thermal distribution during HPF processes on dies insert surface. Finally, all result was analysed and discuss to fulfil all objective.

### 3.3 AISI H13 Tool Steel Die

The die material chosen for this work was the premium grade ASSAB 8407, an equivalent of AISI H13 tool steel. The premium grade of AISI H13 tool steel is the preferred die material in forming and stamping industry. The composition of the ASSAB 8470 steel from energy dispersive X-ray spectroscopy (EDXs) analysis is given in Table 3.1. Premium grade H13 is a chromium hot work steel and is a hypoeutectoid steel with high hardenability and a good combination of strength, hot hardness, toughness, ductility and resistance to tempering. Some typical physical and mechanical properties of H13 used are presented in Table 3.2.

Table 3.1 Chemical composition of ASSAB 8407/ AISI H13 steel

Material	Elements (wt%)					
	C	Si	Mn	Cr	Mo	V
ASSAB 8407/ AISI H13	9.91	0.70	0.14	3.58	0.47	0.23

Table 3.2 Physical and mechanical properties of ASSAB 8407/ AISI H13 steel

AISI H13 Tool Steel	Properties		
	20°C	400°C	600°C
Temperature	20°C	400°C	600°C
Density kg/m <sup>3</sup>	7800	7700	7600
Modulus of elasticity MPa	210 000	180 000	140 000
Coefficient of thermal expansion per °C from 20°C	-	12.6 x 10 <sup>-6</sup>	13.2 x 10 <sup>-6</sup>
Thermal conductivity W/m °C	25	29	30

Source: ASSAB (2008)

The blank materials used in hot press forming process was 22MnB5 steel with 1.8 mm thickness. The hardness of as-received 22MnB5 steel is 202.5 HV<sub>0.1</sub>. Samples were cut using a sheet metal cutting machine into 150 X 70 X 1.8 mm dimension. The properties of 22MnB5 steel used are from energy dispersive X-ray spectroscopy (EDXs) analysis as shown in Table 3.3.

Table 3.3 Chemical composition of 22MnB5

Material	Elements (wt%)									
	C	Mn	Si	Ni	Cr	S	P	Al	Ti	B
22MnB5	0.23	1.18	0.22	0.12	0.16	0.001	0.015	0.03	0.04	0.003

### 3.4 Development of Hot Press Forming Die

HPF dies were designed using NX10 PLM (Product Lifecycle Management) software. The dies consist of three parts, namely die holder, insert holder with cooling channel and die insert with thermocouple hole as shown in Figure 3.2. Thermocouple holes of 3 mm diameter and 45 mm depth were machined at the lower die inserts. Figure 3.3 and 3.4 show the die insert holder size of 140 x 70 x 38 mm while the die inserts size is 70 x 33 x 8 mm is shown in Figure 3.5.

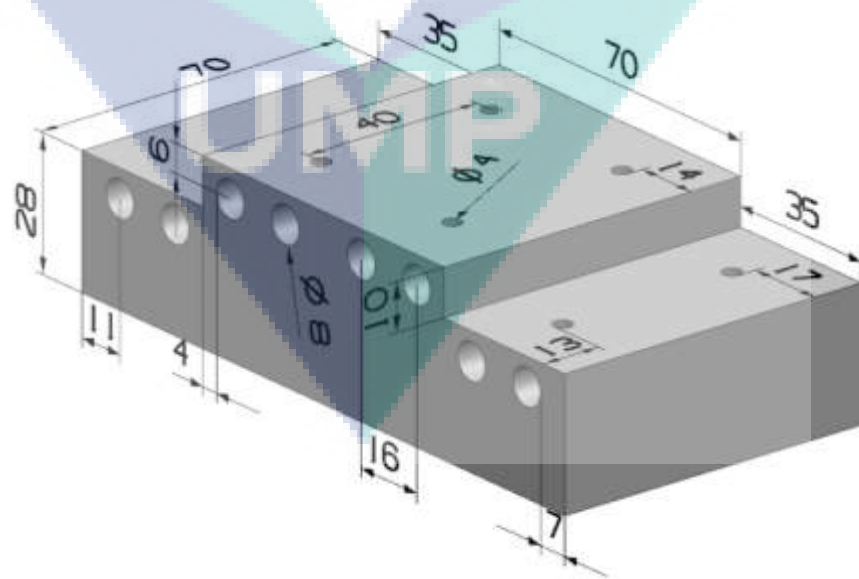
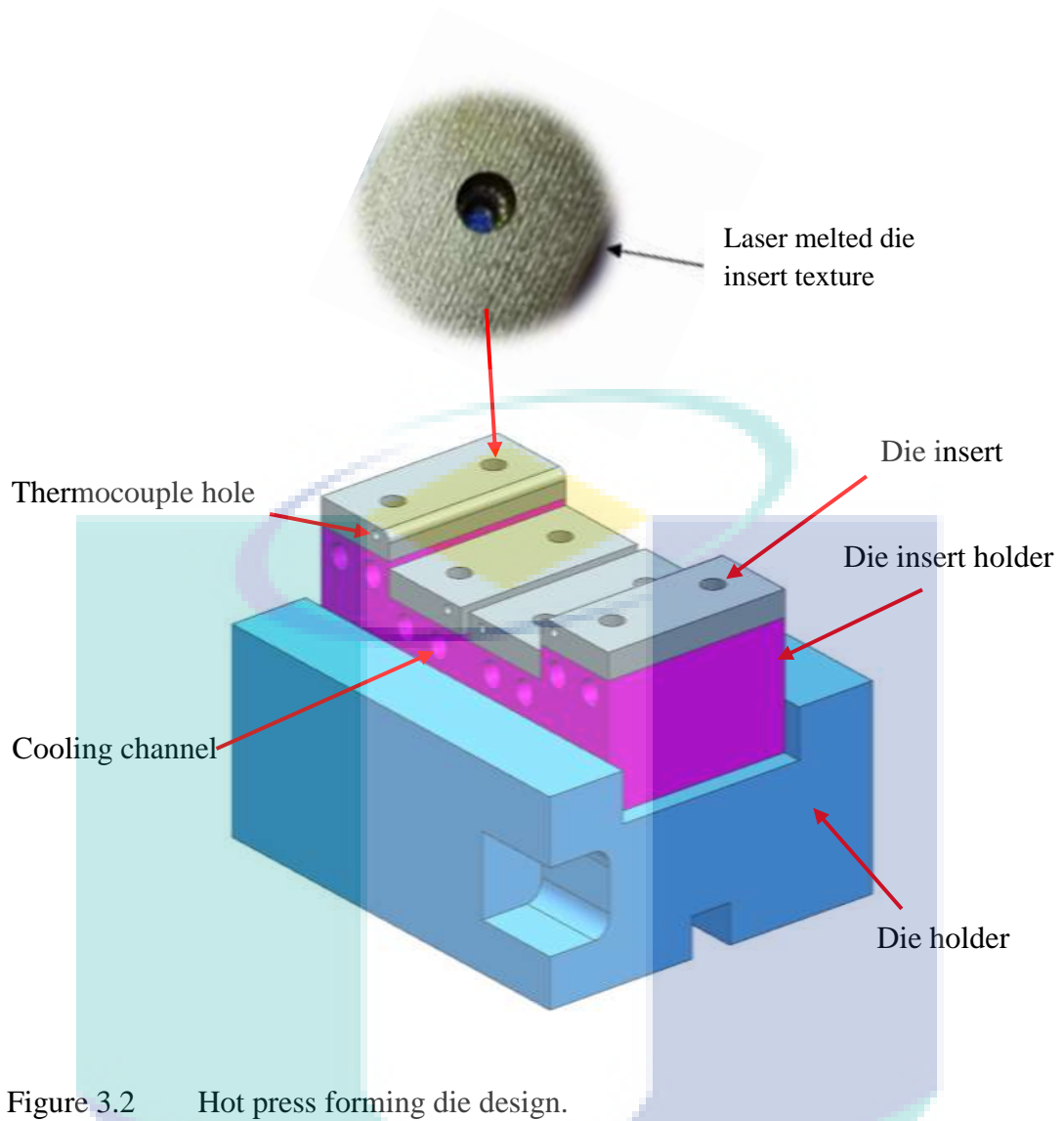


Figure 3.3 Upper die insert holder with dimension



Cooling channel position is very important in designing hot press forming die. Referring to the industrial practice, the diameter range of cooling channel was between 8 and 12 mm; pitch distance was 10 mm while the distance to loading surface was between 10 and 15 mm (Zamri and Yusoff 2015). Referring to previous result (Zamri and Yusoff 2015), to produce better performance of quenching processes during HPF process, the diameter of the cooling channel (a) was 8 mm, the pitch between cooling channels (b) was 8 mm and the distance between cooling channels to loading surface (c) was 10 mm, as shown in Figure 3.6.

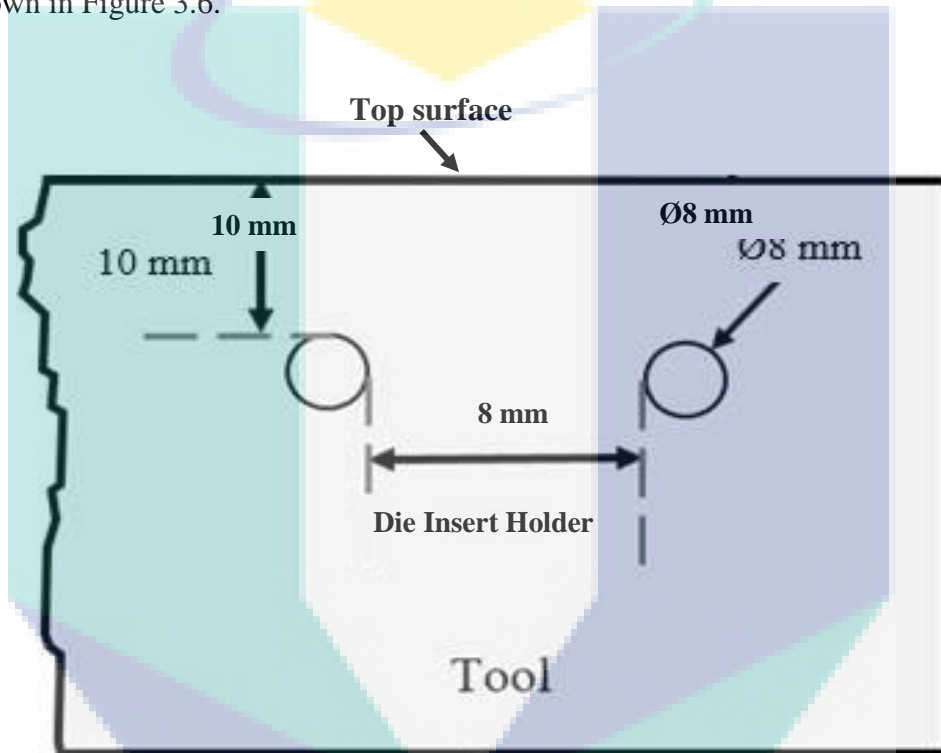


Figure 3.6 Cooling channel design in die insert holder  
Source: Zamri and Yusoff (2015)

Die fabrication was conducted using CNC machining for precision. The ASSAB 8407 steel block was cut using wire cut and using CNC milling into 140 x 70 x 38 mm for die insert holders as shown in Figure 3.7 and while die fitting to its holder is shown in Figure 3.8. Figure 3.9 shows die inserts after machining into 70 x 33 x 8 mm. Screw hole of laser modified die insert was drilled using die sinking process due to its high hardness properties.



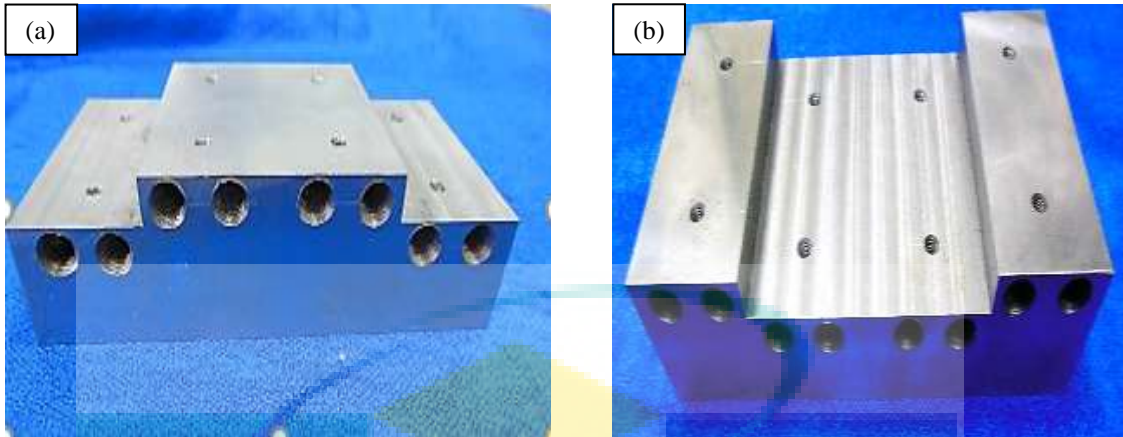


Figure 3.7 As-machined geometry of (a) upper and (b) lower die

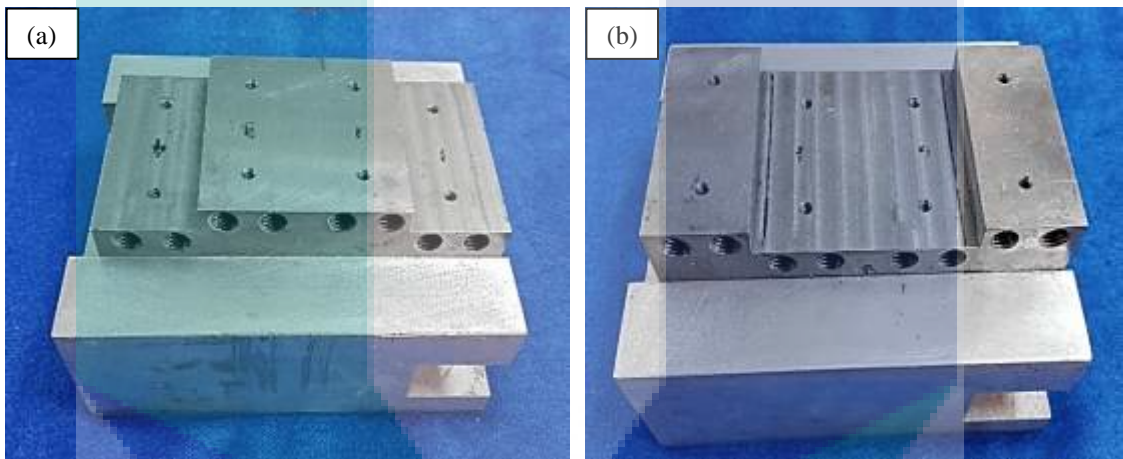


Figure 3.8 Assembly of (a) upper die with holder and (d) lower die with holder



Figure 3.9 Die inserts after machining into 70 x 33 x 8 mm



### 3.5 Laser Surface Melting

Laser surface melting process was conducted using JK300HPS Nd:YAG twin lamp laser source with 1064 nm wavelength with pulsed mode on AISI H13 surface. Laser processing setup is shown by a schematic diagram in Figure 3.10. The sample surface was prepared with methanol before laser processing to avoid contaminations and ensure its cleanliness. Argon gas at 30 kPa pressure was used to protect sample surface from oxidation during laser melting. The Nikon Tool Maker Microscope (MM400/800) was used to observe the laser spot size. Five laser spots without any overlapping were measured before starting the laser melting process to determine the exact spot size. Results from microscope observation show the average spot size was 0.7 mm. Then the laser beam was focused to 0.7 mm spot size onto the sample surface with an average power of 100 W. The laser head was consistently in a vertical position of 90° and was moved linearly in the x-y direction during the melting process of the sample surface.

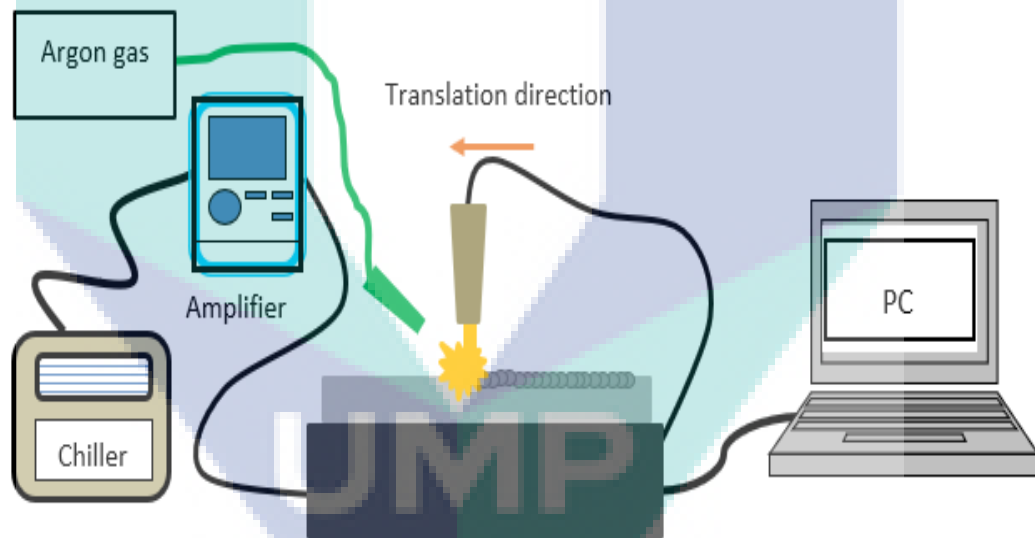


Figure 3.10 Schematic diagram of laser surface melting process setup

Table 3.4 shows the parameters setting used to process the samples. The parameters were opted with try and error method. The controlled parameters are peak power ( $P_p$ ), pulse repetition frequency (PRF) and spot overlap percentage ( $\eta$ ). Constant Average Power at 100 W used for laser melting process. Laser peak power in pulsed laser processing is more important than the average power (Mahmoudi, Torkamany et al. 2010). Varying peak power and PRF at a constant average power altered the surface

properties. The peak power at range of 1700 to 2500 W and PRF range of 50 to 70 Hz. While overlapping rate range of 30 to 70%. The calculated laser melting parameters from the settings were irradiance (I), residence time (T<sub>R</sub>), pulse width (τ), processing speed (v) and pulse energy (E<sub>p</sub>) as shown in Table 3.5.

Table 3.4 Parameter setting for laser melting process.

Parameter	Setting value
Average Power (W)	100 (constant)
Peak Power (W)	1700 – 2500
Pulsed Repetition Frequency, PRF (Hz)	50 – 70
Overlapping Percentage (%)	30 – 70

Laser spots pattern after laser melting process depends on spot overlapping percentage as shown in Table 3.6. The laser spot overlapped,  $L_o$ , can be calculated from Equation 3.1. Where  $L$  is the spot radius plus scanning speed,  $\eta$  is overlapping percentage and  $L_o$  is overlapped distance between two  $L$ .

$$L_o = \left[ 1 - \left( \frac{\eta}{100} \right) \right] \times L \text{ mm} \quad 3.1$$

the processing speed,  $v$ , can be calculated from equation 3.2. Where  $L$  is the length of sample (mm),  $d$  is the diameter of spot size (mm),  $\eta$  is the spot overlap (%) and  $T$  is the pulse period (s).

$$v = \frac{L}{\left( \frac{L}{d} \right) / (\eta)} \times T \text{ mm/s} \quad 3.2$$

the condition of die inserts after laser melting with various laser parameter as shown in Figure 3.11. Figure 3.11 (a) to (c) shows die inserts with laser surface melting at 70, 50 and 30 percent overlapping rate. It took between 4.9 to 16.1 minutes to finish melting process on die insert with 30 to 70% overlapping rate as shown in Figure 3.2.

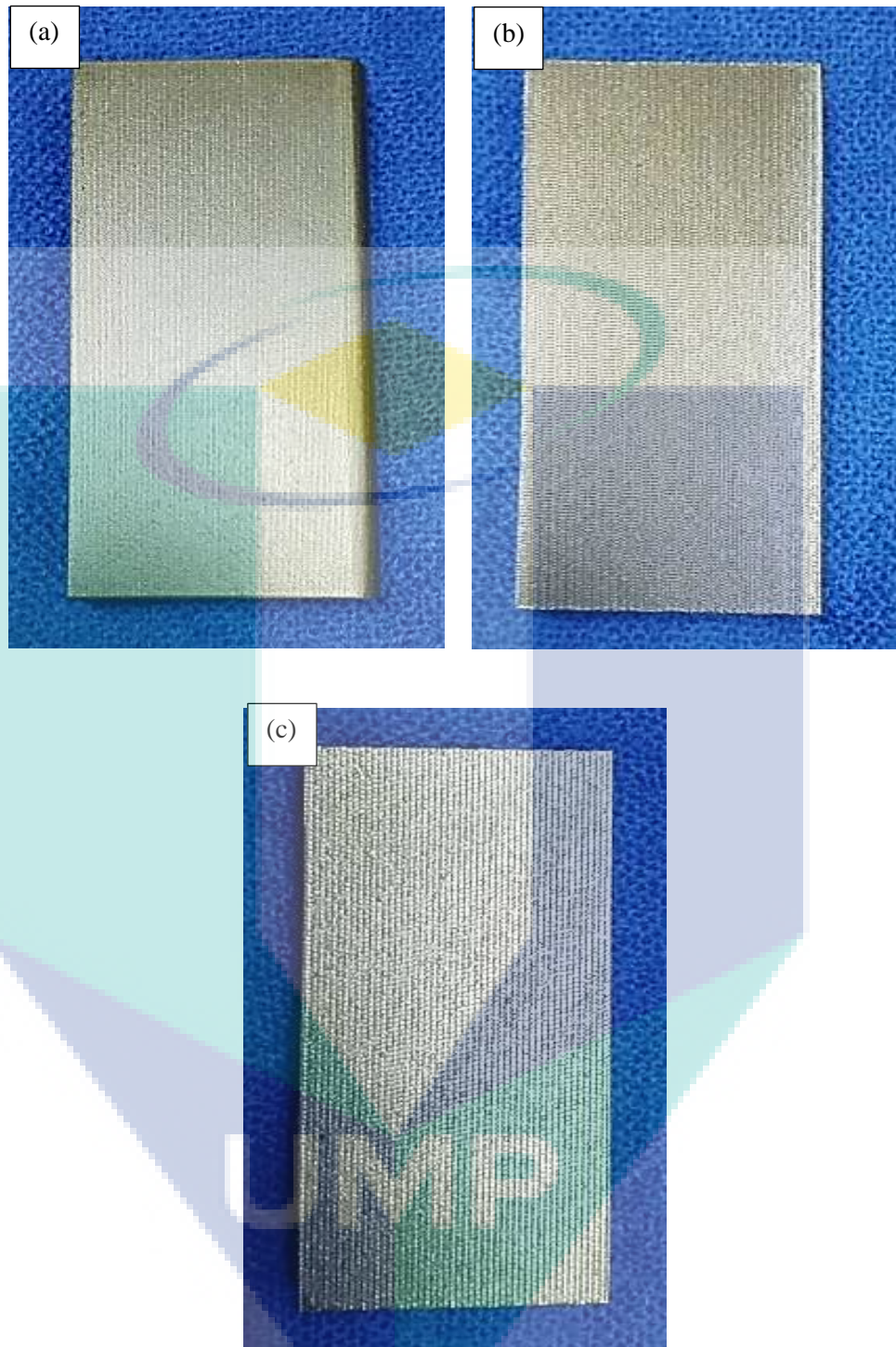
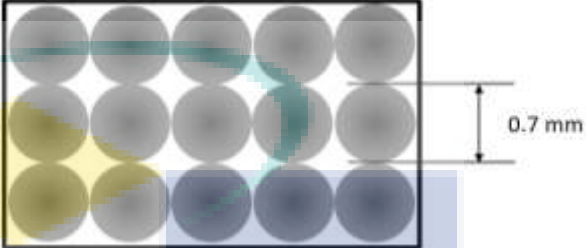
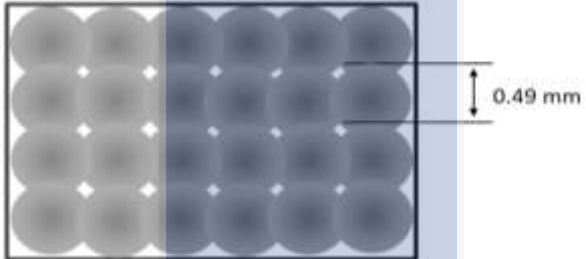
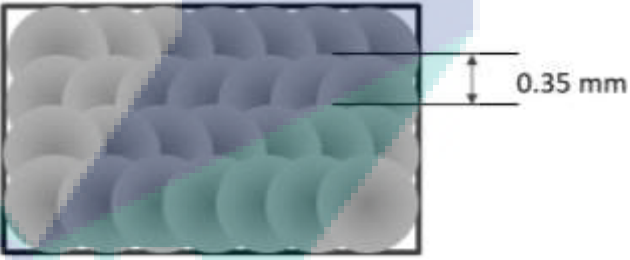
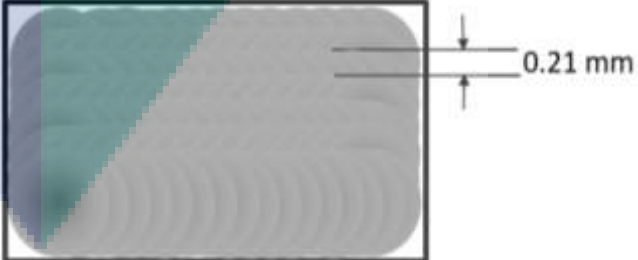


Figure 3.11 Die insert condition after laser melting at (a) 70%, (b) 50% and (c) 30% overlapping rate.

Table 3.5 Parameter for laser surface melting of AISI H13 steel

Sample	Set Parameters					Outcome Parameters			
	Average Power, $P_A$ (W)	Peak Power $P_P$ (W)	Pulse Repetition Frequency PRF (Hz)	Spot overlap, $\eta$ (%)	Processing Speed, $V$ (mm/min)	Pulse Energy, $E$ (J)	Pulsed Width $\tau$ (ms)	Residence Time, TR (s)	Irradiance $I$ (W/mm <sup>2</sup> )
1	100	2100	50	30	1470	2.00	1.0	0.023	1145767.03
2		2500	60	30	1764	1.67	0.7	0.016	1636810.04
11		1700	60	30	1764	1.67	1.0	0.023	1113030.83
10		2100	70	30	2058	1.43	0.7	0.016	1604073.84
8		2500	50	50	1050	2.00	0.8	0.027	974291.69
5		1700	50	50	1050	2.00	1.2	0.039	662518.35
3		2500	70	50	1470	1.43	0.6	0.019	1364008.37
13		1700	70	50	1470	1.43	0.8	0.028	927525.69
6		2100	60	50	1260	1.67	0.8	0.026	982086.02
7		2100	60	50	1260	1.67	0.8	0.026	982086.02
15		2100	60	50	1260	1.67	0.8	0.026	982086.02
16		2100	60	50	1260	1.67	0.8	0.026	982086.02
17		2100	60	50	1260	1.67	0.8	0.026	982086.02
14		2100	50	70	630	2.00	1.0	0.053	491043.01
12		2500	60	70	756	1.67	0.7	0.037	701490.02
4		1700	60	70	756	1.67	1.0	0.054	477013.21
9		2100	70	70	882	1.43	0.7	0.038	687460.22

Table 3.6 Laser spot patterns at different overlap percentages.

Overlapping percentage (%)	Overlapping pattern
0 (without overlap)	
30	
50	
70	

### 3.6 Design of Experiment (DOE) for AISI H13 Tool Steel Sample and Optimisation

A preliminary study was conducted to determine the lower and upper range of peak power, spot overlap and PRF prior to DOE development. Laser surface melting process was designed using Box-Behnken design with three factors. The design produced 17 experiments with 13 different parameter settings and five repetitions as shown in Table 3.7. The laser process was conducted at a constant average power of 100 W, spot overlap of 30 to 50% and PRF of 50 to 70 Hz respectively. The responses were sub-surface hardness, melt depth and surface roughness which were analysed using response surface methodology (RSM). The RSM analysis was to select optimised parameters for laser melting of ASSAB 8407 (AISI H13) steel surface.

Table 3.7 Laser melting parameter produce by Design of Experiment (DOE)

Std	Run	Factor 1	Factor 2	Factor 3
		A:Peak Power watt	B:PRF Hz	C:Overlap %
12	1	2500	60	70
6	2	2100	60	50
1	3	2100	50	30
3	4	2500	70	50
13	5	1700	70	50
7	6	2100	60	50
2	7	2500	60	30
14	8	2100	50	70
5	9	1700	50	50
9	10	2100	70	70
11	11	1700	60	30
16	12	2100	60	50
4	13	1700	60	70
17	14	2100	60	50
8	15	2500	50	50
15	16	2100	60	50
10	17	2100	70	30



Set of laser processing parameter were generated using Design Expert Software. The experimental data were analysed using response surface method (RSM) with Box-Behnken technique to analysed surface response on the melted surface. DOE analysis shows the effect of peak power, pulse repetition frequency (PRF) and overlapping percentage on hardness properties, surface roughness and melted depth. The five centre point was meant for obtaining a precise model and investigate random error of the model.

### 3.6.1 DOE Optimisation

DOE optimisation was conducted to obtain significant model using regression analysis. The model reduction using stepwise regression performed to get fit model with eliminates automatically insignificant term. The analysis variance (ANOVA) and optimisation were performed for hardness, roughness and melted depth response. The optimisation processes start with set desired goal of model factor and response. The goal for response were set to maximum for hardness, in range for roughness and minimize for melted depth as shown in Figure 3.12. The lower and upper limit of factor and response was set and result for optimisation solution and desirability graph were displayed.

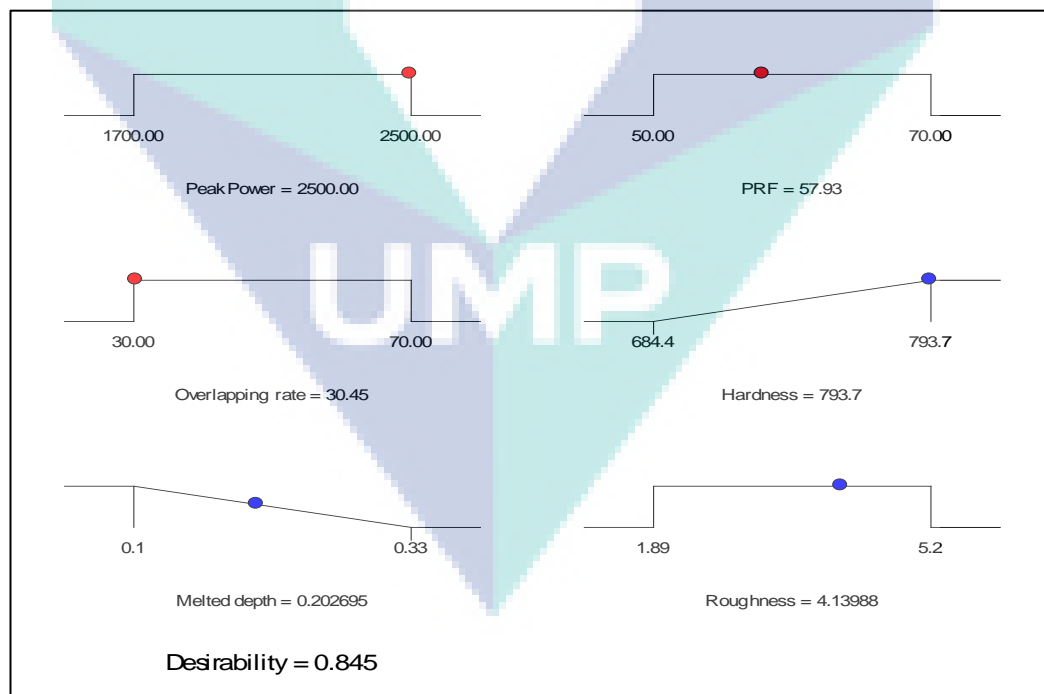


Figure 3.12 Optimisation of parameter setting

## **3.7 Characterization of Laser Modification Surface**

### **3.7.1 Sample Preparation**

Samples were cut using wire cut and cleaned using methanol. Samples were then mounting using BUEHLER SimpliMet 1000 Automatic Mounting Press machine. Sample were ground sequentially using SiC abrasive papers of 150, 320, 400, 600, 800 and 1200 grit. Ground samples were polished using red felt and imperial polishing cloths with 6 and 1  $\mu\text{m}$  size diamond paste. Polished samples were etched with 2% nital for three seconds to reveal the grain structure.

### **3.7.2 Surface Roughness Measurement**

Surface roughness of the melted surface was analysed using 7061 MarSurf PS1 Roughness Tester. The analysis to observed effect of various laser melting parameter on surface roughness ( $R_a$ ). Surface roughness is an important factor to make sure the laser melted surface is suitable to be used without secondary processes and to confirm the melted surface was uniform. The distance measured for surface roughness ( $R_a$ ) was 8 mm with 2 $\mu\text{m}$  stylus tip and 0.7 mN measuring force.

### **3.7.3 Surface Morphology Analysis**

Morphology of laser melted surface samples was observed using MM-320 Mahr Optical Microscope with QUARDA-CHECK-300 software. A 25x magnification was used to observe the overlapping pattern on the melted surface. The overlapping pattern was analysed using ImageJ software to measure the length between each laser spots at different overlapping percentages.

### **3.7.4 Microhardness Test**

Hardness properties of the as-received and melted surface of AISI H13 samples before and after HPF processed were characterised by Wilson hardness tester with Vickers diamond indenter and 100 kN load. The subsurface hardness was measured on the cross-sectional area of the samples. Each indentation was 20  $\mu\text{m}$  distance from sample surface and edge of each indentation mark to avoid distortion due to deformation of the sample surface after hardness test. The samples of 22MnB5 before and after HPF



processed were characterized for surface hardness properties to show the effect of various die insert surfaces on 22MnB5 properties before and after hot press forming process.

### **3.7.5 X-ray diffraction (XRD) analysis**

Phase analysis was carried out using Rigaku Miniflex X-ray diffractometer. The diffraction patterns were scanned from 3 to 90 degrees two-theta scanning range. Phase identification of melted die surface indicated the effect of heating and cooling during laser melting process on the phase transformation and changes of peak intensity. The dimension of samples for XRD analysis was 12 x 12 x 3 mm.

### **3.7.6 Metallographic study**

Metallographic study of as-received and laser melted surface samples was conducted using Hitachi TM3030Plus scanning electron microscope (SEM). Samples were observed using back-scattered detector (BSD) at high vacuum setting with magnification range of 1500-6000x. The effect of thermal and pressure during HPF process on grain size and melted layer depth were analysed from different die insert samples.

### **3.7.7 Chemical Composition and Element Mapping**

Chemical composition and element mapping on melted die surface were analysed using with Hitachi TM3030Plus energy dispersive x-ray spectrometer (EDXS) detector integrated with SEM. Chemical composition was analysed using point and line spectrum across the melted zone, heat affected zone and substrate layer. Element mapping was also conducted to determine the element distribution the in melted layer.

## **3.8 Hot Press Forming Process**

Hot press forming process to form 22MnB5 steel blank with 70X140X1.8 mm was conducted using 60-tonne hydraulic press machines. The hot press forming process of 22MnB5 blank include heating, transferring, pressing and cooling. The hot press forming processes start with heating up 22MnB5 blank at 950°C for 5 minutes and quickly transfer the blank to the hydraulic press machine. The heated blank was pressed and quenched simultaneously for 8 seconds with 5°C water flow in the cooling channel. The flow rate of cooling water was controlled using water pump system at 45 ℓ/min. Figure

3.13 shows the schematic diagram of hot press forming process experimental setup, and Figure 3.14 shows the actual setup for hot press forming processes. The parameters used for hot press forming processes are shown in Table 3.8. The HPF parameter in Table 3.8 was predicted using preliminary study (the try and error method) based on past results of HPF study (Aziz and Aqida 2013). The forming process for each die insert surface was conducted on 40 samples of 22MnB5 steel. Temperature distribution within die insert surface during hot press forming cycle was measured using four type-K thermocouples with four different melted dies surface. The thermocouples were placed at 1 mm depth from surface of the lower die insert and attached with data logger recording. Changes of temperature in the die inserts were recorded throughout 40 cycles of hot press forming process via data logger. The data logger read data from four thermocouples simultaneously. After 40 cycle HPF processed finished, the thermal distribution data from data logger will transfer to Microsoft Excel to evaluate all the data.

Table 3.8 Hot Press Forming Processing Parameter

<b>Hot Press Forming Parameter</b>	
Cooling Temperature (°C)	5
Cooling water flow rate (liters/minutes)	45
Quenching time (second)	8
22MnB5 heating temperature (°C)	950
Cooling medium	Water
Distance between upper and lower die (mm)	20
Press Machine Pressure (Bar)	60

Source: Aziz and Aqida (2013)

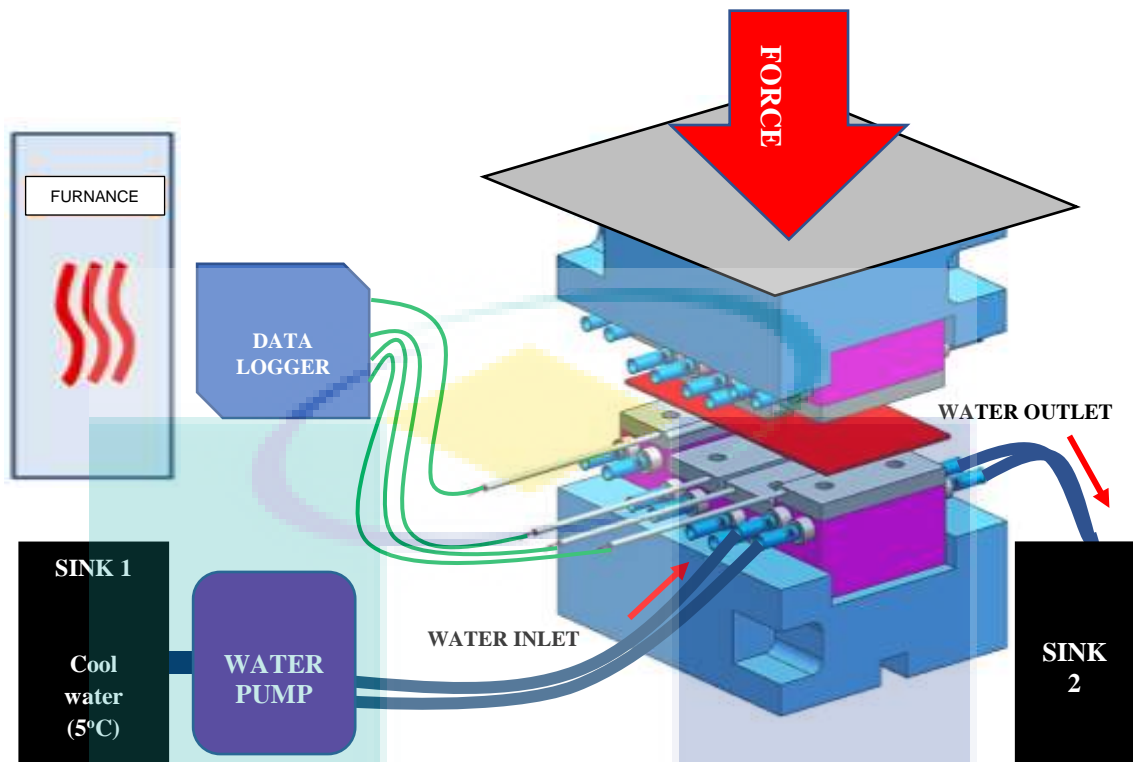


Figure 3.13 Schematic diagram of hot press forming process setup



Figure 3.14 Hot press forming processes setup

The 22MnB5 sample after HPF process is shown in Figure 3.15. After HPF was done on 22MnB5, the 22MnB5 blanks sample were characterized for metallographic,

hardness and martensite distribution after hot press forming process. Hot press formed samples were ground using abrasive paper with 1200 grit size and were polished using imperial cloth with 1  $\mu\text{m}$  diamond paste before image analysis. Phase transformation was analysed using ImageJ software using threshold menu.

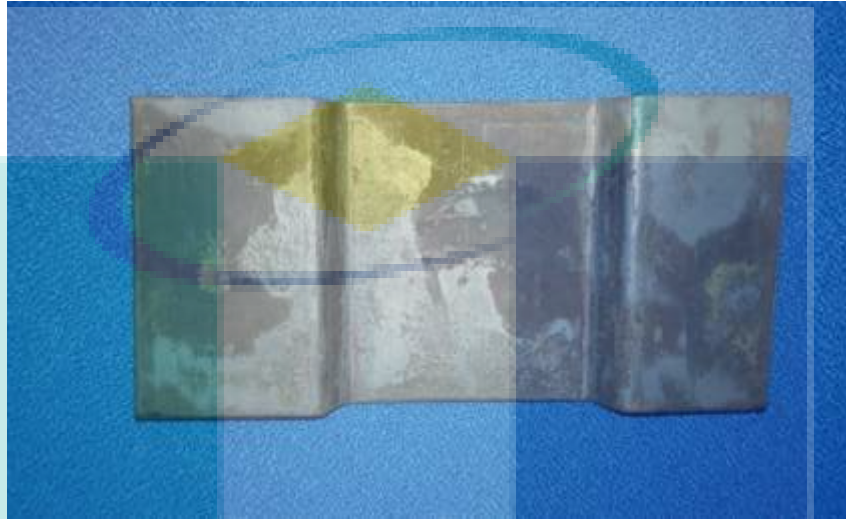


Figure 3.15 Hot press formed of 22MnB5 sample

### 3.9 Image Analysis

Images of grain boundary from scanning electron microscope (SEM) with back-scattered detector and martensite image of 22MnB5 from Wilson hardness tester was analysed using ImageJ software. The images of AISI H13 and 22MnB5 were analysed for average grain size and martensite phase percentage. The “image threshold” and “analyse particle” in pop up menu of ImageJ software used to measure the grain size and percentage of martensite. Analysis of grain and martensite started with scale setting based on the scale of micrograph of known distance. Then, by using the image threshold menu, to the background subtraction was set. The image was contrast using red colour as grain or martensite with black background. The result of average grain size and martensite percentage was indicated by red colour highlight on the image.

ImageJ software is capable of reading many image formats such as GIF, JPEG, TIFF, GIF and PNG. It can also edit, process and analyse micrographs and images (Udalagama, Chen et al. 2013). Most technique of image analysis, filtering and manipulation can be implemented in this software (Domínguez-García and Rubio 2009). Image analysis using ImageJ software performed faster analysis and reliable with

consistent and unbiased results (Grishagin 2015, Lozano-Gerona and García-Otín 2018). ImageJ software was developed at the National Institutes of Health (NIH) and used since 1997.

### 3.10 Thermal Analysis

Thermal analysis of die inserts during hot press forming was analysed using data from thermocouple reader. The thermocouple was attached 1 mm inside die insert surface during HPF processes. Four thermocouples attached at four different dies insert as shown in Figure 3.16. The thermocouple only attached at lower die insert. Thermocouple attached with data logger inside die insert surface for 40 cycle heating and cooling during forming blank of 22MnB5 steel. After 40 cycle HPF process, data from thermocouple reader (data logger) transfer to Microsoft Excel to analysis temperature distribution of die insert. The effect of heating and cooling during HPF process on as-received and melted die insert was characterised.

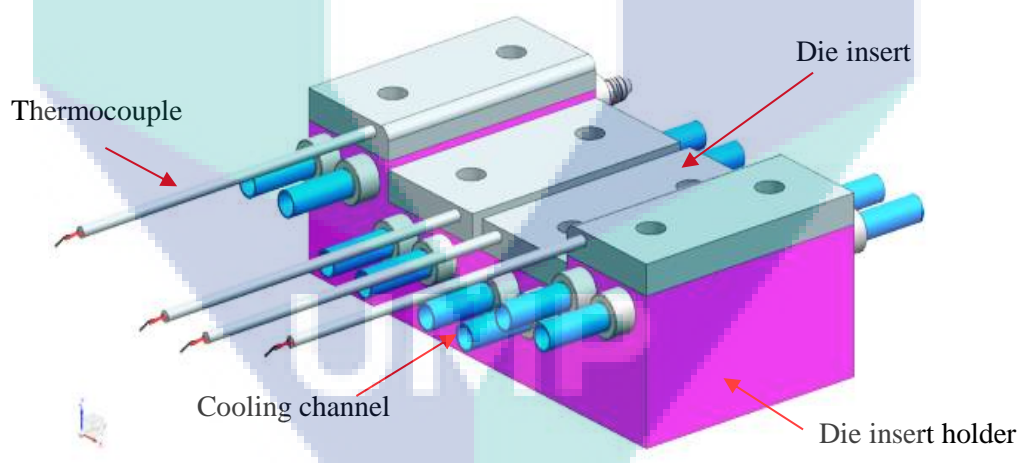


Figure 3.16 Thermocouple attach at lower die insert

## CHAPTER 4

### RESULTS AND DISCUSSION

#### 4.1 Introduction

In this topic, the effect of laser parameter on melted surface and effect of various melted surface on 22MnB5 steel blank properties during HPF process is presented. Initial characterisation is on the as-received AISI H13 steel properties. The laser surface melting statistical models are then presented sequentially based on DOE. From the DOE, the effect of laser parameters on the melted depth, hardness and surface roughness properties are presented. The overlapped geometry results from DOE with different pulsed repetition frequency (PRF), peak power and overlapping percentage settings are shown. Besides that, the effects of overlapping rate on the melted surface properties on morphology, melted depth, hardness, chemical composition, roughness and phase analysis are discussed. The properties of melted die are presented with effect of melted die on 22MnB5 blank surface after HPF processed. Finally, there are results on thermal distribution within die insert surface during hot press forming process.

#### 4.2 Surface Morphology

Various overlapping rates in the laser melting of AISI H13 tool steel yielded different morphologies of overlapping laser spots on the melted surface. Figure 4.1 shows overlapping laser spots on the melted surface of H13 sample at the overlapping rates of 30%, 50%, and 70%. The lowest overlapping rate of 30% produced higher processing speed of between 1470 mm/min and 2058 mm/min compared to the processing speed of the highest overlapping rate of 70%, which ranged between 756 mm/min and 882 mm/min. Meanwhile, the overlapping rate of 50% yielded processing speed of between 1050 mm/min and 1470 mm/min. In other words, lower overlapping rate results in higher



processing speed, but overlapping laser spot increases with increasing peak power. Thus, different overlapping laser spots pattern can be controlled by different overlapping rate, pulse energy, peak power, and processing speed.

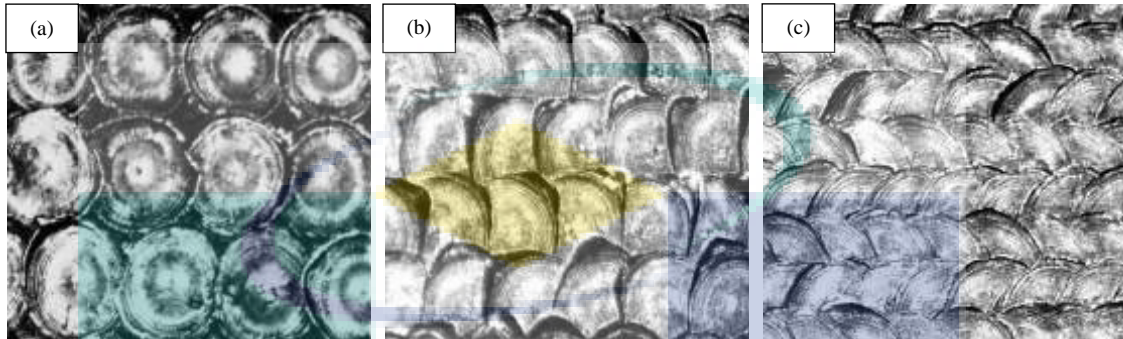


Figure 4.1 Overlapping laser spots of melting sample processed with different overlapping percentage of (a) 30%, (b) 50% and, (c) 70% overlapping rate

Referring to Figure 4.1 (a), overlapping laser spot of 30% less due to the high processing speed, which was attributed to the shorter interaction time between the laser beam and sample surface. Besides that, Figure 4.1 (c) demonstrates the production of more overlapping laser spots on the sample surface during the laser processing, which was contributed by the outcome of high overlapping rate, specifically low processing speed. The observed peak power was also found to contribute significant effect on the overlapping laser spots pattern, where high peak power increased the amount of energy absorbed on the sample surface and subsequently produced deeper molten pool. On the other hand, lower pulsed energy produced lower surface temperature, which improved surface topography. In short, shorter interaction time with high irradiance is required to avoid overheating, burn mark, and spark on the sample surface. Argon gas used to protect the surface from burn mark and spark.

Laser melting processed on die surface produce various laser spot pattern due to overlapping percentage of each melted pool. In this study 30, 50 and 70% overlapping rate with various peak power and PRF used to melt die surface. overlapping laser spot increased with increasing peak power. Different overlapping laser spots pattern control with different overlapping rate, pulse energy, peak power and processing speed. Highest processing speed due to less overlapping rate. Surface morphology depend on overlapping rate, where less overlapping rate produce fast processing speed. The findings

in this study show that 70% overlapping rate produce smooth surface compare 30 and 50% overlapping rate. Result from past study shown, the surface pattern required in HPF processes to decreased effect metal to metal contact (Shihomatsu, Button et al. 2016) during forming process.

### 4.3 Metallographic Study

#### 4.3.1 As-received AISI H13 Steel

Figure 4.2 presents the microstructure of as-received H13 before laser melting using back-scattered scanning electron micrograph at 15000x magnification. In particular, Figure 4.2 (a) depicts the as-received H13 steel with ferrite background as well as the presence of carbide phase distribution. The micrograph shows large grain size with thin grain boundary in the as-received H13 sample. The threshold analysis of as-received H13 using ImageJ yielded 10.7% of grain boundary phase, as shown in Figure 4.2 (b). The hardness properties of as-received H13 recorded 228.1 HV<sub>0.1</sub> before the laser melted analysis using Vickers hardness tester.

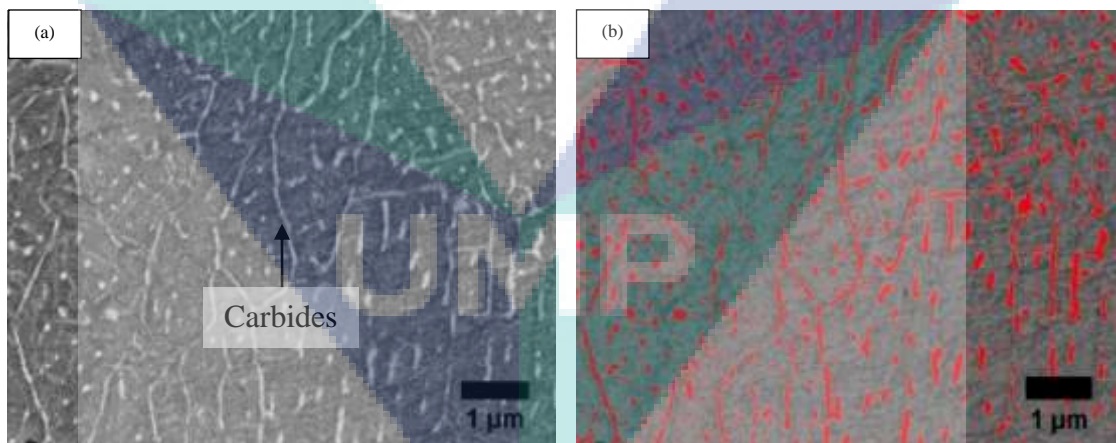


Figure 4.2 (a) Micrograph of as-received H13 steel before laser melting at 15000× magnification and (b) threshold analysis of grain boundary percentage.



## 4.3.2 Laser Melted AISI H13 Surface

### 4.3.2.1 Melted Depth

In this study, the laser parameters, such as pulse repetition frequency (PRF), peak power, overlapping rate, and average power, in laser melting demonstrated varied pulse energy, residence time, and irradiance, which yielded different properties of melted surface. Various overlapping rates in the laser melting of AISI H13 tool steel showed different melt pool of melted surface. The Molten pool and melted depth study were conducted on cross section of the melted surface. Melted surface was cut using EDM Wire Cut and observed using Nikon Tool Maker Microscope (MM400/800). Figure 4.3 shows micrographs of varying molten pool and melted depth at 30, 50 and 70% overlap with different pulse repetition frequency (PRF). In this study, the proposed optimum surface thickness was at 50% overlapping rate with 1050 and 1470 mm/min processing speed, where the range of thickness was 0.20 to 0.26 mm. the optimum surface thickness proposed at 50% overlapping due to optimum production time with better performance that reduce production cost.

Laser energy absorbed on the sample surface depend on peak power and PRF. High peak power produced higher irradiance, while increase the absorption rate will necessitate increase of laser power or irradiance. The irradiance for sample process at 30% overlapping rate range between 1113030.83 to 1636810.04 W/mm<sup>2</sup>. While for 50% overlapping rate, the irradiance range between 662518.35 to 16604073.84 W/mm<sup>2</sup>. The 70% overlapping rate produce lower irradiance between 477013.21 to 701490.02 W/mm<sup>2</sup> due to effect of higher overlapping rate. Low PRF at 50 Hz produce high energy of 2 Joule. While, high PRF at 70 Hz produce energy of 1.43 Joule. The variations of overlap percentage and PRF in laser surface melting process affect the melted layer geometry and thickness. Laser power affects the formation of melted layer width and depth on the substrate. The melted layer depth increased with increasing laser irradiance. High energy and low processing speed cause a large amount of energy absorbed on the sample surface during the laser process, which explains the effect on the melt depth of melted pool. Higher surface temperature which resulted from a higher irradiance promoted energy penetration and efficient surface melting which improved the surface absorptance.

Figure 4.3 depicts the resultant outcomes in terms of different melting thickness of the melted surface. Accordingly, the overlapping rate of 30% produced molten layer thickness of between 0.1 mm and 0.24 mm as shown in Figure 4.3 (a) – (c). Meanwhile, the overlapping rate of 50% produced molten layer thickness of between 0.16 mm and 0.25 mm as shown in Figure 4.3 (d) – (f). As for the highest overlapping rate of 70%, the molten layer thickness was the highest, which ranged from 0.21 mm to 0.33 mm shown in Figure 4.3 (g) - (i). The depth of molten layer decreased with increased PRF from 50 Hz to 70 Hz. The sample with the highest overlapping rate of 70% and PRF of 50 Hz was processed at a higher energy of 2 J, which produced a melted zone (MZ) depth of 0.33 mm due to the higher energy penetration into the sample surface (Aqida, Naher et al. 2011). Meanwhile, higher PRF of 70 Hz reduced laser energy to 1.43 J, reducing the MZ depth of the melted pool (0.1 mm) since lower laser penetration reduced the absorption of laser energy into the sample surface (Shin and Yoo 2008).

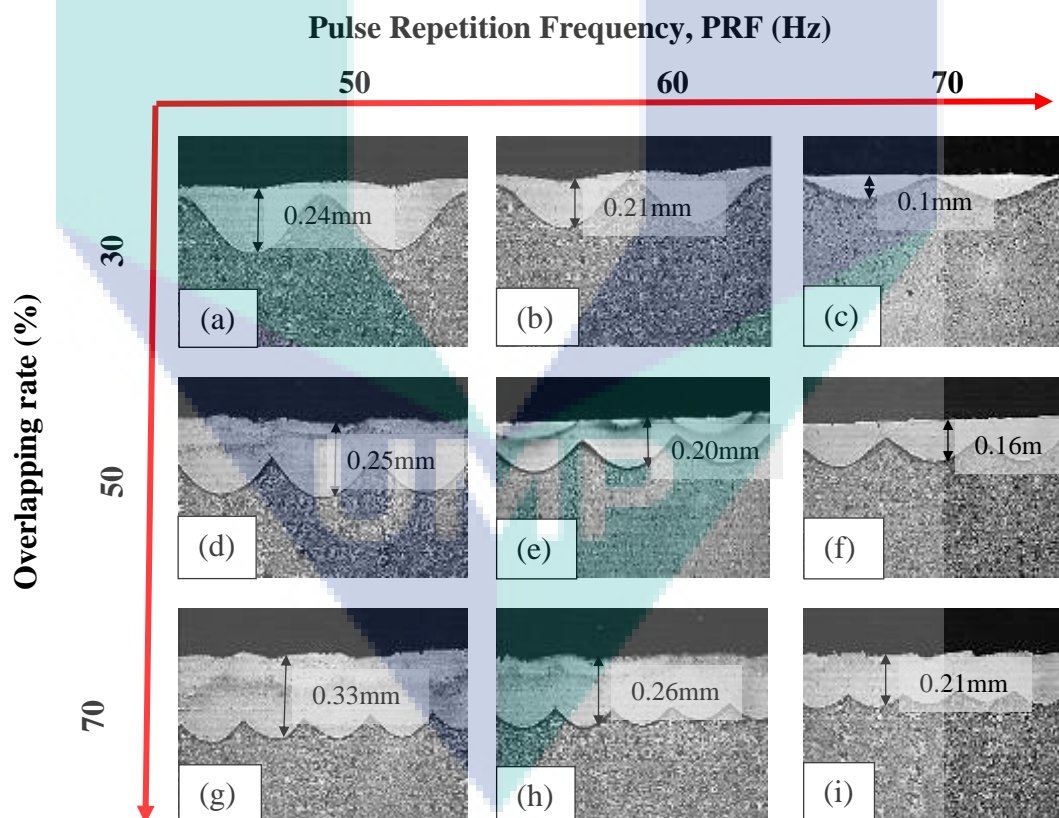


Figure 4.3 Micrographs of varying molten pool and melted depth at 30, 50 and 70% overlap with different pulse repetition frequency.

In this study, a higher depth range was measured at lower power setting and higher duty cycle given the longer pulse widths, considering that pulse width depends on the duty cycle. Longer pulse width was found to promote surface melting, while the addition of particles contributed an insignificant effect on layer thickness formation. The processing speed of the overlapping rate of 30% ranged from 1470 mm/min to 2058 mm/min; the processing speed of the overlapping rate of 50% ranged from 1050 mm/min to 1470 mm/min; the processing speed of the overlapping rate of 70% ranged from 756 mm/min to 882 mm/min. This study demonstrated the relationship between the overlapping rate and the laser processing speed. The overlapping rate of 70% produced more molten pool compared to the sample process at other overlapping rates, as shown in Figure 4.3 (a), (d) and (g). Furthermore, the laser interaction time at the overlapping rate of 70% was found longer than the other laser interaction times of other overlapping rates in this study.

On the other hand, high overlapping rate of 70% caused longer interaction time and rapid solidification in the melted pool. Longer interaction time between the sample surface and laser beam was attributed to the reduced processing speed, producing wider and deeper molten pools. Laser power affects the formation of melted layer width and depth on the substrate. The melted surface depth increased at lower pulse repetition frequency (PRF) of 50 Hz whereas higher peak power was due to the longer pulse width, considering that pulse width depends on the duty cycle. Longer pulse width allows more surface melting and increases the layer depth, while higher pulse energy produces higher penetration into the substrate surface. The distance between melted pools increased at the overlapping rate of 30%. Basically, increased pulse overlap increases the laser interaction time and subsequently, raises the laser energy absorption. As the laser energy penetrates deeper into the sample depth, the melted surface solidifies at lower cooling rate. Overlapping laser spots in the sample causes additional heating of the melted layer, which delays the solidification process.

#### 4.3.2.2 Grain Size and Structure

Laser melting produced a layer with metallurgical changes on H13 substrate due to the localised surface heating and rapid solidification of the micron-sized molten pool from the pulsed laser. The metallographic study of laser melting cross section, specifically the SEM micrographs at 6000x magnification for sample 10 (peak power of 2100 W, PRF of 70 Hz and 30% overlapping rate), is presented in Figure 4.4. Figure 4.4(a) shows the formation of three layers after laser processing, namely melted zone (MZ), heat affected zone (HAZ), and substrate. The grain structure varied according to different melted depths, which was due to the use of different operating temperatures. MZ experienced complete melting due to the absorption of homogenous laser beam energy by substrate layer at sufficient laser-surface interaction time (Kusinski, Kac et al. 2012).

The grain structure at MZ is revealed in Figure 4.4 (b), which revealed refined equiaxed grain structure in relative to the substrate material due to the localised rapid heating and cooling processes. The high temperature interaction between laser power and sample surface leads to localised heating, resulting in grain refinement in MZ. The MZ is deemed important in demonstrating the effect of laser melting process. Meanwhile, the undercooling process at molten pool, specifically the low temperature condition with high grain growth rate, produced equiaxed grain near the edge of substrate. Equiaxed grain structure was seen to be larger at the centre of melted pool when the cooling process was delayed, which was attributed to the latent heat at higher cooling rate (Beckermann 1997). In laser surface melting, rapid localised heating and cooling processes produce smaller grain size and initiate phase transformation (Wang, Zhou et al. 2012). Laser melted surface was reported in prior studies to exhibit enhanced surface properties of the substrate due to grain refinement, secondary carbides, and hard non-equilibrium microstructure formation (Aqida, Brabazon et al. 2011).



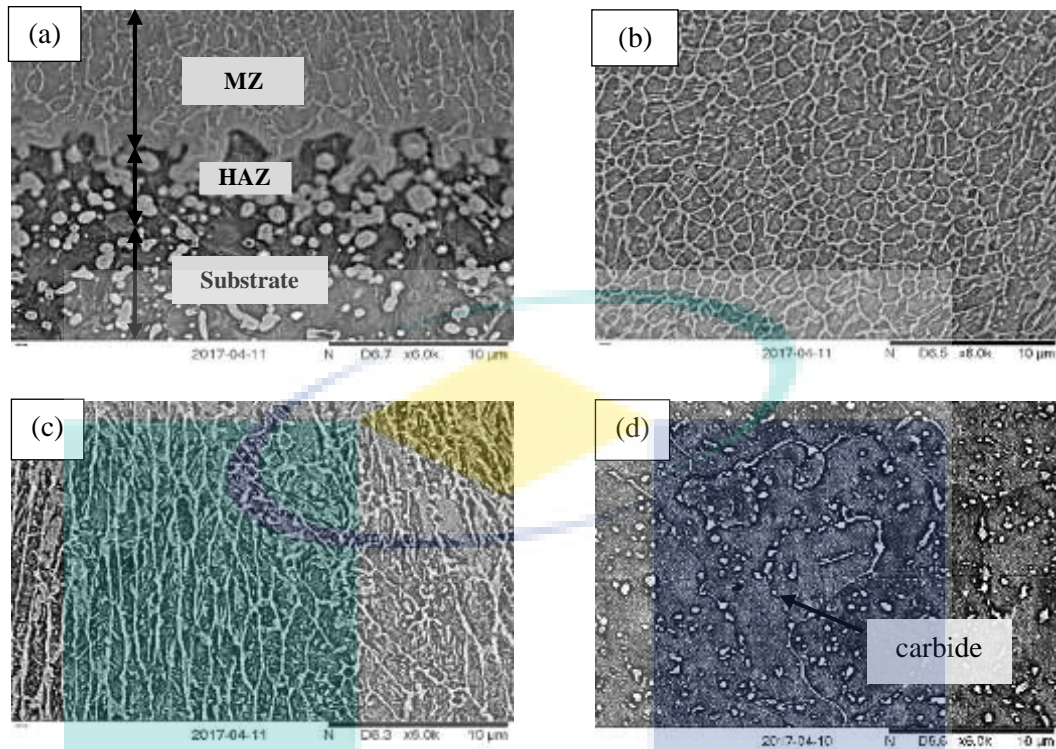


Figure 4.4 SEM micrographs of (a) laser melted AISI H13 tool steel cross section with presence of melted zone (MZ), heat affected zone (HAZ) and substrate material, (b) fine equiaxed grain structure in the MZ, (c) Columnar grain structure in the HAZ, and (d) large equiaxed grain structure at 6000x magnification for sample 10.

Figure 4.4 (c) depicts coarse grain structure in HAZ, which was attributed to lower temperature and different temperature heating in the molten pool depth. The different temperature heating in melted pool reduces hardness between 240.3 to 335.4 HV<sub>0.1</sub> in HAZ, as the latent heat delays solidification (Gao, Zhao et al. 2015). HAZ is basically a transition zone where the substrate is partially melted with altered chemical properties due to the high temperature heat (Aqida, Brabazon et al. 2013). The temperature between liquidus and solidus causes partial melting in HAZ, resulting in the formation of columnar grain structure (Kusiński, Kac et al. 2010). The reduced energy penetration leads to the increase of grain size as the energy travels deeper into the substrate and produces various energy distribution as it collides with high temperature carbides (Calcagnotto, Ponge et al. 2009). Thus, uneven melting occurs, resulting in inhomogeneous solidification (Montealegre, Castro et al. 2010).

Referring to Figure 4.4 (d), the distribution of carbides in the form of white particles can be observed in the substrate material. More overlapping laser spots delay the

solidification process on the surface of molten pool; thus, producing larger grain size at the top region of melted surface. The penetration of laser energy into the substrate was found to reduce the cooling rate and form HAZ between the substrate and cladding layer. The formation of three regions in clad layer was attributed to the beam interaction time and laser power. When the laser energy penetrates into the surface, the upper region solidification occurs sooner than the lower region in the presence of high purity particles. New melted phase can be developed by controlling the heating and solidification rates (SN, LH et al. 2014). When the heating hit, substrate melted by high irradiance laser beam. As the laser energy penetrates deeper, the melted surface solidifies at lower cooling rate. Thus, this explains why grain refinement appeared in MZ and varied according to the heating and cooling rates at different laser parameter settings in this study. The overlapping laser spots cause additional heating of the melted layer, which subsequently delays the solidification. Besides that, in laser surface melting, rapid localised heating and cooling processes produce smaller grain size and initiate phase transformation. Figure 4.5 presents the melted area observed for SEM micrographs of grain structure of the laser melted AISI H13 for sample 5. Sample 5 was processed at 1700 W peak power, 50 Hz PRF and overlapping rate of 50%.

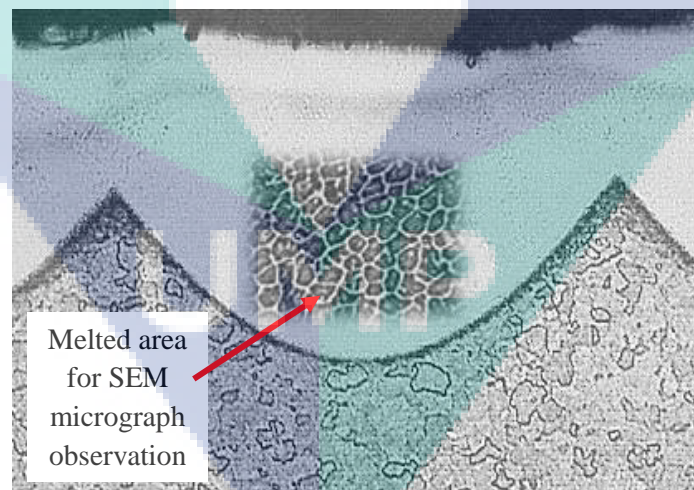


Figure 4.5 Area observed for SEM micrograph of grain structure evolution laser melted zone of AISI H13 at sample 5.

Meanwhile, Figure 4.6 presents the SEM micrographs of the evolved grain structure of melted die surface in MZ at various overlapping rate. Rapidly melted and solidified H13 die surface yielded smaller grain boundary size in the melted layer Figure

4.6. The grain boundary structure expanded with the increase of overlapping rates from 30 to 70%, as shown in Figure 4.6 (a) – (c). Referring to these figures, the grain boundary size decreased as the overlapping rate decreased. The grain boundary at the overlapping rate of 70% shown in Figure 4.6 (c) appeared coarser with less boundary, as the slow cooling process in melted pool raises the grain size. On the other hand, the grain size at the overlapping rate of 30% in Figure 4.6 (a) was smaller since lower overlapping rate produces faster cooling rate. During the laser processing, the sample surface melted and solidification occurred, resulting in the formation of new layer with new microstructure and grain refinement.

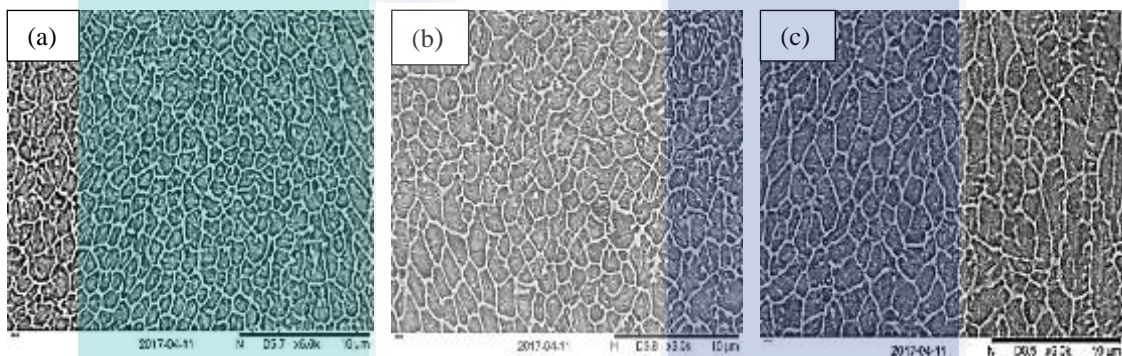


Figure 4.6 SEM Micrographs of grain structure evolution laser melted zone of AISI H13 samples which were processed at (a) 30%, (b) 50% and 70% overlapping rate at 15000x magnification.

The observed discontinuous grain boundary was attributed to latent heat that delays the solidification rate. Fundamentally, the solidification process that involves different laser processing parameters produces various grain boundary formation. Accordingly, the value of PRF and overlapping rate influence the evolution of grain boundary, where lower PRF produces higher laser energy and higher overlapping rate produces slower solidification process. The grain size decreases with the increase of solidification rate. In this study, laser melting processes produce molten liquid during laser melting process on as-received H13 die. The higher overlapping rate of 70% produced a slower processing speed of 630 mm/min with 491043.01 W/mm<sup>2</sup> irradiance, which caused delayed solidification due to more molten pool formation. As the laser energy penetrated deeper into the sample depth, the melted surface solidified at lower cooling rate. While, high irradiance of 1636810.04 W/mm<sup>2</sup> at 30% overlapping rate produced higher temperature with less overlapping rate due to higher processing speed



produced higher surface hardness. Apart from higher processing speed, lower overlapping rate with higher temperature produces faster cooling rate and causes grain refinement during the solidification process (Ren, Fu et al. 2019), which improve the surface properties (Gao, Song et al. 2016). During the laser melting process, molten pool is formed along with the occurrence of solidification process. The solidification process transforms melted pool from hot liquid to solid and subsequently, produces new properties according to the operating temperature and time during heating and cooling processes.

Table 4.1 Average grain size of melted layer at various parameter settings

Overlapping rate (%)	Parameter				Average Grain size ( $\mu\text{m}$ )
	Peak Power (Watt)	Irradiance ( $\text{W}/\text{mm}^2$ )	Processing speed (mm/min)	Pulse Energy (J)	
30	2100	1145767.03	1470	2.00	0.81
	2500	1636810.04	1764	1.67	0.84
	1700	1113030.83	1764	1.67	0.82
	2100	1604073.84	2058	1.43	0.78
50	2100	1364008.37	1470	1.43	0.99
	2500	1604073.84	1050	2.00	1.12
	1700	662518.35	1050	1.43	1.07
	2100	927525.69	1470	1.67	1.01
70	2100	491043.01	630	2.00	1.28
	2500	701490.02	756	1.67	1.21
	1700	477013.21	756	1.67	1.19
	2100	687460.22	882	1.43	1.08

The laser melting process in this study produced melted zone (MZ), heat affected zone (HAZ), and substrate. The grain structure of melted layer refined due to high temperature interaction between laser power and sample surface caused localised heating at the melted pool. Table 4.1 shows average grain size of melted layer at various parameter settings. The parameters were opted with try and error method. Parameter setting produced from DOE analysis. The average grain size for 30% overlapping was  $0.81\mu\text{m}$ . While for 50% overlapping rate produce average grain size of  $1.05\mu\text{m}$ . Overlapping rate of 70% produce average grain of  $1.19\mu\text{m}$ . The average grain size in the

melted layer was 1.02  $\mu\text{m}$ , while the average grain size in substrate was 3.02  $\mu\text{m}$ . It shown, the grain size in substrate decreased up to 66.2% after laser melting processed. Table 4.1 shown overlapping percentage give significant effect of grain size formation. High overlapping rate produce slow processing speed, it caused delay solidification on melted pool and produce bigger grain size. This study clearly demonstrated that the grain refinement in melted layer improves the properties of the melted layer in terms of increased hardness.

#### **4.4 Chemical Composition**

The chemical composition of melted layer in MZ and substrate based on the results of energy dispersive X-ray spectroscopy (EDXS) spectrum line is summarised in Table 4.2. The presence of carbon (C), manganese (Mn), and sulphur (S) increased in MZ. However, presence of silicon (Si), titanium (Ti), vanadium (V), chromium (Cr), molybdenum (Mo), iron (Fe), and nickel (Ni) decreased in MZ. The obtained lines spectrum revealed that MZ contained carbon of between 11.494 wt% and 18.28 wt%, which was higher than the range of carbon in substrate of between 9.907 wt% and 18.077 wt%. Higher temperature from the absorption of laser energy and rapid solidification diffused the carbon content from substrate to MZ. In other words, the results revealed high carbon content in the melted layer. A prior study had discussed the various elements in the chemical composition of melted layer as a result of high temperature (Aqida, Brabazon et al. 2013). Adding to that, this study also demonstrated that high carbon content distributed in melted layer during melting process enhances hardness properties.

The distribution of the elements of melted surface at line spectrum analysis varied at different ranges for all samples (Table 4.3). These identified elements were detected by 10-line spectra along the depth of MZ in the melted layer, as shown in Figure 4.7(a) and (b). Si and Ti were not detected in samples 1, 4, and 5. As for samples 2, 6, 9, and 13, ten elements were detected where nine elements were detected in samples 3 and 11 and Ti and Ni were not present in samples 8, 10, and 12. The laser parameters used in melting process such as irradiance, residence time and laser energy caused variation of elements composition in melted die insert surface. During laser heating on die surface, composition in the melted layer changed from its substrate due to elements diffusion in the molten region. In particular, the increase or decrease of certain elements in the melted layer can be contributed by atomic diffusion at high surface temperature from the

substrate to melted layer during laser processing. The diffusion in steel occurred at high temperature, where at higher irradiance and shorter residence time, the temperature of the melted surface increased rapidly.

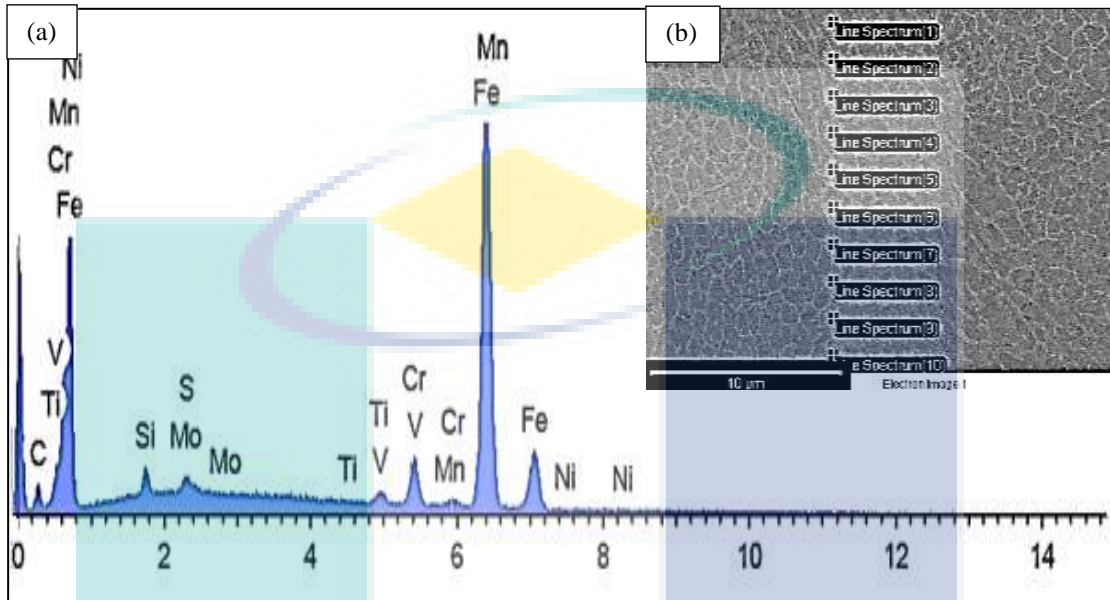


Figure 4.7 (a) EDX Spectrum analysis of melted layer for sample 6 and (b) line spectrum along the depth at modify layer

The element mapping using line spectrum shows the elements distribution in a selected area of the laser melted layer for sample 9 as presented in Appendix L by various colours; blue, green, yellow, magenta, purple, white and red to differentiate the elements presence in the melted layer. The distribution of white colour was less than other colours and representing only 0.05% Ni content in the laser melted layer. The carbon (red colour) represented of 14.99% C, silicon (green) represented of 0.92% Si, chromium (purple) represented of 4.71% Cr, and manganese (magenta) represent of 0.18% Mg respectively. The blue colour represented iron which is the highest element in the melted layer at 77.12%. Various element distribution in the melted layer depends on the laser irradiance and interaction time with sample surface. Increased and decreased of some elements in the laser melted layer was due to high surface temperature diffused from substrate layer during laser processing. The findings in this study shows a high carbon content distributed in the laser melted layer during melting processed that caused increase of hardness in the layer.

Table 4.2 Chemical composition of AISI H13 tool steel in melted zone, heat affected zone and substrate material

	Element (wt.%)									
	C	Si	S	Ti	V	Cr	Mn	Fe	Ni	Mo
<b>Melted Zone (MZ)</b>	11.440	0.704	0.028	0.021	0.775	4.180	0.159	71.229	0.047	0.428
	-	-	-	-	-	-	-	-	-	-
	18.280	1.070	0.379	0.064	1.139	5.058	0.647	79.221	0.338	1.895
<b>Heat Affected Zone (HAZ)</b>	10.389	0.675	0.006	0.090	0.354	3.571	0.209	74.069	0.027	0.378
	-	-	-	-	-	-	-	-	-	-
	17.882	1.717	0.322	0.038	1.892	7.373	0.499	83.499	0.655	1.383
<b>Substrate</b>	9.907	0.704	0.003	0.006	0.234	3.578	0.143	67.327	0.021	0.466
	-	-	-	-	-	-	-	-	-	-
	18.077	1.627	0.250	0.156	7.276	7.436	0.554	81.73	0.466	7.942

Table 4.3 Element distribution of melted surface at line spectrum 1

Sample	Element									
	C	Si	S	Ti	V	Cr	Mn	Fe	Ni	Mo
1	14.496	0.983	n/a	n/a	1.049	4.508	0.647	76.805	n/a	1.511
2	12.411	1.031	0.351	0.014	0.892	4.759	0.177	79.702	0.178	0.485
3	17.345	0.882	0.019	0.019	0.759	4.417	0.255	75.317	n/a	0.986
4	15.413	0.956	n/a	n/a	1.080	4.356	0.108	76.595	0.147	1.346
5	10.638	0.916	n/a	n/a	0.886	4.699	0.275	80.874	0.326	1.387
6	11.643	0.953	0.109	0.036	0.849	4.726	0.144	80.130	0.327	1.082
7	19.682	0.853	n/a	0.070	0.828	4.446	0.244	72.422	n/a	1.454
8	17.150	0.943	0.004	n/a	0.905	4.452	0.188	75.082	n/a	1.276
9	14.993	0.924	0.213	0.107	0.888	4.706	0.179	77.121	0.050	0.819
10	12.659	0.968	0.035	n/a	1.009	4.745	0.180	78.915	n/a	1.489
11	9.427	0.974	0.106	n/a	1.037	4.561	0.164	82.365	0.364	1.001
12	10.330	1.135	0.169	n/a	0.925	4.638	0.369	81.352	n/a	1.082
13	12.425	1.152	0.220	0.005	1.014	4.557	0.395	78.664	0.291	1.276

#### 4.5 Surface Roughness Properties

Surface roughness is another key factor for the manufacturing process to produce better surface finishing. Table 4.4 shown surface roughness of melted layer at various parameter setting. The laser settings produced surface roughness of between 1.89  $\mu\text{m}$  and 5.19  $\mu\text{m}$ . The lowest surface roughness of 1.89  $\mu\text{m}$  was processed at 2100 W with the lowest pulse energy of 1.43J and the highest overlapping rate of 70%. On the other hand, the highest surface roughness of 5.19  $\mu\text{m}$  was produced with the highest pulse energy of 2 J and low PRF of 50 Hz. Higher laser energy absorption produces higher temperature at the surface and subsequently forms irregular geometries, which explains the increasing surface roughness. The increase of overlapping rate increases the laser interaction time and laser energy absorption. Lower duty cycle at higher power setting can minimise the surface roughness at any overlap setting due to the dominance of duty cycle effect at the higher power setting.

High absorption of pulse energy into the sample surface increased the surface roughness of the melted surface. Apart from higher pulse energy, higher peak power also increased the surface roughness, as the amount of energy penetrated affects the

overlapping laser spots (Zhang, Ren et al. 2010). The interaction time between the laser and sample surface during processing was reduced as the overlapping rate decreased at higher processing speed. Low PRF tends to produce high pulse energy, which causes higher absorption of laser energy and increased temperature of the material surface, resulting in increased surface roughness. Meanwhile, lower duty cycle with higher irradiance produces lower surface roughness (Aqida, Naher et al. 2011). Higher laser absorption due to high peak power produces larger spot size; thus, increasing the roughness on the material surface (Fauzun, Aqida et al. 2014).

Table 4.4 Surface roughness of melted layer at various parameter settings

Parameter				
Overlapping rate (%)	Processing speed (mm/min)	Irradiance (W/mm <sup>2</sup> )	Pulse Energy (J)	Roughness (Ra)
30	1470	1145767.03	2.00	3.73
	1764	1636810.04	1.67	3.89
	1764	1113030.83	1.67	3.01
	2058	1604073.84	1.43	2.43
50	1470	1364008.37	1.43	3.86
	1050	974291.69	2.00	4.17
	1050	927525.689	1.43	2.09
	1470	982086.023	1.67	2.10
70	630	491043.01	2.00	3.41
	756	701490.02	1.67	2.96
	756	477013.21	1.67	2.12
	882	687460.22	1.43	1.89

In this study, the surface roughness reduced with the increase of PRF and peak power. In this case, average surface roughness at the overlapping rate of 30% was the highest at 3.89  $\mu\text{m}$  whereas the surface roughness at the overlapping rate of 70% was the lowest at 1.89  $\mu\text{m}$ . The surface roughness quality of melted surface highly depends on the processing speed factor, which contributes to the overlapping laser spot pattern (Aqida, Maurel et al. 2009). The surface roughness quality of melted surface was found to be highly dependent on the processing speed and overlapping percentage, which contributed to the overlapping laser spot patterns. Basically, higher surface roughness increases thermal conductivity during HPF process. In this study, the targeted surface roughness was less than 5  $\mu\text{m}$  which was deemed suitable for engineering applications (Aqida, Naher et al. 2011), and surface roughness increased heat transfer during HPF processed due to less effect metal to metal contact during HPF processed.

#### **4.6 Hardness Properties**

Micrograph of Vickers indentation on melted zone, heat affected zone, and substrate presents in Figure 4.8. Smaller indenter marks shown in melted zone compared to the substrate. The smaller indenter marks in the melted zone reveals that the melted surface is capable of withstanding higher load, and thus indicates the hardness of melted zone higher than the substrate. Whereas Figure 4.9 presents the hardness profile of the melted layer across the substrate for different samples. Due to various laser parameter settings, the heating and cooling rates varied and resulted in a range of high hardness values from 684.4 to 793.7  $\text{HV}_{0.1}$ . The maximum hardness was caused by the rapid heating rate of surface using high pulse energy of 2 J that melted the surface at a processing speed of 1764 mm/min. Consequently, solidification occurred at the approximate same quick period. High hardness properties of laser melted layer increased threefold of its substrate due to grain refinement. Nevertheless, the reduced hardness properties of melted layer were directly proportional to the processing speed. The minimum hardness was acquired when the pulse energy was 1.43 J and the processing speed was 882 mm/min. Despite the rapid heating time, the pulse energy may be insufficient to raise the surface temperature for the melting process at 0.6 ms to 1.2 ms.



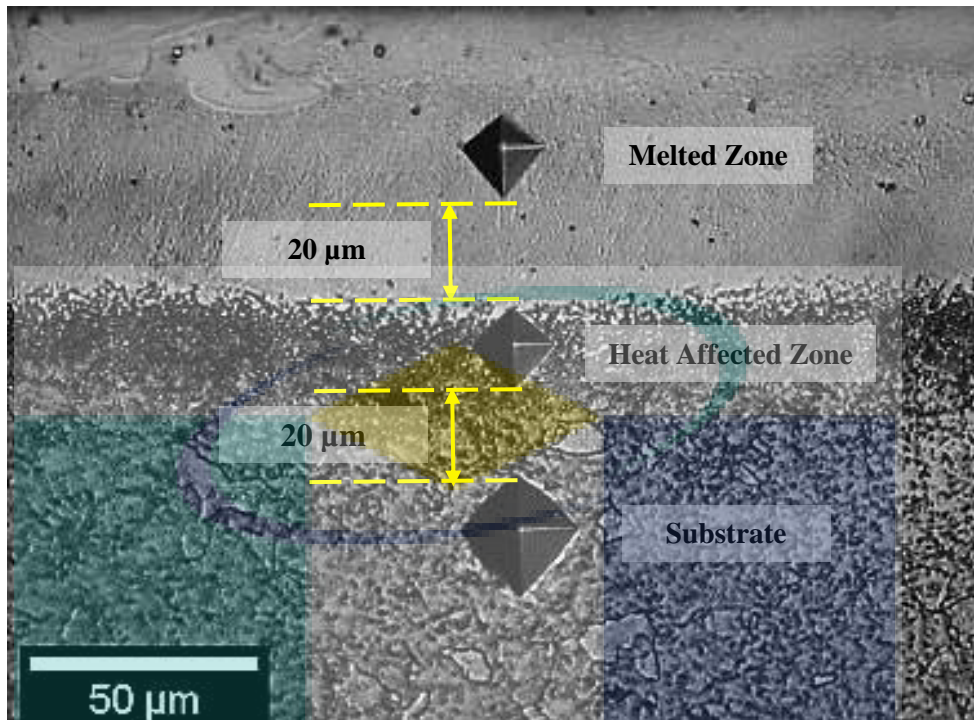


Figure 4.8 Cross-section surface of melted zone (MZ), heat affected zone (HAZ) and substrate with Vickers hardness indentation

Variation of hardness in the melted zone as shown in Figure 4.9 was due to effect of various laser parameters like peak power, pulse energy, pulse repetition frequency and overlapping rate. Hardness properties in the melted zone increased with increasing PRF. The pulse energy was lower at a higher PRF and caused a faster cooling rate. Besides that, hardness values in melted layer increased as the PRF decreased and peak power increased. The properties of melted surface changes due to the constant average power with changing duty cycle and peak power (Mahmoudi, Torkamany et al. 2010). The surface hardness also decreased with increasing overlapping rate.

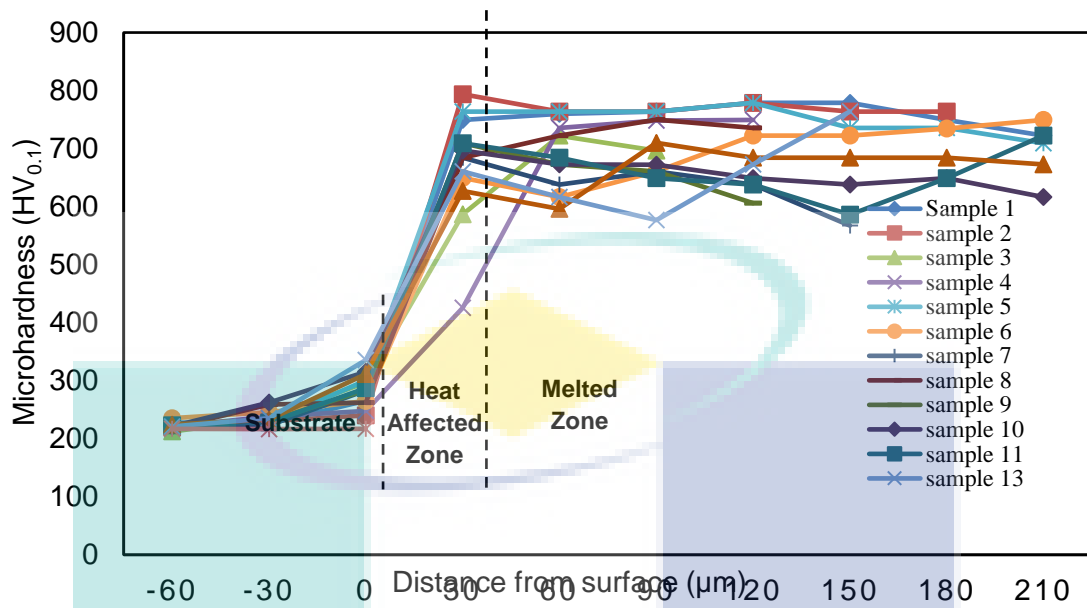


Figure 4.9 Microhardness as a function of distance from surface of laser melting H13 steel cross section

Meanwhile, higher irradiance of  $6.495 \times 10^3 \text{ W/mm}^2$  with higher processing speed of 1764 mm/min reduced the heating time, resulting in higher solidification rate. Rapidly melted and solidified H13 surface yielded smaller grain size in the melted layer, which exhibited high hardness. Besides that, grain refinement led to higher volume of grain boundary development, which enhanced the hardness properties. On the other hand, lower hardness was measured across the HAZ to the substrate. Lesser grain boundary was revealed by the as-received H13, which produced the lowest hardness properties as compared to that of the melted surface with higher volume of grain boundary. The reduced hardness in HAZ due to shorter interaction time between laser beam and substrate or latent heat that delays the solidification rate (Gao, Zhao et al. 2015). Evidently, the increase in surface hardness is an attribute that improves wear resistance (Telasang, Majumdar et al. 2015). As for the die application, higher surface hardness is significant for the improvement of wear resistance, which enhances the lifetime of the die (Sohi, Ebrahimi et al. 2012).

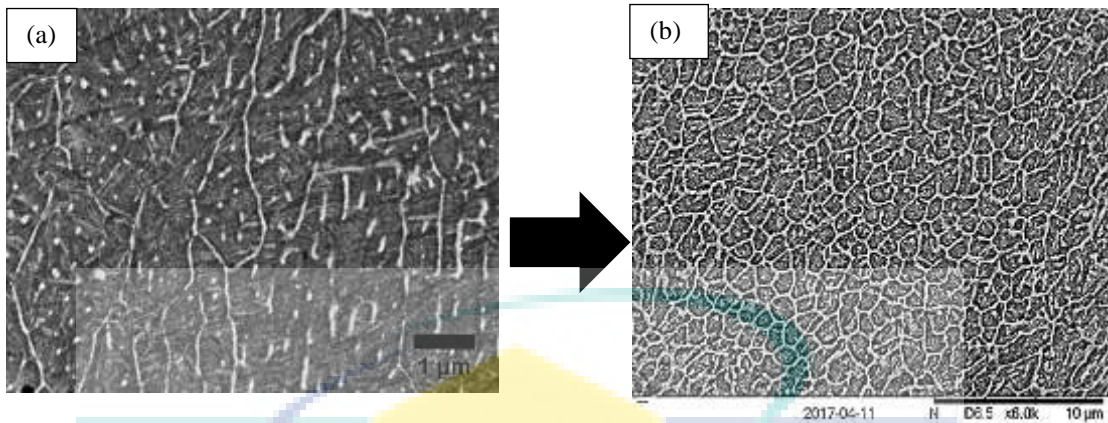


Figure 4.10 Grain of AISI H13 surface (a) before and (b) after melting processed

Heating and cooling rates are significant values in laser surface melting to control the size of the micro structurally altered region and comply with the Hall-Petch relation (Aqida, Brabazon et al. 2011). After laser melting processed of as-received AISI H13, the grain or crystallite amount of melted layer increased as shown in Figure 4.10 (b) thus increased hardness on melted layer as shown in Figure 4.9. Referring to Hall-Petch relation, the surface hardness of melted layer increased due to laser melting processed changes microstructure and produced new properties on AISI H13 die surface. Besides, increase of grain boundary volume fraction of the interphase region caused the grain size decreased (Cherkaoui and Capolungo 2009). The hall-patch relation describes that the yield strength of a material increases proportional to square root of the grain size. Hall-Patch is the only classic strengthening mechanism that does not reduce ductility.

The hardness properties of as-received H13 were 228.1 HV<sub>0.1</sub> before laser melted analysis using Vickers hardness tester. After laser melting processes, the hardness of melted layer increased between 684.4 and 793.7 HV<sub>0.1</sub>. It shown, the surface hardness on melted layer increased up to three time after laser melting process. The findings in this study show that the laser melted surface can be used to enhance thermal properties of dies surface and improved quality of 22MnB5 after HPF processed.

#### 4.7 X-ray Diffraction (XRD) Analysis

The results of phase analysis of AISI H13 before and after the laser melting process using XRD are revealed in Figure 4.11. The XRD analysis detected  $\alpha$ -Fe (110) and (200) phases at different Bragg's angle (2 theta). The phases for the melted surface

of H13 at various laser processing parameters were diffracted at different intensities. The samples were processed at different peak power from 1700 W to 2500 W and PRF of between 50 Hz and 70 Hz, and overlapping rates from 30% to 70%. In particular, samples 1, 2, 3, and 4, which were processed at the overlapping rate of 30%, demonstrated Bragg's angle (2 theta) of 44.30° to 44.90° and 64.46° to 64.89°. Samples 5, 6, 7, 8, and 9 were processed at the overlapping rate of 50%, which revealed Bragg's angle (2 theta) of 44.04° to 45.10° and 64.21° to 65.98°. Meanwhile, samples 10, 11, 12, and 13 presented Bragg's angle (2 theta) of 44.66° to 44.93° and 64.80° to 65.01° after the laser melting process. The XRD analysis for as-received H13 sample presented phase at Bragg's angle (2 theta) of 44.60° and 65.00°. Various Bragg's angle of melted surface through the laser melting process on H13 die surface produced new texture in the melted surface.

The intensity peak of as-received H13 and melted surface of samples at the overlapping rates of 30%, 50%, and 70% are presented in Figure 4.11(a–d). Higher peak intensity produced Bragg's angle of between 44.63° and 44.90°. The melted surface of sample at the overlapping rate of 30% (Figure 4.11(a)) recorded maximum peak intensity of 393.65 cps, which was lower than the recorded maximum peak intensity of samples at the overlapping rates of 50% (497.42 cps) and 70% (645.13 cps), as shown in Figure 4.11(b) and Figure 4.11(c), respectively. The peak intensity of the diffracted phases changed for the case of melted surface given the effect of various laser melting parameters on the surface crystallite. Higher peak intensity led to larger crystallite formation for the case of as-received H13 (Kim and Chung 2003) whereas lower peak intensity led to smaller crystallite for the case of melted surface. The maximum peak intensity of as-received H13 was 990.39 cps with lesser grain boundary (Figure 4.11(d)).



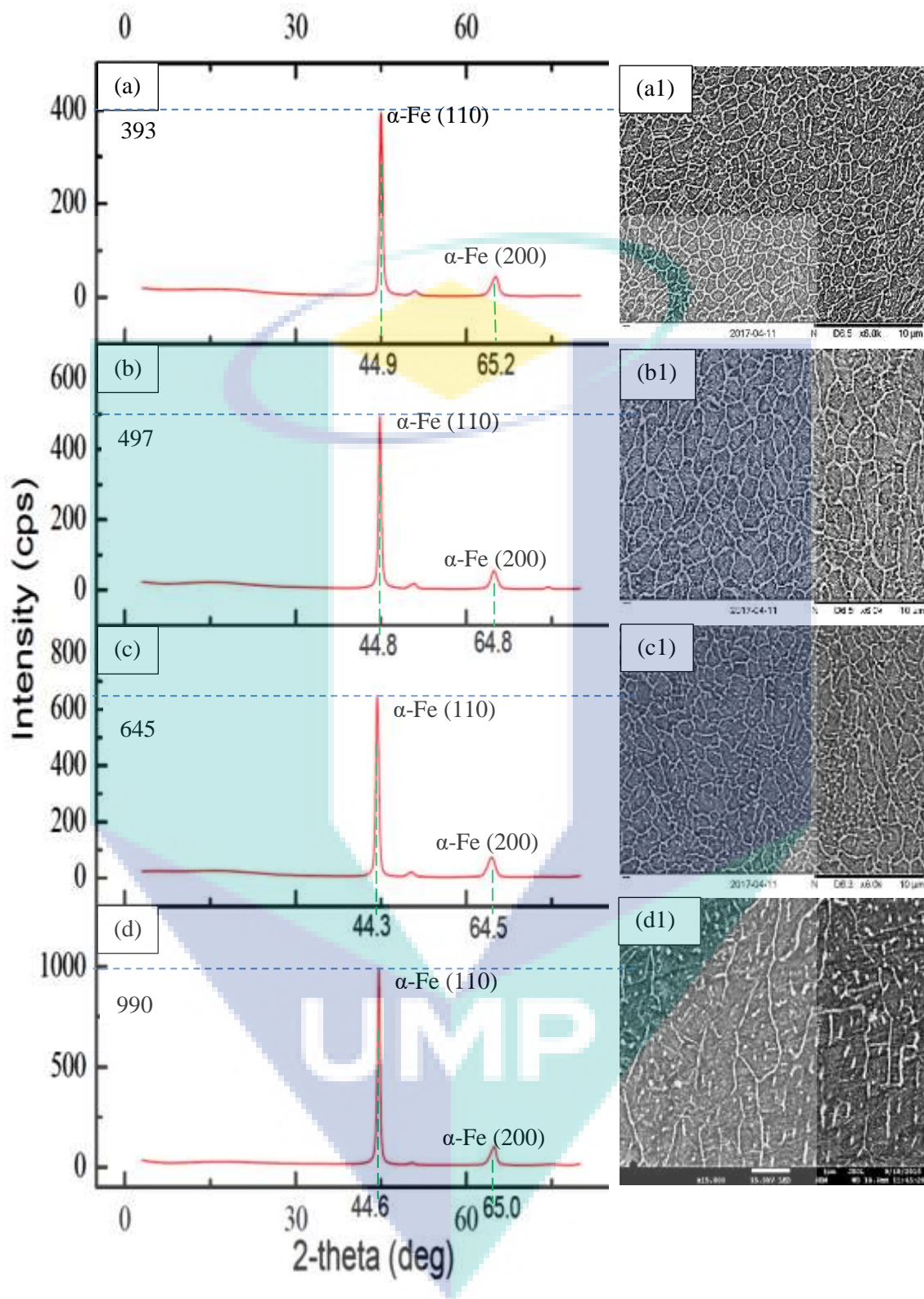


Figure 4.11 X-ray diffraction pattern of die insert surface with the corresponding micrograph of laser melted surface of overlapping rate (a) 30%, (b) 50%, (c) 70% and (d) As-received H13 steel

The grain boundary of melted surface and as-received H13 at the overlapping rates of 30%, 50%, and 70% are presented in Figure 4.11(a1–d1). The crystallite of the melted surface was lower than the crystallite of as-received H13. The sample at the overlapping rate of 30% yielded the lowest crystallinity and contained higher grain boundary and crystallite volume. The as-received H13 recorded grain boundary of 8.97% whereas, at the melted surface, its grain boundary was between 12.61% and 22.13%. In other words, grain boundary size refinement occurs due to the heating and cooling processes during the laser melting process. On the other hand, the intensity of  $\alpha$ -Fe phase peak at (110) and (200) diffraction was contributed by the heating and cooling processes at the melted pool.

The peak intensity diffraction corresponds with grain structure refinement, which affects the hardness properties. In this study, the surface hardness of sample at the lowest overlapping rate of 30% was the highest at 778.9 HV<sub>0.1</sub>; the surface hardness of sample at the overlapping rate of 50% recorded 749.4 HV<sub>0.1</sub>; the surface hardness of sample at the highest overlapping rate of 70% was the lowest at 709.9 HV<sub>0.1</sub>. Meanwhile, the surface hardness of as-received H13 was the lowest at 228.1 HV<sub>0.1</sub>. The peak intensity analysis further revealed that the melted surface produces low peak intensity compared to as-received H13. The obtained results of analysis also revealed refined grain structure of as-received H13 after laser melting process due to heating and cooling processes during laser melting process. High crystallite increases surface hardness of melted layer. The hardness of melted layer increased from 684.4 and 793.7 HV<sub>0.1</sub>. The surface hardness of melted layer increased up to three time after laser melting process.

The peak intensity analysis shown, melted surface produce low peak intensity compares as-received H13. Low peak intensity produced high crystallite or grain boundary on melted surface. The peak intensity of as-received H13 were 990.39 cps and for melted surface between 393.65 to 645.13 cps. Peak intensity analysis shown the grain structure of as-received H13 become refinement after laser melting processed due to heating and cooling during laser melted processed. The findings in this study show that high crystallite increased surface hardness at melted layer.

## 4.8 Respond Surface Method (RSM) Analysis

The response surface (RSM) analysis was performed on the experimental data to examine the hardness, melted depth and roughness properties using Box-Behnken design as shown in Table 4.5, which involved the quadratic model with model reduction (to improve the model). The box-Behnken analysis was used to identify the independent variables or factors that affect the process and product, and also to study the effects of dependent variables or responses.

Table 4.5 Laser parameters for process optimisation

Std	Run	Factor 1 A:Peak Power watt	Factor 2 B:PRF Hz	Factor 3 C:Overla P %	Response 1 Hardness HV0.1	Response 2 Melt Depth mm	Response 3 Roughness $\mu\text{m}$
8	1	2500	60	70	722.6	0.21	2.96
15	2	2100	60	50	719.5	0.20	3.86
9	3	2100	50	30	778.9	0.24	3.73
4	4	2500	70	50	684.4	0.16	3.07
3	5	1700	70	50	749.9	0.16	2.10
16	6	2100	60	50	709.2	0.22	3.91
6	7	2500	60	30	793.7	0.21	3.89
11	8	2100	50	70	749.5	0.33	3.41
1	9	1700	50	50	749.4	0.27	4.17
12	10	2100	70	70	763.9	0.21	1.89
5	11	1700	60	30	722.1	0.10	3.01
13	12	2100	60	50	728.9	0.19	3.83
7	13	1700	60	70	719.7	0.26	2.12
17	14	2100	60	50	709.3	0.20	3.90
2	15	2500	50	50	778.9	0.25	5.20
14	16	2100	60	50	718.8	0.21	3.88
10	17	2100	70	30	749.4	0.19	2.43

### 4.8.1 Hardness Properties

The model F-value of 10.07 demonstrates the significance of the model. In other words, the chance for the model to obtain this particular model F-value is only 0.19% given the presence of noise. The value of “Prob > F” that is less than 0.05 reflects the significance of the model terms. In this case, A, C, AB, AC, B<sup>2</sup>, C<sup>2</sup>, A<sup>2</sup>B, and AB<sup>2</sup> were



significant model terms as shown in Table 4.6. On the other hand, value that exceeds 0.1 indicates that the model terms are not significant. The “lack of fit F-value” of 3.60 implies that the “lack of fit” is not significant in relative to the pure error. In other words, the chance for “lack of fit F-value” to achieve this value is 12.14% given the presence of noise. The non-significant result indicated good “lack of fit”; in other words, the model was deemed fit.

Table 4.6 ANOVA result for melted surface hardness response using quadratic model with stepwise elimination

<i>Source</i>	<i>Sum of Squares</i>	<i>df</i>	<i>Mean Square</i>	<i>F Value</i>	<i>p-value Prob &gt; F</i>	<i>Remarks</i>
<i>Model</i>	12550.74	8	1568.84	10.07	0.0019	<i>significant</i>
<i>A-Peak Power</i>	1387.56	1	1387.56	8.91	0.0175	
<i>C-Overlapping rate</i>	976.82	1	976.82	6.27	0.0367	
<i>AB</i>	2256.25	1	2256.25	14.48	0.0052	
<i>AC</i>	1179.92	1	1179.92	7.57	0.0250	
<i>B<sup>2</sup></i>	2094.72	1	2094.72	13.45	0.0063	
<i>C<sup>2</sup></i>	1888.46	1	1888.46	12.12	0.0083	
<i>A<sup>2</sup>B</i>	2209.00	1	2209.00	14.18	0.0055	
<i>AB<sup>2</sup></i>	1526.28	1	1526.28	9.80	0.0140	
<i>Residual</i>	1246.35	8	155.79			
<i>Lack of Fit</i>	975.22	4	243.81	3.60	0.1214	<i>not significant</i>
<i>Pure Error</i>	271.13	4	67.78			
<i>Cor Total</i>	13797.09	16				
Std. Dev.	12.48		R-Squared	0.9097		
Mean	738.12		Adj R-Squared	0.8193		
C.V. %	1.69		Pred R-Squared	0.3947		
PRESS	8351.24		Adeq Precision	11.228		

Figure 4.12 shows the contour plot of hardness properties against peak power and PRF at the overlapping rate of 50%. The elliptical contour plot demonstrated significant interaction between the variables. The reduce of PRF from 60 HZ to 50 Hz and the increase of peak power from 2100 W to 2500 W increased the contour from 730.963

HV<sub>0.1</sub> to 762.463 HV<sub>0.1</sub>. The highest peak power of 2500 W with the highest PRF of 70 Hz produced lower surface hardness on the melted surface.

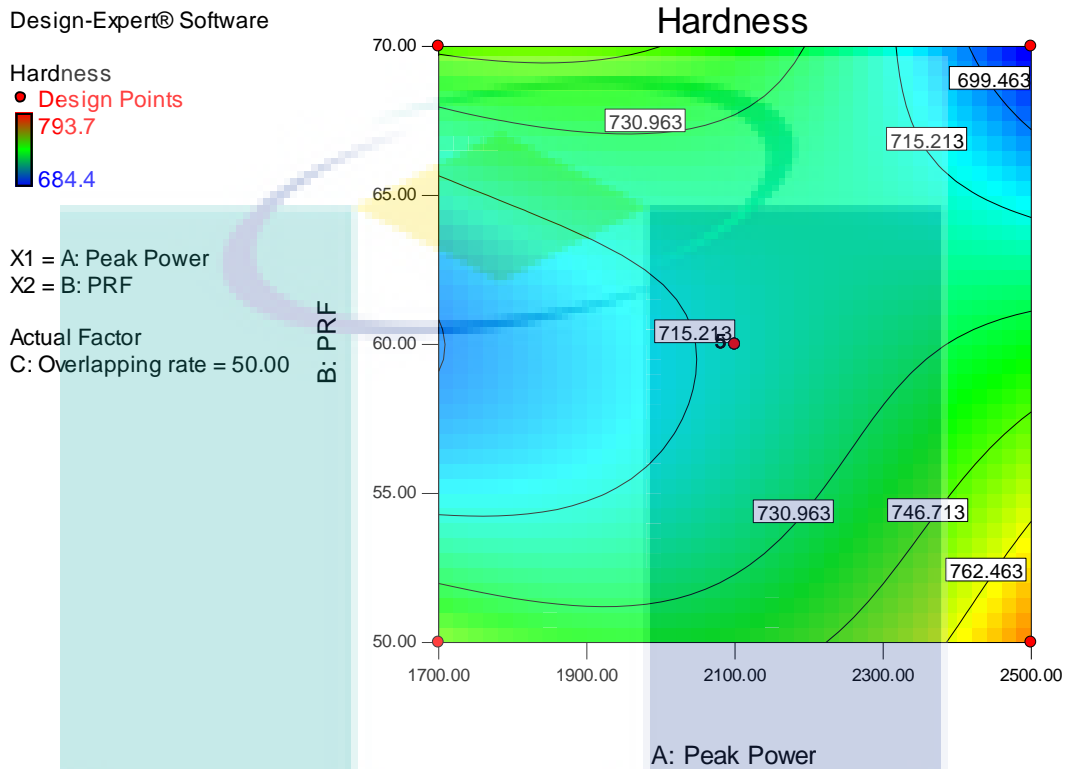


Figure 4.12 Contour plot of hardness properties responding to various peak power and PRF at 50% overlapping rate

#### 4.8.2 Melt Depth

The quadratic model was improved using stepwise elimination shown in Table 4.7, where the model F-value of 24.12 implies that the model in this study was significant. The chance to obtain this value was only 0.01% due to noise. Furthermore, the obtained values of “Prob > F” that are less than 0.05 indicate that the model terms in this study were significant. In this case, B, C, AC, A<sup>2</sup>, and B<sup>2</sup> were deemed significant model terms. As previously indicated, values that exceed 0.1 indicate that the model terms are not significant, while the “lack of fit F-value” of 2.74 implies that the “lack of fit” is not significant in relative to the pure error. Hence, the chance of BC model to improve “lack of fit F-value” was higher than 10%. After model reduction, the chance for “lack of fit F-

value” to achieve this value is 17.43% due to noise. The non-significant result indicated good “lack of fit”; in other words, the model was deemed fit.

Table 4.7 ANOVA result for melted surface melted depth response using quadratic model with stepwise elimination

Source	Sum of Squares	df	Mean Square	F Value	p-value Prob > F	Remarks
<i>Model</i>	0.038	6	6.408E-003	24.12	< 0.0001	<i>significant</i>
<i>B-PRF</i>	0.017	1	0.017	64.41	< 0.0001	
<i>C-Overlapping rate</i>	9.045E-003	1	9.045E-003	34.05	0.0002	
<i>AC</i>	6.480E-003	1	6.480E-003	24.39	0.0006	
<i>BC</i>	1.225E-003	1	1.225E-003	4.61	0.0573	
<i>A^2</i>	1.689E-003	1	1.689E-003	6.36	0.0303	
<i>B^2</i>	3.135E-003	1	3.135E-003	11.80	0.0064	
<i>Residual</i>	2.657E-003	10	2.657E-004			
<i>Lack of Fit</i>	2.137E-003	6	3.561E-004	2.74	0.1743	<i>not significant</i>
<i>Pure Error</i>	5.200E-004	4	1.300E-004			
<i>Cor Total</i>	0.041	16				
Std. Dev.	0.016	R-Squared	0.9354			
Mean	0.21	Adj R-Squared	0.8966			
C.V. %	7.67	Pred R-Squared	0.7135			
PRESS	0.012	Adeq Precision	20.891			

The effect of overlapping rate and peak power on melt depth properties at constant PRF of 60 Hz is presented in Figure 4.13. The increase of overlapping rate from 50% to 70% and the reduction of peak power from 2300 W to 1700 W raised melt depth contour from 0.214 mm to 0.238 mm. The melt depth contour decreased when the peak power and overlapping rate decreased from 2300 W to 1700 W and 50% to 30%, respectively. Referring to the obtained contour plot, the maximum melted depth was achieved at the overlapping rate of more than 50%. On the other hand, the elliptical contour plot demonstrated significant interaction between the variables.

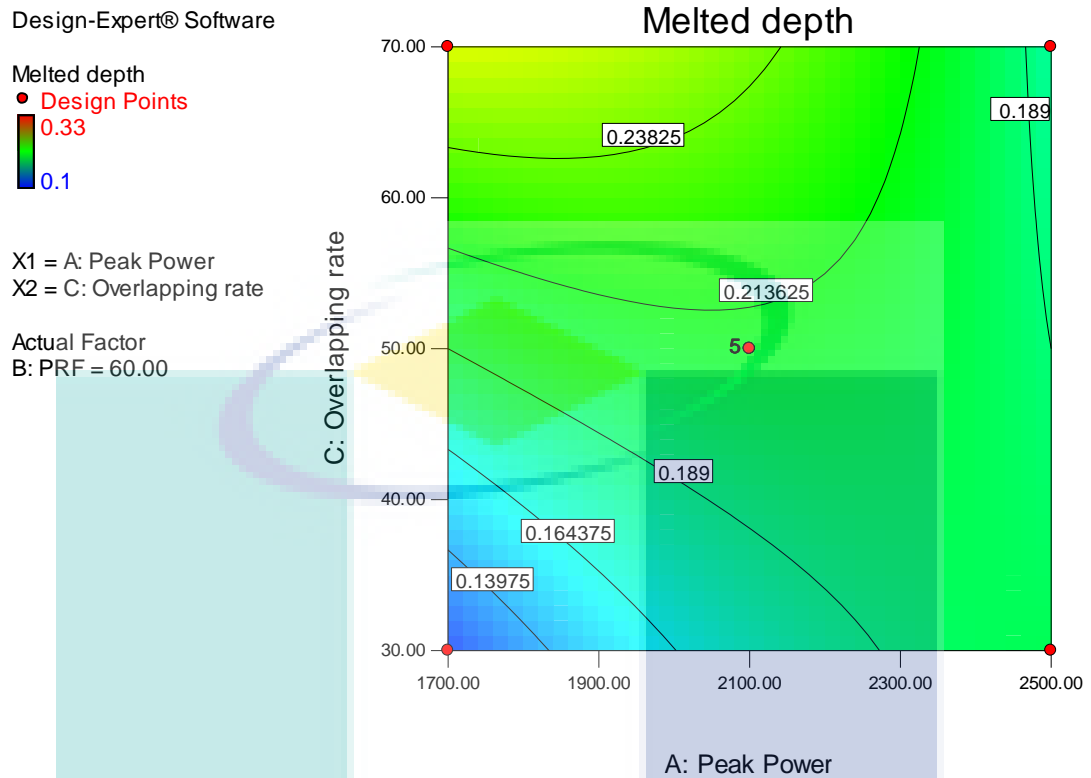


Figure 4.13 Contour plot of melt depths at various overlapping rate and peak power at 60Hz PRF

### 4.8.3 Surface Roughness

Analysis varians (ANOVA) of melted depth respond using quadratic model is shown in Table 4.8. The obtained model F-value of 628.37 implies that the model was significant with only 0.01% chance that the value occurred due to noise). Values of “Prob > F” that are less than 0.05 indicate that the model terms were significant. In this case, A, B, C,  $A^2$ ,  $B^2$ ,  $C^2$ ,  $A^2B$ ,  $A^2C$  were significant model terms. The “lack of fit F-value” of 3.59 implies the “lack of fit” was not significant in relative to the pure error. In particular, BC was selected to increase “lack of fit F-value” by more than 10% to reflect that the model is fit to optimise all the responses, where the chance that the value occurred was 12.43% due to noise. The non-significant result indicated good “lack of fit”; in other words, the model was deemed fit.

Table 4.8 ANOVA result for melted surface roughness response using quadratic model with stepwise elimination

Source	Sum of Squares	df	Mean Square	F Value	p-value Prob > F	Remarks
<i>Model</i>	12.30	9	1.37	628.37	< 0.0001	<i>significant</i>
<i>A-Peak Power</i>	1.73	1	1.73	795.57	< 0.0001	
<i>B-PRF</i>	1.99	1	1.99	914.37	< 0.0001	
<i>C-Overlapping rate</i>	0.18	1	0.18	85.04	< 0.0001	
<i>BC</i>	0.012	1	0.012	5.57	0.0504	
<i>A^2</i>	0.013	1	0.013	5.96	0.0446	
<i>B^2</i>	0.14	1	0.14	66.64	< 0.0001	
<i>C^2</i>	2.87	1	2.87	1319.64	< 0.0001	
<i>A^2B</i>	0.24	1	0.24	109.48	< 0.0001	
<i>A^2C</i>	0.12	1	0.12	52.98	0.0002	
<i>Residual</i>	0.015	7	2.174E-003			
<i>Lack of Fit</i>	0.011	3	3.700E-003	3.59	0.1243	<i>not significant</i>
<i>Pure Error</i>	4.120E-003	4	1.030E-003			
<i>Cor Total</i>	12.31	16				
Std. Dev.	0.047		R-Squared		0.9988	
Mean	3.37		Adj R-Squared		0.9972	
C.V. %	1.38		Pred R-Squared		N/A	
PRESS	N/A		Adeq Precision		91.156	

Figure 4.14 presents the ANOVA contour plot reflects the roughness properties in response to the overlapping rate and PRF with constant peak power of 2100 W. The model revealed that relatively uniform surface roughness was achieved for the sample at PRF of less than 60 Hz and the overlapping rate of between 31% and 61%. The maximum surface roughness recorded 3.84  $\mu\text{m}$ . On the other hand, the minimum surface roughness of melted surface was 2.31  $\mu\text{m}$  at PRF of over 65 Hz and the overlapping rate of under 60%. The contour plot also revealed that the surface roughness increased at the maximum overlapping rate of 50% and peak power of less than 2300 W. Meanwhile, the surface roughness at the peak power of 2100 W decreased with the increase of PRF. The elliptical contour plot demonstrated significant interaction between the corresponding variables.

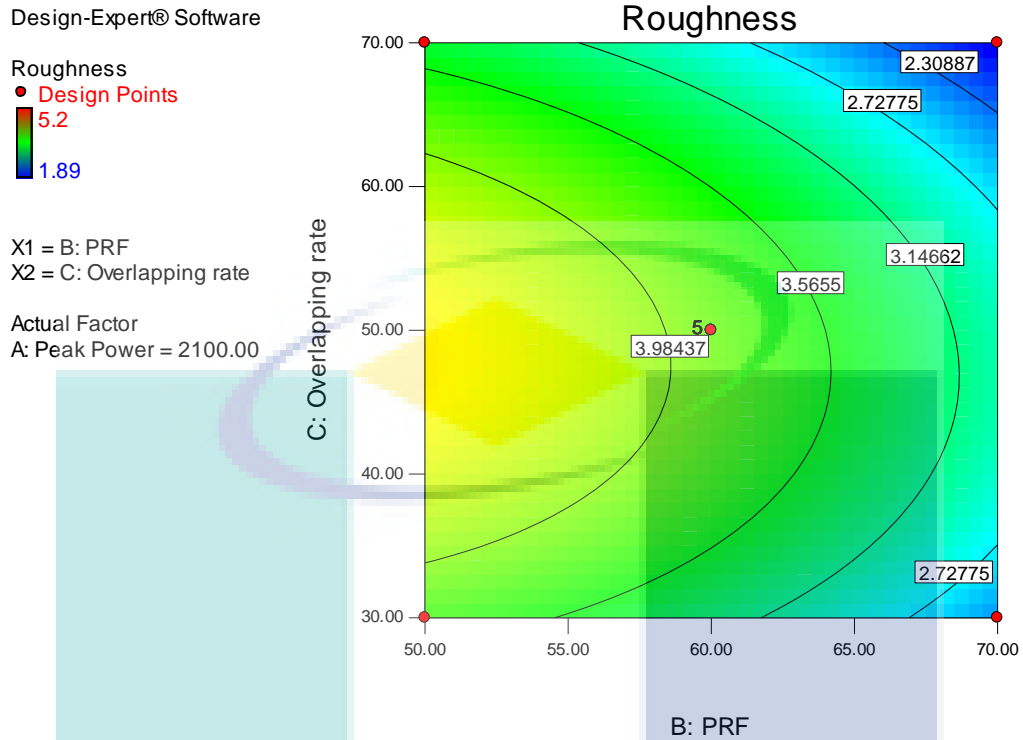


Figure 4.14 Contour plot of surface roughness at different overlapping rate and PRF at 2100 W peak power

#### 4.9 Design Optimization

The goal, limit and importance level for setting and outcome parameter from DOE are shown in Table 4.9. The goals of peak power, PRF, and overlapping rates were set within the appropriate range of is in range. The hardness properties goals were set to maximize, while melted depth was set to minimize and surface roughness set is in range. The importance level for factor parameters were set at Level 3 for all parameters. The importance levels of hardness were set at Level 5, while the roughness was set at Level 3 and melted depth was set at Level 2. The changes on the importance level would affect the desirable solution.

Table 4.9 Constrain selected in design optimization of laser melted processes

Name	Goal	Lower	Upper	Lower	Upper	Importance
		Limit	Limit	Weight	Weight	
Peak Power	is in range	1700	2500	1	1	3
PRF	is in range	50	70	1	1	3
Overlapping rate	is in range	30	70	1	1	3
Hardness	maximize	684.4	793.7	1	1	5
Melted depth	minimize	0.10	0.33	1	1	2
Roughness	Is in range	1.89	5.20	1	1	3

Design solution in Table 4.10 shows 23 solution of parameter setting. The highest desirability factor was 0.847 and the lowest solution was 0.416. As for optimisation analysis, the surface hardness was set to maximum limit, while the surface roughness was set to in range limit, and melted depth set to minimize to ensure the highest hardness with better surface roughness after laser melting process. The prediction of setting parameters included peak power of 2500 W, PRF of 58.27 Hz, overlapping rate of 30% produce maximum surface hardness of 793.7 HV<sub>0.1</sub>, roughness of 4.08 μm, and melted depth of 0.2 mm at the highest desirability factor of 0.847. Table 4.10 shown solution number 1 and 9 with peak power of 2500 W, PRF of 58.27 and 60.1 Hz with overlapping rate of 30% similar with parameter used during experimental process with (peak power of 2500, PRF of 60 Hz and overlap rate of 30%).



Table 4.10 Design solution for maximised surface hardness and melted depth

Number	Peak power	PRF	Overlap rate	Hardness	Melted depth	Roughness	Desirability
<u>1</u>	<u>2500.00</u>	<u>58.27</u>	<u>30.00</u>	<u>793.7</u>	<u>0.20</u>	<u>4.08</u>	<u>0.847</u>
2	2496.63	58.18	30.00	793.7	0.20	4.08	0.846
3	2499.90	58.02	30.32	793.7	0.20	4.12	0.845
4	2500.00	57.80	30.61	793.7	0.20	4.16	0.844
5	2398.23	54.60	30.00	793.7	0.22	4.12	0.815
6	1864.27	70.00	30.00	773.2	0.14	2.10	0.812
7	1861.26	70.00	30.00	773.1	0.14	2.10	0.812
8	1850.11	70.00	30.00	772.7	0.14	2.08	0.812
<u>9</u>	<u>2500.00</u>	<u>60.10</u>	<u>30.00</u>	<u>785.2</u>	<u>0.20</u>	<u>3.91</u>	<u>0.810</u>
10	2496.75	53.34	30.00	814.2	0.23	4.48	0.795
11	2500.00	60.79	30.00	781.9	0.19	3.83	0.794
12	2184.03	68.95	30.00	765.2	0.18	2.63	0.715
13	1803.07	50.00	30.25	760.9	0.19	3.69	0.670
14	2076.59	50.00	30.00	770.4	0.23	3.70	0.666
15	1846.89	70.00	63.74	761.1	0.21	1.89	0.644
16	1886.24	70.00	65.18	761.5	0.21	1.89	0.643
17	1941.68	70.00	66.89	760.7	0.21	1.89	0.636
18	1750.79	70.00	53.49	752.0	0.18	2.17	0.623
19	2005.62	70.00	68.45	757.9	0.21	1.89	0.622
20	2009.76	70.00	68.53	757.7	0.21	1.89	0.620
21	2046.41	69.99	69.23	755.0	0.21	1.89	0.607
22	2500.00	51.74	61.33	762.5	0.25	4.53	0.581
23	2251.86	61.97	70.00	726.4	0.21	2.80	0.416

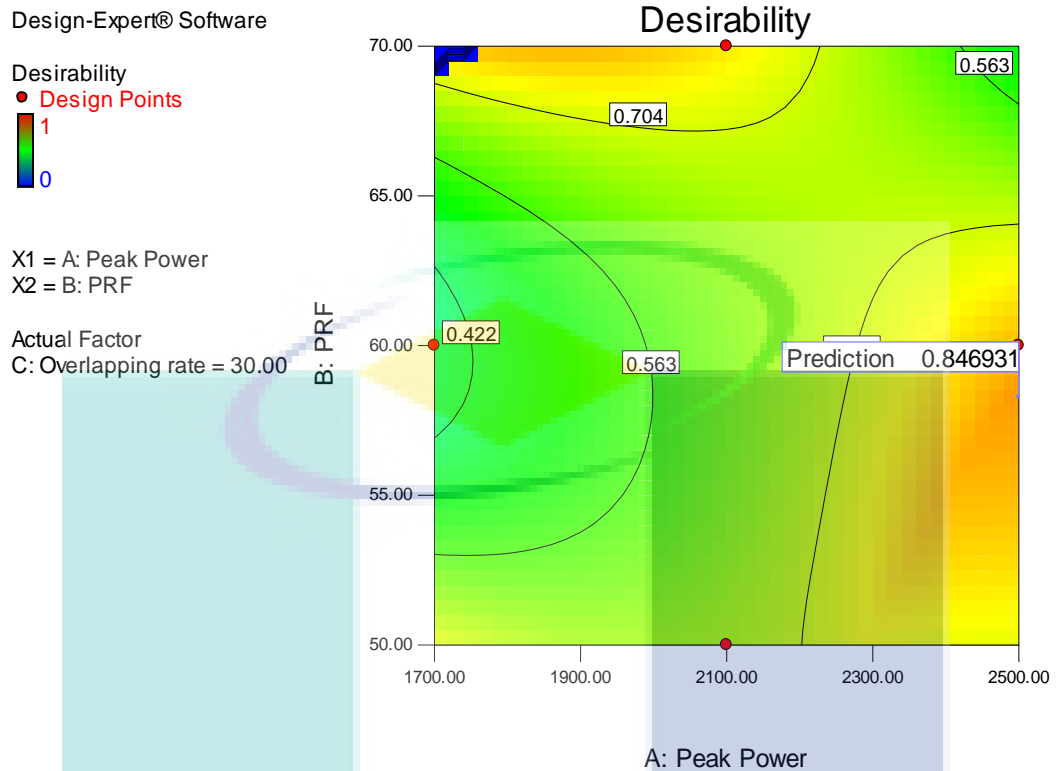


Figure 4.15 Desirability Contour plot of melted surface with highest desirability factor of 0.847

The generated optimal condition criteria in the desirability contour plot are shown in Figure 4.15. The desirability function served to optimise the experimental conditions for maximised surface hardness. The best combination of factors included peak power of 2500 W, PRF of 58.27 Hz, and overlapping rate of 30%. The plotted desirability contour graph of peak power and PRF at the overlapping rate of 30% revealed that desirability factor increased with the increase of peak power. The predicted desirability in the contour plot after model reduction recorded the value of 0.847. The contour plot of optimised surface hardness, melted depth and roughness of melted surface is presented in the Appendix B, C and D.

#### 4.10 Validation process

Based on the result from DOE optimization of laser melted die insert, the optimum parameter of 2500 W peak power, 58.27 PRF and 30% overlapping rate with maximum surface hardness of 793.7 HV<sub>0.1</sub>, melted depth of 0.2 mm and 4.08 μm surface roughness with 0.847 desirability factor. While, the experimental data shown highest surface hardness were 793.7 HV<sub>0.1</sub> with 0.21 mm melted depth and 3.89 μm surface roughness using laser processing parameter of 2500 W peak power, 60 Hz PRF and 30% overlapping rate. The validation processes done to assess amount of the 95% confidence interval between the predicated value from DOE optimisation and experimental result. The 95% confidence interval for surface hardness and roughness was calculated by using the formula as shown;

$$95\% \text{ confidence interval} = \frac{\text{Predicted value} - \text{Actual value}}{\text{Predicted value}} \times 100 \quad 4.1$$

The amount of the 95% confidence interval between the predicated value from DOE optimisation and experimental at 2500 W peak power, 60 Hz PRF and 30% overlapping shown hardness of predicted value was 785.2 HV<sub>0.1</sub> while the experiment value was 793.7 HV<sub>0.1</sub> with 95% confidence interval of 1.1%. While the surface roughness value from experiment yield 3.89 mm and the predicted value was 3.91 with 0.5% of 95% confidence interval. It can be validated, that the laser parameter used can be produce the expected properties within the investigated range. The 95% confidence interval of surface hardness and roughness of melted surface is presented in the appendix D and E.

#### 4.11 Analysis of Hot Press Forming Process

The results of the analysis of laser melted die inserts surface were compared to the results of as-received H13 die inserts in terms of thermal stability after the HPF of 22MnB5 steel blanks. In order to determine the effect of simultaneous cooling and forming in HPF process for laser melted inserts, the findings on the characterisation of 22MnB5 steel blanks, specifically the results of metallographic study, hardness properties, and martensite transformation of 22MnB5, were included in this study.

### 4.11.1 Metallographic Study

The microstructure of as-received 22MnB5 steel blank before HPF process is presented in Figure 4.16(a), while Figure 4.16 (b) shows the resulted of 22MnB5 steel blank shape after HPF process. The micrograph in Figure 4.17 shows the martensite structure of 22MnB5 steel after HPF process in the case of as-received H13 die insert. The various laser melting parameter on die insert surface produced various martensite structure in 22MnB5 steel component.

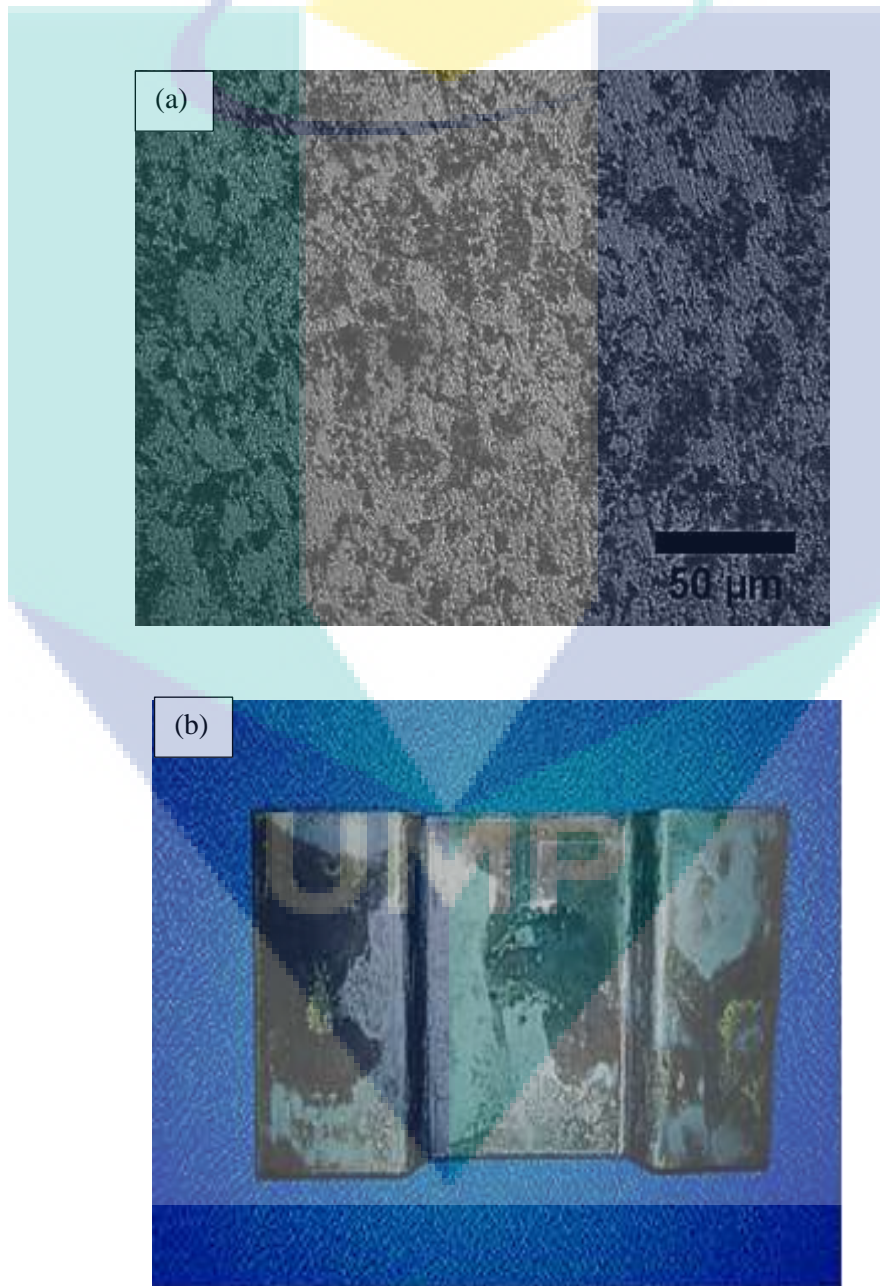


Figure 4.16 As-received 22MnB5 boron steel (a) microstructure of cross section before HPF process, (b) shape after HPF processes



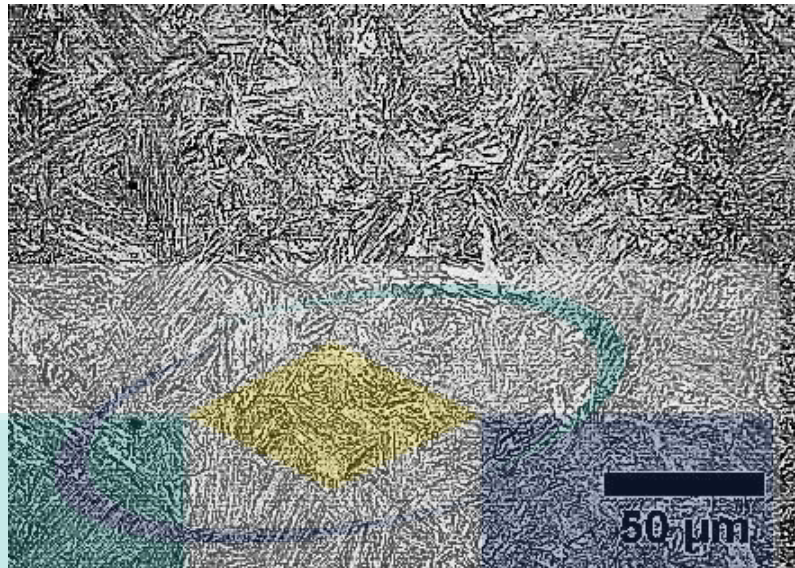


Figure 4.17 Micrograph of 22MnB5 blank after HPF process using as-received H13 die

On the other hand, referring to Figure 4.18, laser melted die insert was found to affect the martensitic structure of hot press formed 22MnB5 steel components. The cross-section of die inserts with melted depth of 0.21, 0.25 and 0.33 mm is shown by Figure 4.18 (b) - (d). Micrographs in Figure 4.18 (e) - (h) compare the martensite structure of hot press formed 22MnB5 steel components responding to the die inserts used respectively. Figure 4.19 (a) shown die insert of as-received AISI H13. The laser melted die inserts shown at Figure 4.18 (b) was processed at 30% overlapping rate and 2100W peak power, while Figure 4.18 (c) was processed at 50% overlapping rate and 2500W peak power and Figure 4.18 (d) was processed at 70% overlapping rate and 2100W peak power with same PRF at 50Hz. Martensite structure at Figure 4.18 (e) – (h) produce after HPF process using various die insert surface. Different overlapping rate on die insert surface produce higher surface roughness caused reduce effect metal to metal contact during HPF process. Effect of roughness on melted die surface can prevent die surface from effect metal to metal contact during HPF processed. Less metal to metal contact between die surface and 22MnB5 blank can improve die lifetime due to lubrication affect when quenching processed in HPF (Fauzun, Aqida et al. 2017). High hardness of die surface can improve die lifetime and produce high quality component.



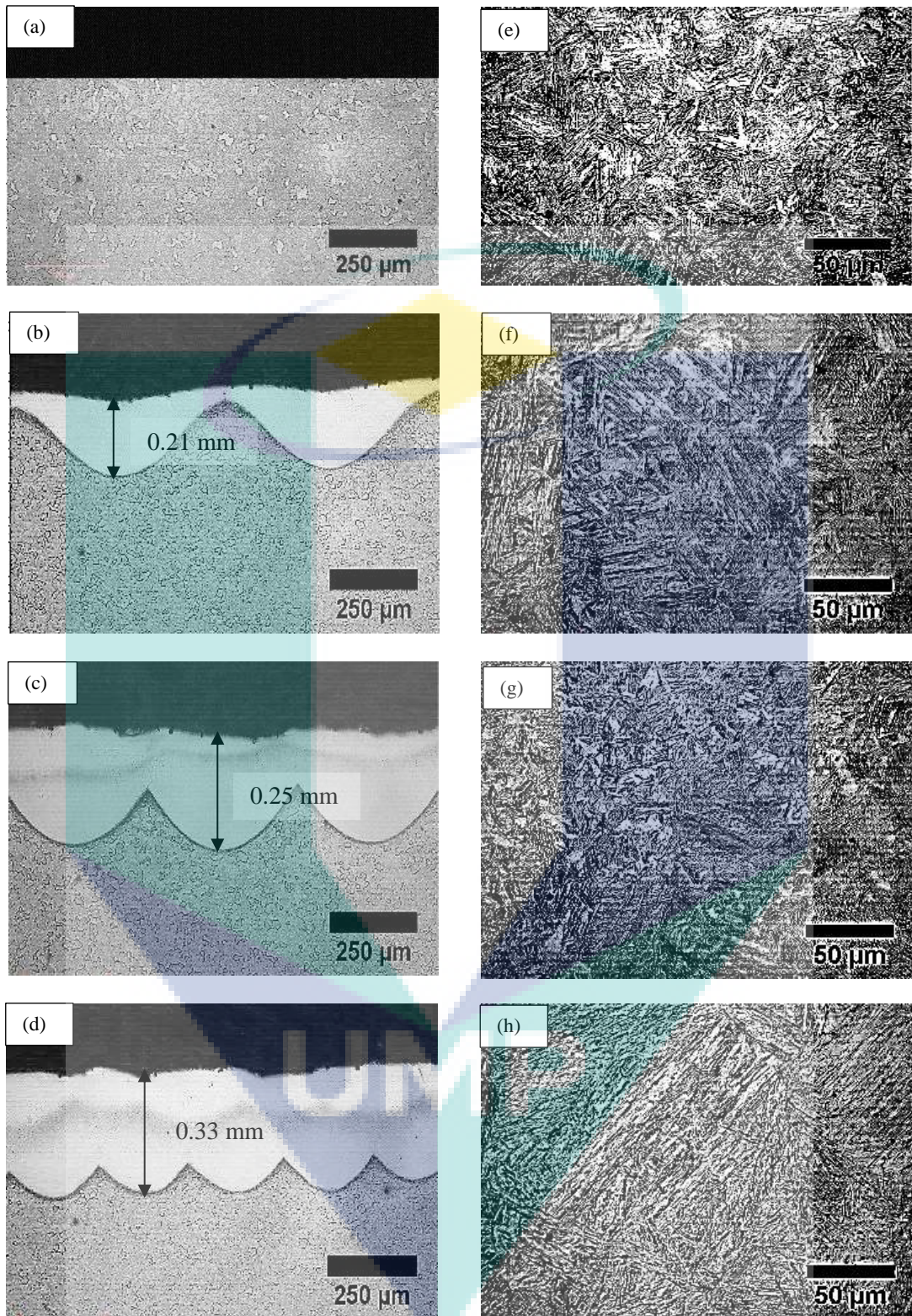


Figure 4.18 Die insert cross section micrograph of (a) as-received AISI H13, (b) laser melted of overlapping rate at (b) 30%, (c) 50%, and; (d) 70% with corresponding of 22MnB5 steel blank structure (e)-(h) after HPF processes



#### 4.11.2 Martensite Percentage

The effect of overlapping rates and peak power on the martensite distribution of 22MnB5 are shown in Figure 4.19, where the martensite structure increased with decreasing overlapping rate. On the contrary, the increase of peak power from 2100 W to 2500 W reduced martensite structure. The martensite structure at the overlapping rates of 50% shown in Figure 4.19 (b) and (e), and martensite structure in Figure 4.19 (a) and (d) produced at 70% overlapped appeared coarser compared to the martensite structure at the overlapping rate of 30% shown in Figure 4.19 (c) and (f). When the overlapping rate for the melted die insert reduced to 30% and peak power increased to 2500 W, the martensite structure of 22MnB5 improved with homogenous distribution. Figure 4.20 shown threshold analysis for micrograph of martensite formation on 22MnB5 steel after HPF processed.

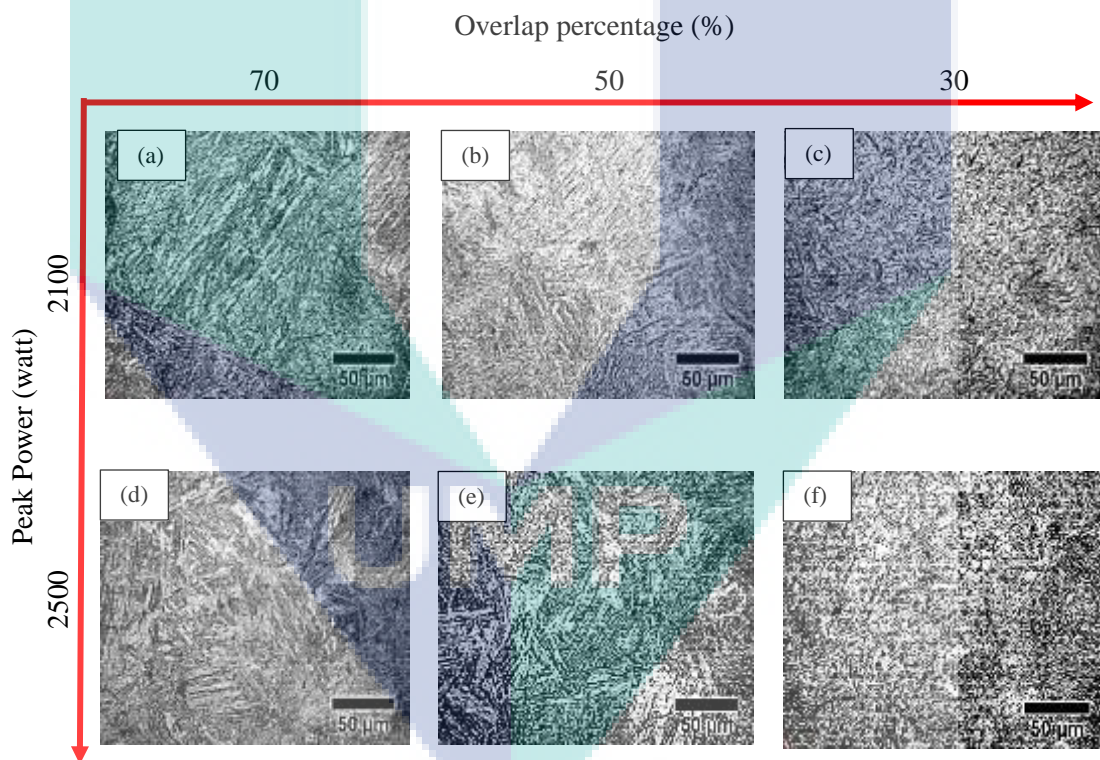


Figure 4.19 Micrograph of martensite formation in 22MnB5 steel blank after HPF process responding to the parameters of laser melted die insert.

The percentages of various martensite phase formation of 22MnB5 after HPF process was analysed using ImageJ software with threshold highlight analysis as revealed in Figure 4.20. The martensite structure formation of 22MnB5 blank increased up to 80.6% when formed using laser melted die surface at the overlapping rate of 30% shown in Figure 4.20 (a). Figure 4.20 (b) yielded martensite structure of 78.5% using laser melted die insert at the overlapping rate of 50%, while Figure 4.20 (c) exhibited martensite structure of 76.3% using laser melted die insert at the overlapping rate of 70%. On the other hand, the martensite structure content of sample was formed using as-received die, which is presented in Figure 4.20 (d), recorded 58.7%. The martensite percentage of 22MnB5 using laser melted die insert increased as much as 27.2% compared to as-received H13 die insert. Overall, the martensite formation for all 22MnB5 samples using different laser melted die inserts recorded a range of between 74.8% and 80.6%.

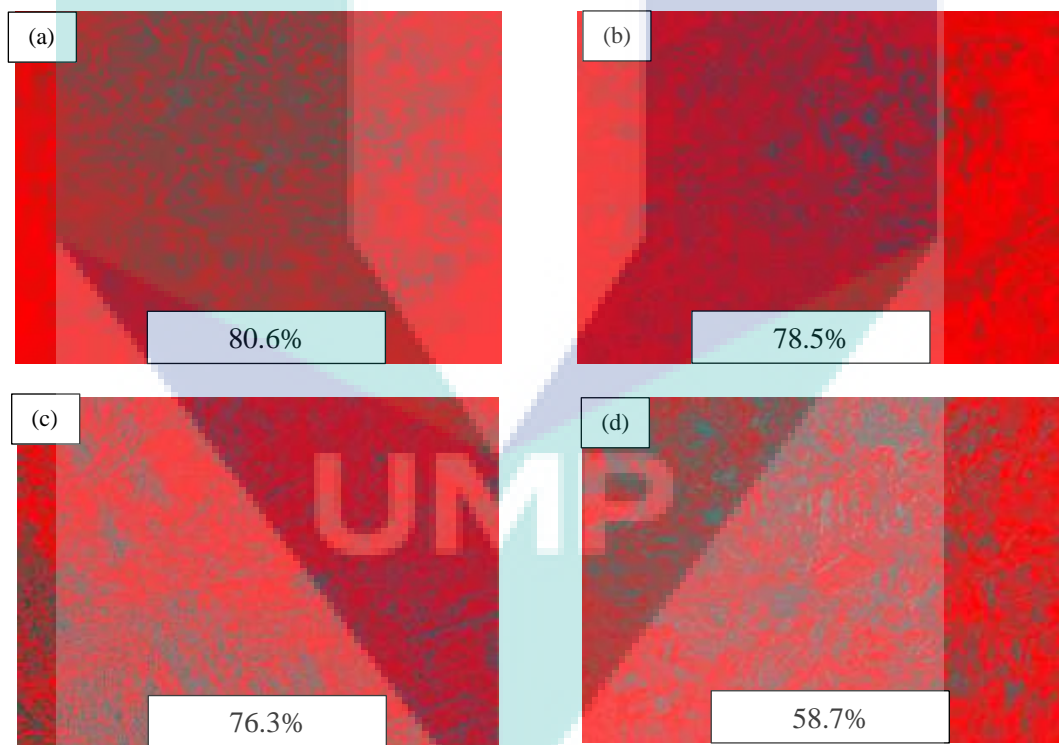


Figure 4.20 Micrograph of martensitic structure in hot press formed 22MnB5 steel with red threshold formed using die insert of (a) 30% overlap, (b) 50% overlap, (c) 70% overlap and (d) as-received die.

### 4.11.3 Hardness Properties of 22MnB5 after HPF

The hardness properties of 22MnB5 steel blank before and after HPF process using as-received H13 die and laser melted die with various laser parameters are demonstrated in Figure 4.21. Hardness properties of as-received 22MnB5 before HPF process recorded 202.5 HV<sub>0.1</sub>. The hardness properties of 22MnB5 with melted die surface after HPF process increased in direct proportional to the laser processing parameter. Meanwhile, the surface hardness of 22MnB5 steel after HPF process using as-received H13 die increase to 386.6 HV<sub>0.1</sub>. On the other hand, HPF process using laser melted die surface increased the surface hardness of 22MnB5 up to 508.1 HV<sub>0.1</sub>. Adding to that, the lowest surface hardness of 22MnB5 after HPF process using laser melted die surface recorded 471.1 HV<sub>0.1</sub>. However, the surface hardness of 22MnB5 increased up to twofold of the as-received blank after HPF process using the laser melted die inserts.

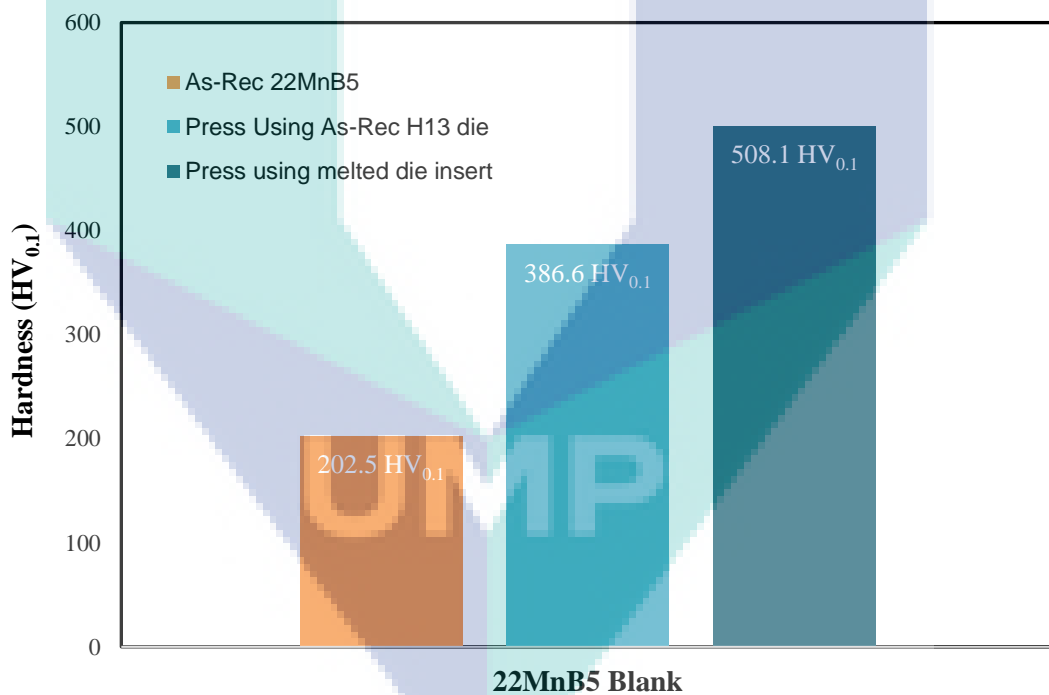


Figure 4.21 Average hardness properties of 22MnB5 steel blank before and after HPF using different die insert

In particular, the hardness properties of samples B1 to B4, which were processed using laser melted die insert at the overlapping rate of 30%, ranged between 500.2 HV<sub>0.1</sub> and 508.1 HV<sub>0.1</sub>. Laser melted die inserts at the overlapping rate of 50% produced hot

press formed components for samples B5 to B9 with hardness properties of between 485.2 HV<sub>0.1</sub> and 500.4 HV<sub>0.1</sub>. The hardness properties of samples B10 to B13 ranged from 471.1 HV<sub>0.1</sub> to 492.7 HV<sub>0.1</sub> after HPF process using melted die surface at the overlapping rate of 70%. Overall, the hardness properties of 22MnB5 after hot press formed using laser melted die inserts increased in relative to the case of as-received H13 die insert. Decreased surface hardness of samples B10, B11, B12, and B13 (at the overlapping rate of 70%) after HPF process, as compared to the surface hardness of samples B1, B2, B3, and B4 (at the overlapping rate of 30%), occurred due to the effect of surface roughness on the die surface. Surface roughness of die surface after laser melting process produced various surface morphologies or roughness (known as texture).

Essentially, the different roughness values for the melted die surface can affect the hardness properties of 22MnB5 steel blank after HPF process. The effect of surface roughness and thermal properties of melted die insert can be improved to produce higher strength surface on 22MnB5 during HPF process (Valls, Hamasaiid et al. 2017). Besides that, higher strength surface of 22MnB5 after press using melted die occurs due to the rapid cooling rate as a function of thermal conductivity on the melted die surface (Valls, Casas et al. 2010). In particular, faster cooling rate during HPF process was found to improve the martensite transformation of 22MnB5, which subsequently increased the hardness of 22MnB5 after HPF using melted die surface, as compared to the use of as-received die (Figure 4.21). Increased hardness of 22MnB5 after HPF using melted die (due to faster cooling rate) allows the contact surface to rapidly cool down, which reflects the thermal properties of melted die surface. Basically, the melted die surface exhibits new surface with different roughness value according to the applied overlapping rate during laser melting process whereas the as-received die exhibits smoother surface.

Laser melted die insert surface contributed to higher martensite structure in hot press formed 22MnB5 components; in other words, the hardness properties were enhanced. High strength components involve martensite structure of 80.6% with tensile strength up to 1630 MPa. Notably, the martensite structure is the common strengthening component for high strength boron steel. The laser melted die insert surface produced higher cooling rate due to refined grain structure and high volume of grain boundary. In fact, grain size affects the thermal conductivity due to the grain boundaries and their effect on the heat transfer during HPF process. When grain size increases, the thermal



conductivity of particles increases too because lesser grain boundaries in material exist. Furthermore, heating steel at high temperature enhances hardenability since the grains involved are larger.

The surface hardness of 22MnB5 after HPF process using melted die surface in this study increased up to 508.1 HV<sub>0.1</sub> compared to the sample with the as-received H13 die insert (386.6 HV<sub>0.1</sub>). The increase of hardness for 22MnB5 after HPF process using melted die may be attributed to the faster cooling rate that allows the contact surface to rapidly cool down; thus, reflecting the thermal properties of melted die surface. Basically, the melted die surface exhibits new surface with different roughness values according to the applied overlapping rate during the laser melting process. The martensite structure of 22MnB5 with melted die surface in this study increased up to 37% compared to the martensite structure of 22MnB5 with as-received die. The roughness on melted die surface can prevent the die surface from the effect of metal-to-metal contact during HPF process. Less metal-to-metal contact between the die surface and 22MnB5 blank can prolong the lifetime of die due to the lubrication effect in quenching process of HPF. This study proved the significance of laser melted surface in enhancing the thermal properties of die surface and improving the quality of 22MnB5 after HPF process.

#### **4.12 Hardness Properties of Die insert after HPF**

Thermal stability of laser melted die inserts was examined after 40 cycles of forming. After the exposure to high temperature of 740°C from 22MnB5 steel during HPF process, the subsurface hardness properties of die inserts did not show significant changes (slightly increased). Figure 4.22 shows the hardness of laser melted die inserts for samples 1, 5, and 10 before and after HPF process. Before HPF process, sample 1 recorded the highest hardness of 778.9 HV<sub>0.1</sub> (with surface hardness of 825.3 HV<sub>0.1</sub> after HPF process), followed by sample 5 with the hardness of 763.9 HV<sub>0.1</sub> (with surface hardness of 763.9 HV<sub>0.1</sub> after HPF process), and sample 10 with the hardness of 672.5 HV<sub>0.1</sub> (with surface hardness of 696.7 HV<sub>0.1</sub> after HPF process). The percentage of hardness increased by 3.5% to 5.7%, which may be due to the exposure of die surface to higher temperature (around 550°C) when it was transferred from blank surface to die insert surface with rapid cooling temperature of 5°C on the die insert surface.

Most steels and refined grain structure are unstable at elevated temperatures of more than 550°C (Sadak 2015). The hardness of the die inserts after HPF process increased due to the effect of thermal cyclic loading (heating and cooling processes). The heating temperature significantly affects the increase or decrease of surface hardness during thermal loading cyclic (heating and cooling processes) and no significant effect by the increase of thermal loading cycles only (Sadak 2015). A prior study on hot work tool steel revealed that the steel hardness decreased when the hot work tool steel surface work at elevated temperature of 575°C and thermal cycle time increased caused the surface start softening at elevated temperature with increased thermal cycle (Caliskanoglu, Siller et al. 2002). The surface hardness of hot work tool steel decreased after 100 cycles of thermal loading due to particle coarsening (Caliskanoglu, Siller et al. 2002). Besides that, decreased surface hardness increases the wear rate at elevated temperature of above 400°C due to recrystallisation (Mori, Bariani et al. 2017). Though high temperature is known to move the grain boundaries and merge the grains size (Busboom, Lytton et al. 1963).

However, the pressure effect during forming of blank is possible in order to retain the fine grain structure of the laser melted die insert (Ventura 2017). After all, the properties of die insert may change due to cyclic thermal loading at elevated temperature. Basically, the effect of thermal cycle on the hardness of die insert depends on the operating temperature and time. The results in Figure 4.23 demonstrated increased hardness of melted die insert after 40 cycles of HPF process due to the effect of quenching processes (heating and cooling processes) during thermal loading cyclic. The effect of heating and cooling processes at elevated temperature improved surface hardness due to cyclic heating and cooling function as heat treatment for the die surface to refine its grain structure. Cyclic thermal loading with constant surface temperature (without increasing the temperature of die inserts) possibly improve or increase the surface hardness of the melted die surface.



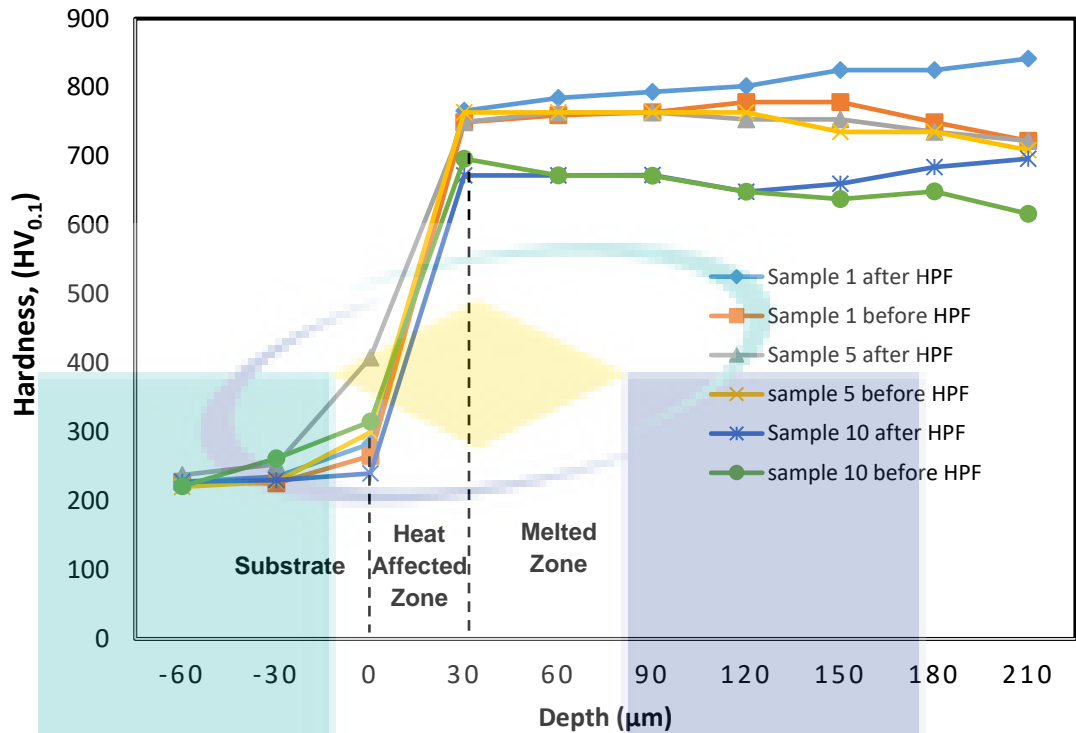


Figure 4.22 Hardness properties of melted surface before and after HPF of 22MnB5 steel blank as a function of distance from surface

The hardness of melted die inserted after 40 cycles of HPF process in this study increased due to the effect of quenching process during thermal loading cyclic. The effect of heating and cooling processes at elevated temperature increased the surface hardness of die insert surface due to the cyclic heating and cooling function as heat treatment for the die surface to refine its grain structure. The cooling rate of laser melted die surface was higher than the cooling rate of as-received die insert given the roughness effect of melted die surface. Higher cooling rate causes the melted die surface to rapidly cool down during HPF process. Thermal loading cyclic with constant surface temperature at elevated temperature can improve the surface hardness of melted die surface. Furthermore, the effect of thermal cycle on die insert hardness depends on the cyclic temperature exposure.

#### 4.13 Thermal Analysis of Die Insert After HPF Processes

Thermal analysis of die inserts was based on temperatures of die surface collected by data logger from thermocouple during HPF process. Thermocouple was attached at 1 mm inside lower die insert surface before HPF process start until HPF process finish

formed 40 pieces of 22MnB5 steel for every die insert surface. During HPF processes, the temperature of melted die surface stabilised after eight 8 cycles of forming process (heating and cooling). The first eight cycles were the transient phase while the following cycles were at a steady state phase where the temperature of HPF die inserts is consistent during the forming process. While for the as-received H13 die insert, the temperature was stable after 10 cycles of HPF process. The initial temperature for all die inserts before the HPF process was at 5°C while the temperature for 22MnB5 blank was at 950°C. In particular, Figure 4.23 (a – d) shows the thermal distribution of the laser melted die surface during HPF process at an overlapping rate of 30% for sample 11, 50% for sample 5, 70% for sample 4 and the as-received H13 steel (in this order).

Temperature distribution at various die insert surface during quenching in HPF process is shown in Figure 4.23. The average quenching temperature within 1 mm of die insert surface at 30%, 50% and 70% overlapping rate was 40.4°C, 50.2°C and 58.5°C, while for the as-received die insert, the average quenching temperature was at 60.9°C. This result shows that the as-received H13 die absorbed more heat during quenching process compared to the melted die surface, while the melted die surface can transfer heat rapidly. The less effect of metal to metal contact (die surface and 22MnB5) shows that flat surface of as-received H13 absorbed more heat up to 20.7°C when the austenised 22MnB5 blank was in contact with die surface. In the laser melted die insert, the contact was the lowest with the die insert temperature of 23.6°C. But no significant effect is shown in the thermal distribution. The effect of temperature distribution in the die insert surface was also analysed by corresponding it to the results of 22MnB5 blanks properties after HPF forming where, the surface hardness of 22MnB5 increased up to twofold of the as-received blank after HPF using melted die insert.

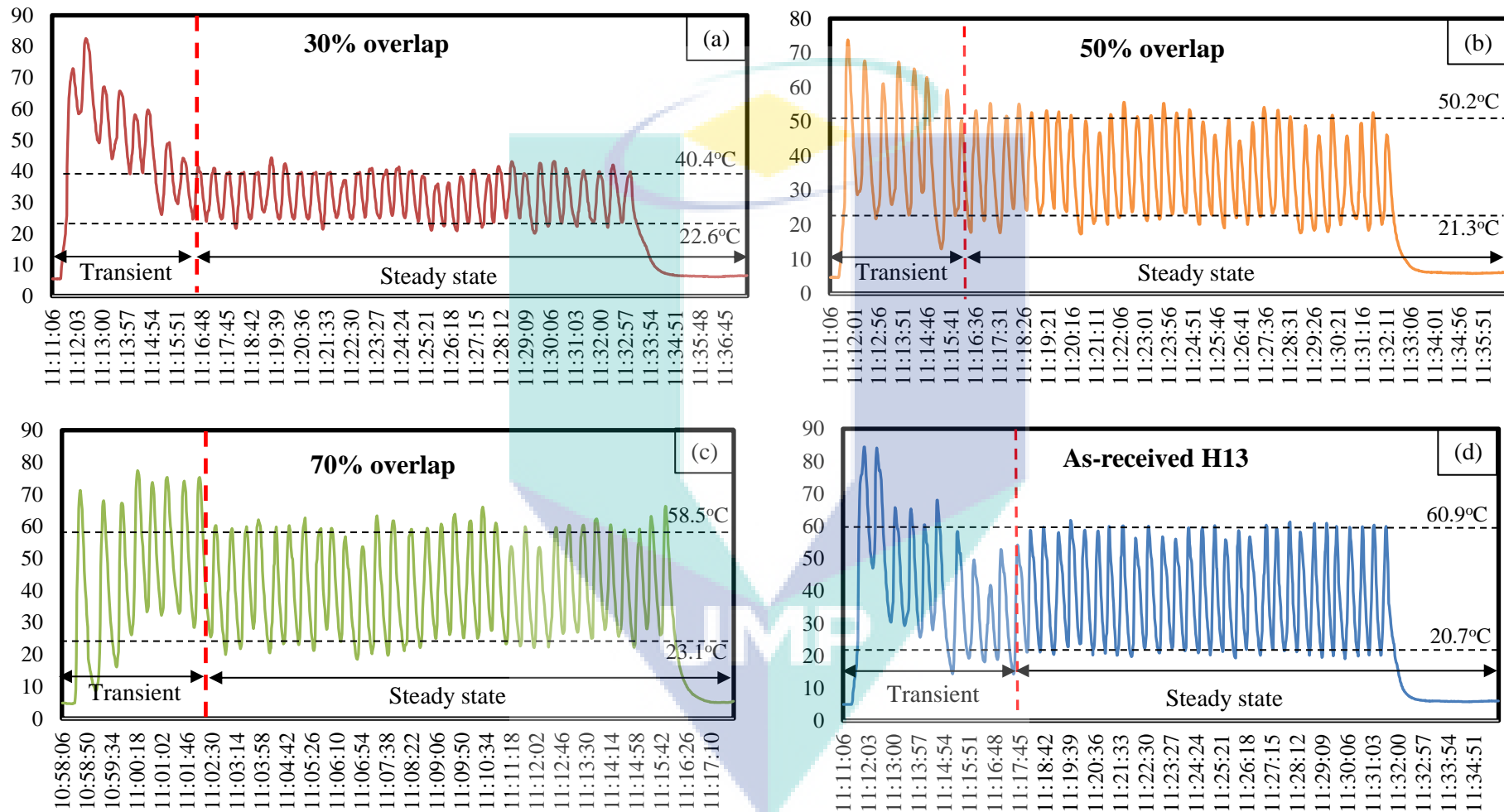


Figure 4.23 Maximum and minimum thermal distribution in die inserts with (a) melted surface of 30% overlap, (b) melted surface of 50% overlap, (c) laser melted surface of 70% overlap and; (d) as-received AISI H13 condition during 40 cycles of HPF.

The die inserts for sample 11 at 30% overlapping rate absorbed an average temperature of 40.4°C from 22MnB5 blank during HPF process as shown in Figure 4.23 (a). The laser melted die insert with 50% and 70% overlap absorbed an average temperature of 50.2°C and 58.5°C as shown in Figure 4.23 (b) and (c). The highest average temperature absorbed by the as-received H13 die insert surface during HPF process was 60.9°C as shown in Figure 4.23 (d). Less temperature was absorbed in sample 11 with 30% overlap due to less effect of metal to metal contact during HPF process, which contributed fast heat transfer. High cooling rate in the laser melted die insert allows fast cooling when the die insert surface was in contact with the 950°C temperature 22MnB5 blank. The fast cooling rate enhanced the properties of 22MnB5 blank after forming by the laser melted die insert. High cooling or quenching rate is required to produce high strength component in HPF.

Efficient heat transfer contributes to the increase of cooling rate during HPF process and produced high strength of 22MnB5 blanks. This can prevent materials from premature degradation due to substantial overheating which caused heat to diffuse very fast from material. The different rate of heat transfer on die surface depends on the grain structure or microstructure resulted from the formed blanks. Other than, enhanced surface properties (hardness) of melted die insert after laser melting process affects the heat transfer during forming process. Other than that, thermal conductivity changes in the laser melted die insert varies the ability of the surface to transport heat energy from high temperature region to low temperature region. The thermal conductivity of materials depends on its crystallinity or grain size. High quenching rate require high thermal conductivity on die surface to increased cooling rate during HPF processed (Zulhishamuddin and Aqida 2015). Sample at 30% overlapping rate indicates that the smaller grain size has improved thermal conductivity when HPF was conducted using sample 11. Sample 11 shows a high cooling rate (fast heat transfer) followed by sample 4 during HPF process.

In addition, thermal stability is another important factor to conduct material at high temperature. With thermal stability, the laser melted surface has the tendency to retain its properties at high working temperature of forming process. The die insert surface temperature was lower than (austenite temperature) of 950°C due to the heat loss during the transfer of 22MnB5 blank from the furnace to the HPF die. The blank and die inserts

were held for 8 seconds (quenching process), while the temperature of die insert decreased over time due to the consistent water flow at 5°C within the cooling channels that were positioned underneath the die insert surface.

#### 4.13.1 Thermal Stability and Performance of Hot Press Forming Die Insert

. Laser melting was used to modify the surface properties of die insert. Various selected parameter chooses to melted die surface. The surface hardness of laser melted die insert was in the range of 684.4 – 793.7 HV<sub>0.1</sub>. Conducting HPF using both as-received and laser melted die inserts produced 22MnB5 steel components with high hardness properties due to rapid heating and cooling (quenching) processed on 22MnB5 during HPF processes.

The hardness properties of as-received 22MnB5 were 202.5 HV<sub>0.1</sub> before hot press forming process. Hardness properties range of formed 22MnB5 components was 386.6 – 508.1 HV<sub>0.1</sub>. The surface hardness of 22MnB5 after HPF using melted die surface increased up to 508.1 HV<sub>0.1</sub> compared to the samples (of 386.6 HV<sub>0.1</sub>) that were formed using as-received H13 die insert. Increased hardness of 22MnB5 after HPF using melted die due to faster cooling rate allow faster cool down the contact surface which related to thermal properties of melted die surface. All melted die surface has new surface with different roughness value depend on overlapping rate during laser melting processed. While as-received die has smooth surface without any roughness increased effect metal to metal contact.

Die insert surface efficiency to cooled down blanks during HPF process is an important factor that influence the heat transfers during quenching process. The martensite composition of 22MnB5 depends on the properties of die insert and cooling factor during quenching process. The laser melted die surface produced 22MnB5 blanks which consists of martensite structure up to 80.6%. While the 22MnB5 blank that was formed using the as-received die produced 58.7% martensite structure. The martensite phase formation for all 22MnB5 samples processed using different laser melted die insert ranged between 74.8% and 80.6%. The martensite structure formation was due to the effect of overlapping rate. Besides, laser parameter produced a higher surface roughness that reduced the effect of metal to metal contact. The effect of surface roughness on the

laser melted die surface prevents the die surface from fully in contact during HPF processed. Less metal to metal contact between die surface and 22MnB5 blank can improved die lifetime (Shihomatsu, Button et al. 2016)

The surface hardness properties of melted die insert range before HPF processed were 672.5 -778.9 HV<sub>0.1</sub>. After HPF processed of 40 cycles, hardness of melted die inserts increased up to 825.3 HV<sub>0.1</sub>. Hardness of melted die insert after 40 cycle HPF processes increased due to effect of quenching processes during thermal loading cyclic. The effect of heating and cooling at elevated temperature caused surface hardness improved due to cyclic heating and cooling function as heat treatment of die surface and refine grain structure. The cooling rate of laser melted die surface higher than cooling rate of as-received die insert caused due to roughness effect of melted die surface. Higher cooling rate caused the melted die surface cool down much faster during HPF processed. Thermal loading cyclic with constant surface temperature at elevated temperature possibly improve or increased surface hardness of melted die surface. The effect of thermal cycle on die insert hardness influence by cyclic of temperature exposure. Increased hardness in die surface possibility increased die lifetime.

#### **4.13.2 Thermal Distribution of Die Insert**

The average thermal distribution analysis of die insert surface indicates heat transfer from high temperature blank surface to the die insert sub-surface processed at 30% overlapping rate was up to 40.4°C. The temperature was measured at 1 mm depth from die surface during HPF processing. The melted and as-received die insert surface experienced fast cooling between 20.7°C and 23.1°C temperature respectively when the upper and lower die opened. Rapid heat transfer across melted die surface during HPF processed produced high surface hardness of 22MnB5 blank. These findings shown hardness of 22MnB5 increased up to two times after HPF process using laser melted die insert. This was due to rapid cooling of the high temperature blank on die insert surface. A higher heat transfer of the laser melted die surface during HPF process was contributed by its surface texture refined structure and high volume of grain boundary. Thus, the laser melted die insert surface has a significant impact to the forming of 22MnB5 blank steel properties.



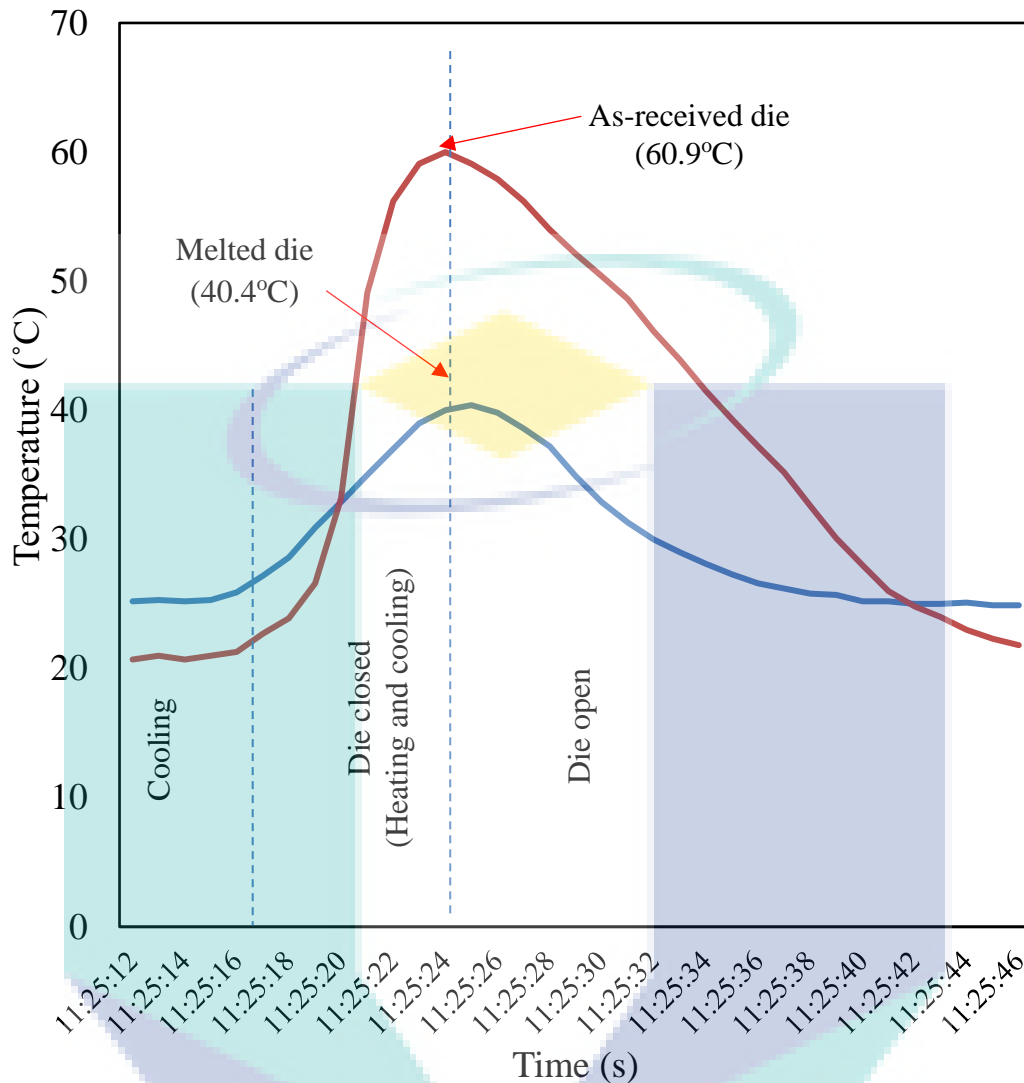


Figure 4.24 Temperature history of as-received and laser melted HPF die inserts from experimental measurement.

Figure 4.24 shows the temperature history of the as-received and the laser melted die insert  $t$  at the depth of 1 mm from the die surface for one HPF cycle. The temperature of melted die surface during HPF process when both upper and lower die in close position was 40.4°C. Whereas the temperature for the as-received die was recorded at 60.9°C. The results show a temperature difference up to 33.7% between the laser melted die and the as-received die insert. Besides that, the cooling rate of the laser melted die surface was higher than the cooling rate of as-received die insert due to less metal to metal contact effect. The higher cooling rate rapidly cools down the melted die surface during HPF process. The above results indicated the thermal properties were relatively enhanced in the laser melted die insert surface, which attributed to the rapid heat transfer across the

die surface within the depth of 1 mm from the surface during HPF process, apart from producing high strength component with improved twofold hardness of 22MnB5 blank.

#### 4.14 Summary

This chapter discussed the findings to fulfil the main and sub-objectives of the research; which is to enhance the surface properties via laser processing, properties of 22MnB5 that formed using laser melted die insert and thermal behaviour of the laser melted die insert in HPF environment. The laser melted and the as-received die insert were characterised to show the effect of laser melting process on the surface properties. All samples were characterised for surface roughness, melt depth, surface morphology, hardness properties, metallographic study, chemical composition and phase analysis. The effect of laser parameter was discussed related to the surface properties after the laser melting process. Results were compared between the melted die and the as-received die properties. The findings from objective one shows that the surface properties of the laser melted die insert enhanced due to refined grain structure which influence to surface hardness properties. The surface hardness of melted die inserts increased up to 793.7 HV<sub>0.1</sub>, that increased up to three times from its substrate. The laser processing parameter; namely overlapping rate, peak power and PRF shows a significant effect to the melted die surface properties. The laser processing parameters at high laser energy with low PRF produced a deeper melt depth up to 0.33 mm with the influence of overlapping rate. While varied chemical composition on the melted die surface contributed by atomic diffusion at high surface temperature from the substrate to the melted layer during melting process as a result of laser energy absorption. The analysis for surface roughness shows a high overlapping rate produced smoother surface compared to samples processed at a lower overlapping rate. The phase analysis shows a lower peak intensity in samples that were processed at a lower overlapping rate. The optimisation analysis shows optimum laser parameter to produce suitable die insert for HPF process is at 2500 W peak power, 60 Hz PRF and 30% overlapping rate.

The melted and the as-received die insert then was used to form 22MnB5 using HPF process. The properties of 22MnB5 after formed using melted die insert were then characterized to show the effect of melted die surface properties on 22MnB5 blank after HPF processes. The results show that the hardness properties of 22MnB5 increased in

direct proportional to the laser processing parameter after formed using the melted die surface. The surface hardness of 22MnB5 increased up to 508.1 HV<sub>0.1</sub> after formed using melted die insert. Meanwhile, the surface hardness of 22MnB5 steel after HPF process using the as-received H13 die increase to 386.6 HV<sub>0.1</sub>. On the other hand, the surface hardness of 22MnB5 increased up to twofold of the as-received blank after HPF process using the laser melted die inserts. The hardness of 22MnB5 blank increased after forming using melted die surface due to martensite transformation. The higher hardness of 22MnB5 sample contain 80.6% martensite structure. Effective cooling rate during quenching processes contributed to improve surface properties of 22MnB5. The thermal behaviour during HPF process indicates the temperature during quenching process in the melted die insert was less than the as-received die inserts. The temperature absorbed in melted die insert was 40.4°C, while as-received die inserted absorbed temperature up to 60.9°C. This result shown during HPF processes, high thermal properties of melted die insert material transfers heats rapidly during quenching process. Rapid heat transfer in melted die surface during quenching process improved the surface hardness of 22MnB5 sample. The above findings fulfilled the main objective to produce high strength component via hot press forming with laser modified die inserts.

The logo for UMP (Universiti Malaysia Perlis) is a large, stylized letter 'U' composed of several overlapping triangles in shades of teal and light blue. The letters 'UMP' are printed in white, bold, sans-serif font across the center of the 'U' shape.

UMP

## CHAPTER 5

### CONCLUSION AND RECOMMENDATION

#### 5.1 Conclusion

This research was conducted to produce high strength component via hot press forming with laser modified die inserts. Overall, the obtained results of this study demonstrated revealed the effect of laser processing parameters on the properties of the modified layer. The laser melting process on the die surface in this study exhibited various laser spot patterns due effect of laser processing parameter. The surface morphology was depended on the overlapping rate, where higher processing speed produced lower overlapping rate and vies versa. This study showed that the overlapping rate of 70% produced smoother surface compared to other overlapping rates of 30% and 50%. Furthermore, the depth of the molten pool at the overlapping rate of 70% was the highest due to high laser energy and more molten pool caused delay solidification. High energy and low processing speed cause a large amount of energy absorbed on the sample surface during the laser process, which explains the effect on the melt depth of melted pool. The melted layer depth increased with increasing laser irradiance. Higher surface temperature which resulted from a higher irradiance promoted energy penetration and efficient surface melting which improved the surface absorptance. While the lowest melt depth produced at 30% overlapping. During laser heating on die surface, the elements diffused from the substrate region to the molten region. Increased element distribution in the melted layer is the effect of laser irradiance and interaction time. This study shows the melted die insert produced smaller crystallite and affect to increased surface hardness of melted layer. From the metallographic study, the grain structure of the melted layer refined as much as 66.4% compared to the as-received H13 steel. The average grain size for the melted depth was at 1.02  $\mu\text{m}$  while the as-received sample was at 3.02  $\mu\text{m}$ . This is parallel with the

hardness findings. where the surface hardness of melted layer increased three time from its substrate (228.1 HV<sub>0.1</sub>) up to 793.7 HV<sub>0.1</sub>.

From the HPF process, the laser melted surface can be used to enhance thermal properties of dies surface and improved the properties of 22MnB5 blank after forming process. Rapid heat transfer across the die surface during HPF process produced high surface hardness of 22MnB5 blank up to 508.1 HV<sub>0.1</sub> when formed using melted die insert compared to the samples (of 386.6 HV<sub>0.1</sub>) that were formed using as-received H13 die insert. The hardness of 22MnB5 can be improved using laser melted die insert. The thermal properties of melted die surface enhanced due to refined grain boundary and high hardness surface. Textured effect on the melted die surface can reduce the die surface from metal to metal contact during HPF process. Less metal to metal contact between die surface and 22MnB5 blank can thus prolong die lifetime. The martensite structure of 22MnB5 increased up to 80.6% when formed using melted die insert. Increased percentage of martensite structure in 22MnB5 subsequently increased the surface hardness of 22MnB5 after HPF using melted die surface that produce high strength component up to 1600 MPa.

The thermal distribution analysis of die insert surface indicates that heat transfer from high temperature blank surface to the melted die insert during quenching process was measured as 40.4°C. While the temperature for the as-received die was recorded at 60.9°C. This shows that the cooling rate of laser melted die surface was higher than the cooling rate of as-received die insert with 33.7% difference. A higher cooling rate rapidly cools down the melted die surface during quenching process. This study demonstrated the significance of laser melted surface in enhancing the thermal properties of die surface and improving the quality of 22MnB5 in HPF process. When the upper and lower die opened, the temperature in all die insert reduced between 20.7°C and 23.1°C. Rapid heat transfer across the melted die surface during HPF processed produced high surface hardness of 22MnB5 blank. The above results indicated that thermal properties were enhanced relatively in the laser melted die insert surface that produced high strength component of 22MnB5 blank steel after HPF process.

## 5.2 Recommendation

Surface modification using laser melting technique on die surface shown surface and sub-surface properties improved. However, more test and analysis should be conduct on melted surface such as;

- i. Hot press forming processed on melted die insert more than 100 cycle need to be study in future to shows more effect of cyclic heating and cooling on melted die surface during HPF processes.
- ii. Thermal wear test and analysis on melted die insert surface to predict die lifetime.
- iii. Attach temperature reader on 22MnB5 blank steel surface to show actual blank temperature when die close and open during HPF process to formed 22MnB5 blank steel and get temperature profile of 22MnB5 during HPF process.
- iv. Toughness test of melted die insert to test and analysis the ability of a die insert surface absorb energy and plastically deform.

The logo for UMP (Universiti Malaysia Perlis) is a large, stylized letter 'U' shape. The top part of the 'U' is a light blue horizontal bar. The two vertical sides of the 'U' are light blue on the left and light purple on the right. The bottom part of the 'U' is a light blue triangle pointing downwards. The letters 'UMMP' are written in white, bold, sans-serif font across the bottom of the 'U' shape.

UMMP



## REFERENCES

- Altan, T. (2007). "Hot-stamping boron-alloyed steels for automotive parts Part II: Microstructure, material strength changes during hot stamping." *Stamping Journal* **19**(1): 14-15.
- Altan, T. and M. Deshpande (2011). "Selection of die materials and surface treatments for increasing die life in hot and warm forging." *ERC for Net Shape Forming, Paper(644-FIA)*: 1-32.
- Aqida, S., D. Brabazon and S. Naher (2011). "Designing pulse laser surface modification of H13 steel using response surface method."
- Aqida, S., D. Brabazon and S. Naher (2013). "Atomic diffusion in laser surface modified AISI H13 steel." *Applied Physics A* **112**(1): 139-142.
- Aqida, S., D. Brabazon and S. Naher (2013). "An investigation of phase transformation and crystallinity in laser surface modified H13 steel." *Applied Physics A* **110**(3): 673-678.
- Aqida, S., M. Maurel, D. Brabazon, S. Naher and M. Rosso (2009). "Thermal stability of laser treated die material for semi-solid metal forming." *International Journal of Material Forming* **2**(1): 761.
- Aqida, S., M. Maurel, D. Brabazon, S. Naher and M. Rosso (2009). "Thermal stability of laser treated die material for semi-solid metal forming." *International Journal of Material Forming* **2**: 761-764.
- Aqida, S., S. Naher and D. Brabazon (2011). Laser surface modification of H13 die steel using different laser spot sizes. *AIP Conference Proceedings, AIP*.
- Aqida, S., S. Naher and D. Brabazon (2011). "Laser surface modification of H13 die steel using different laser spot sizes."
- Aqida, S. N., S. Ahmad, S. Naher and D. Brabazon (2012). Thermal simulation of laser surface modification of H13 die steel. *Key Engineering Materials, Trans Tech Publ*.
- Aqida, S. N., D. Brabazon and S. Naher (2011). "Designing pulse laser surface modification of H13 steel using response surface method."
- ASSAB (2008). ASSAB 8407 SUPREME.
- Aziz, N. and S. Aqida (2013). Optimization of quenching process in hot press forming of 22MnB5 steel for high strength properties for publication in. *IOP Conference Series: Materials Science and Engineering, IOP Publishing*.
- Azushima, A., K. Uda and A. Yanagida (2012). "Friction behavior of aluminum-coated 22MnB5 in hot stamping under dry and lubricated conditions." *Journal of Materials Processing Technology* **212**(5): 1014-1021.

- Bariani, P., S. Bruschi, A. Ghiotti and A. Turetta (2008). "Testing formability in the hot stamping of HSS." *CIRP Annals-Manufacturing Technology* **57**(1): 265-268.
- Bariman, N., S. N. Aqida and F. Fauzun (2017). Laser Melting of High Thermal Conductivity Steel (HTCS) Surface. *Materials Science Forum*.
- Beckermann, C. (1997). "Modeling segregation and grain structure development in equiaxed solidification with convection." *JOM* **49**(3): 13-17.
- Bergeron, J. C., E. Burns, J. Bushie, H. Sandberg, A. V. Heuvel, A. Carrico and W. Forge (2004). "Failure Analysis of H13 Gear Blank Forging Dies." Michigan Technological University: 1-25.
- Burger, N., A. Laachachi, M. Ferriol, M. Lutz, V. Toniazzo and D. Ruch (2016). "Review of thermal conductivity in composites: mechanisms, parameters and theory." *Progress in Polymer Science* **61**: 1-28.
- Busboom, H. J., J. L. Lytton and O. D. Sherby (1963). Influence of Grain Boundaries on High Temperature Strength of Polycrystalline Solids, STANFORD UNIV CA.
- Calcagnotto, M., D. Ponge, Y. Adachi and D. Raabe (2009). Effect of grain refinement on strength and ductility in dual-phase steels. Proceedings of the 2nd International Symposium on Steel Science Strength, Plasticity and Fracture in Steels, Fundamentals and Novel Approaches for New Demands, Kyoto, Japan.
- Caliskanoglu, D., I. Siller, R. Ebner, H. Leitner, F. Jeglitsch and W. Waldhauser (2002). Thermal fatigue and softening behavior of hot work tool steels. Proceedings of the 6th International tooling conference, The use of tools steels.
- Cao, J., F. Liu, X. Lin, C. Huang, J. Chen and W. Huang (2013). "Effect of overlap rate on recrystallization behaviors of Laser Solid Formed Inconel 718 superalloy." *Optics & Laser Technology* **45**: 228-235.
- Chen, C., Y. Wang, H. Ou, Y. He and X. Tang (2014). "A review on remanufacture of dies and moulds." *Journal of Cleaner Production* **64**: 13-23.
- Cherkaoui, M. and L. Capolungo (2009). Structure, Mechanical Properties, and Applications of Nanocrystalline Materials. *Atomistic and Continuum Modeling of Nanocrystalline Materials*, Springer: 29-52.
- Cong, D., H. Zhou, Z. Ren, H. Zhang, L. Ren, C. Meng and C. Wang (2014). "Thermal fatigue resistance of hot work die steel repaired by partial laser surface remelting and alloying process." *Optics and Lasers in Engineering* **54**: 55-61.
- Cong, D., H. Zhou, Z. Ren, Z. Zhang, H. Zhang, C. Meng and C. Wang (2014). "The thermal fatigue resistance of H13 steel repaired by a biomimetic laser remelting process." *Materials & Design* **55**: 597-604.
- Cong, D., H. Zhou, M. Yang, Z. Zhang, P. Zhang, C. Meng and C. Wang (2013). "The mechanical properties of H13 die steel repaired by a biomimetic laser technique." *Optics & Laser Technology* **53**: 1-8.

- Dobrzański, L., M. Piec, A. Klimpel and Z. Trojanowa (2007). "Surface modification of hot work tool steel by high-power diode laser." *International Journal of Machine Tools and Manufacture* **47**(5): 773-778.
- Domínguez-García, P. and M. A. Rubio (2009). "JChainsAnalyser: an ImageJ-based stand-alone application for the study of magneto-rheological fluids." *Computer Physics Communications* **180**(10): 1956-1960.
- Du, C., J. Hoefnagels, S. Kölling, M. Geers, J. Sietsma, R. Petrov, V. Bliznuk, P. Koenraad, D. Schryvers and B. Amin-Ahmadi (2018). "Martensite crystallography and chemistry in dual phase and fully martensitic steels." *Materials Characterization* **139**: 411-420.
- Elhamali, S. M., K. Etmimi and A. Usha (2013). The Effect of Laser Surface Melting on the Microstructure and Mechanical Properties of Low Carbon Steel. *Proceedings of World Academy of Science, Engineering and Technology, World Academy of Science, Engineering and Technology (WASET)*.
- Fan, Z., X. Lei, L. Wang, X. Yang and R. E. Sanders (2018). "Influence of quenching rate and aging on bendability of AA6016 sheet." *Materials Science and Engineering: A* **730**: 317-327.
- Farahmand, P. and R. Kovacevic (2014). "An experimental–numerical investigation of heat distribution and stress field in single-and multi-track laser cladding by a high-power direct diode laser." *Optics & Laser Technology* **63**: 154-168.
- Fauzun, F., S. N. Aqida and M. bin Wahab (2013). Laser Surface Modification of AISI 1025 Low Carbon Steel Using Pulsed Nd: YAG Laser for Enhance Surface Properties. *Key Engineering Materials, Trans Tech Publ.*
- Fauzun, F., S. N. Aqida, I. Ismail and N. Bariman (2017). Micro-Bulges Investigation on Laser Modified Tool Steel Surface. *MATEC Web of Conferences, EDP Sciences.*
- Fauzun, F., S. N. Aqida, M. S. Wahab and W. Saidin (2014). Optimisation of Pulsed Nd: YAG Laser Processing of Gray Cast Iron for Enhanced Surface Properties. *Advanced Materials Research, Trans Tech Publ.*
- Fracasso, F. (2010). Influence of quench rate on the hardness obtained after artificial ageing of an Al-Si-Mg alloy.
- Freiburg, D., D. Biermann, A. Peuker, P. Kersting, H.-J. Maier, K. Möhwald, P. Knödler and M. Otten (2014). "Development and Analysis of Microstructures for the Transplantation of Thermally Sprayed Coatings." *Procedia CIRP* **14**: 245-250.
- Fuchs, K. (2002). Hot-work tool steels with improved properties for die casting applications. 6th International Tooling Conference, Karlstad University.
- Ganeev, R. (2002). "Low-power laser hardening of steels." *Journal of materials processing technology* **121**(2-3): 414-419.

- Ganesh, P., R. Sundar, H. Kumar, R. Kaul, K. Ranganathan, P. Hedao, P. Tiwari, L. Kukreja, S. Oak and S. Dasari (2012). "Studies on laser peening of spring steel for automotive applications." *Optics and Lasers in Engineering* **50**(5): 678-686.
- Gao, K., S. Song, S. Li and H. Fu (2016). "Characterization of microstructures and growth orientation deviating of Al<sub>2</sub>Cu phase dendrite at different directional solidification rates." *Journal of Alloys and Compounds* **660**: 73-79.
- Gao, W., S. Zhao, Y. Wang, Z. Zhang, C. Zhou and X. Lin (2015). "Refinement of Fe-based alloy doped Ti cladding layer." *Surface and Coatings Technology* **270**: 16-23.
- Ghiotti, A., F. Sgarabotto and S. Bruschi (2013). "A novel approach to wear testing in hot stamping of high strength boron steel sheets." *wear* **302**(1): 1319-1326.
- Go, S. (2014). "Failure Analysis of Fractured Tool Steel Die Plate." 1–6.
- Gordillo, N., C. G. de Castro, E. Tejado, J. Pastor, G. Balabanian, M. Panizo-Laiz, R. Gonzalez-Arrabal, J. Perlado and J. del Rio (2017). "On the thermal stability of the nanostructured tungsten coatings." *Surface and Coatings Technology* **325**: 588-593.
- Grishagin, I. V. (2015). "Automatic cell counting with ImageJ." *Analytical biochemistry* **473**: 63-65.
- Group, A. I. R. C. R. A. F. T. E. (1970). "Introduction to surface integrity."
- Gui, Z.-X., K. Wang, Y.-S. Zhang and B. Zhu (2014). "Cracking and interfacial debonding of the Al–Si coating in hot stamping of pre-coated boron steel." *Applied Surface Science* **316**: 595-603.
- Guler, H. and R. Ozcan (2014). "Comparison of hot and cold stamping simulation of Usibor 1500 prototype model." *Indian Journal of Engineering & Materials Sciences* **21**: 387-396.
- Houndri, A., S. Polymenis, Y. Chryssoulakis and D. Pantelis (1992). "Laser melting treatment by overlapping passes of preheated nickel electrodeposited coatings on Al– Si alloy." *Metallurgical Transactions A* **23**(6): 1801-1806.
- Hu, Y. and Z. Yao (2008). "Overlapping rate effect on laser shock processing of 1045 steel by small spots with Nd: YAG pulsed laser." *Surface and Coatings Technology* **202**(8): 1517-1525.
- Huang, C., Y. Zhang, J. Shen and R. Vilar (2011). "Thermal stability and oxidation resistance of laser clad TiVCrAlSi high entropy alloy coatings on Ti–6Al–4V alloy." *Surface and Coatings Technology* **206**(6): 1389-1395.
- Jae-Ho, L., J. Jeong-Hwan, J. Byeong-Don, Y. Hong-Sup and M. Young-Hoon (2009). "Application of direct laser metal tooling for AISI H13 tool steel." *Transactions of Nonferrous Metals Society of China* **19**: s284-s287.

- Jae-Ho, L., J. Jeong-Hwan, J. Byeong-Don, S. Young-Myung and M. Young-Hoon (2009). "Laser surface hardening of AISI H13 tool steel." *Transactions of Nonferrous Metals Society of China* **19**(4): 917-920.
- Jeong-Hwan, J., L. Jae-Ho, J. Byeong-Don and M. Young-Hoon (2009). "Flow characteristics of aluminum coated boron steel in hot press forming." *Transactions of Nonferrous Metals Society of China* **19**(4): 913-916.
- Jhavar, S., C. Paul and N. Jain (2013). "Causes of failure and repairing options for dies and molds: A review." *Engineering Failure Analysis* **34**: 519-535.
- Jia, Z.-x., Y.-w. Liu, J.-q. Li, L.-J. Liu and H.-l. Li (2015). "Crack growth behavior at thermal fatigue of H13 tool steel processed by laser surface melting." *International Journal of Fatigue* **78**: 61-71.
- Jiang, J., L. Xue and S. Wang (2011). "Discrete laser spot transformation hardening of AISI O1 tool steel using pulsed Nd: YAG laser." *Surface and coatings technology* **205**(21-22): 5156-5164.
- Jiang, W. and P. Molian (2001). "Nanocrystalline TiC powder alloying and glazing of H13 steel using a CO2 laser for improved life of die-casting dies." *Surface and Coatings Technology* **135**(2-3): 139-149.
- Jung, H., N. Mangelinck-Noël, H. Nguyen-Thi and B. Billia (2009). "Columnar to equiaxed transition during directional solidification in refined Al-based alloys." *Journal of Alloys and Compounds* **484**(1-2): 739-746.
- Karbalaian, H., A. Yousefi-Koma, M. Karimpour and S. Mohtasebi (2015). "Investigation on the Effect of Overlapping Laser Pulses in Laser Shock Peening with Finite Element Method." *Procedia Materials Science* **11**: 454-458.
- Kattire, P., S. Paul, R. Singh and W. Yan (2015). "Experimental characterization of laser cladding of CPM 9V on H13 tool steel for die repair applications." *Journal of Manufacturing Processes* **20**: 492-499.
- Kim, J.-M. and H.-T. Chung (2003). "Electrochemical characteristics of orthorhombic LiMnO<sub>2</sub> with different degrees of stacking faults." *Journal of power sources* **115**(1): 125-130.
- Kosec, B., M. Sokovic and G. Kosec (2005). "Failure analysis of dies for aluminium alloys die-casting." *Journal of Achievements in Materials and Manufacturing Engineering* **13**: 339-342.
- Kumar, V. (2006). "Process parameters influencing melt profile and hardness of pulsed laser treated Ti-6Al-4V." *Surface and Coatings Technology* **201**(6): 3174-3180.
- Kurz, W., C. Bezencon and M. Gäumann (2001). "Columnar to equiaxed transition in solidification processing." *Science and technology of advanced materials* **2**(1): 185.



- Kusinski, J., S. Kac, A. Kopia, A. Radziszewska, M. Rozmus-Górnikowska, B. Major, L. Major, J. Marczak and A. Lisiecki (2012). "Laser modification of the materials surface layer—a review paper." *Bulletin of the Polish Academy of Sciences: Technical Sciences* **60**(4): 711-728.
- Kusiński, J., S. Kaç and G. Kusiński (2010). "Microstructure and properties of laser remelted iron base amorphous coatings." *Inżynieria Materiałowa* **31**(3): 316-319.
- Lehto, P., H. Remes, T. Saukkonen, H. Hänninen and J. Romanoff (2014). "Influence of grain size distribution on the Hall–Petch relationship of welded structural steel." *Materials Science and Engineering: A* **592**: 28-39.
- Leunda, J., V. G. Navas, C. Soriano and C. Sanz (2012). "Improvement of laser deposited high alloyed powder metallurgical tool steel by a post-tempering treatment." *Physics Procedia* **39**: 392-400.
- Leunda, J., C. Soriano, C. Sanz and V. G. Navas (2011). "Laser cladding of vanadium-carbide tool steels for die repair." *Physics Procedia* **12**: 345-352.
- Li, C., Y. Wang, Z. Zhang, B. Han and T. Han (2010). "Influence of overlapping ratio on hardness and residual stress distributions in multi-track laser surface melting roller steel." *Optics and Lasers in Engineering* **48**(12): 1224-1230.
- Li, Y., D. Liu, W. Zhang, J. Kang, D. Chen, G. Yuan and G. Wang (2018). "Quenching above martensite start temperature in quenching and partitioning (Q&P) steel through control of partial phase transformation." *Materials Letters* **230**: 36-39.
- Li, Y., L. Ying, P. Hu, D. Shi, X. Zhao and M. Dai (2013). Coupled numerical simulation of hot stamping process and experimental verification. *Aip Conf Proc*.
- Liu, Q., Y. Wang, H. Zheng, K. Tang, H. Li and S. Gong (2016). "TC17 titanium alloy laser melting deposition repair process and properties." *Optics & Laser Technology* **82**: 1-9.
- Liu, X., G. Laplanche, A. Kostka, S. Fries, J. Pfetzinger-Micklich, G. Liu and E. George (2019). "Columnar to equiaxed transition and grain refinement of cast CrCoNi medium-entropy alloy by microalloying with titanium and carbon." *Journal of Alloys and Compounds* **775**: 1068-1076.
- Lozano-Gerona, J. and Á.-L. García-Otín (2018). "ImageJ-based semiautomatic method to analyze senescence in cell culture." *Analytical biochemistry* **543**: 30-32.
- Mahmoudi, B., M. Torkamany, A. S. R. Aghdam and J. Sabbaghzade (2010). "Laser surface hardening of AISI 420 stainless steel treated by pulsed Nd: YAG laser." *Materials & Design (1980-2015)* **31**(5): 2553-2560.
- Majumdar, J. D. and I. Manna (2003). "Laser processing of materials." *Sadhana* **28**(3-4): 495-562.
- Meier, H. and C. Haberland (2008). "Experimental studies on selective laser melting of metallic parts." *Materialwissenschaft und Werkstofftechnik* **39**(9): 665-670.



- Mellouli, D., N. Haddar, A. Köster and H. F. Ayedi (2014). "Hardness effect on thermal fatigue damage of hot-working tool steel." *Engineering Failure Analysis* **45**: 85-95.
- Merklein, M. and J. Lechler (2006). "Investigation of the thermo-mechanical properties of hot stamping steels." *Journal of materials processing technology* **177**(1-3): 452-455.
- Mohd Fawzi, Z., Y. AR, M. Farid, M. Sharif and S. Mohd Ali Hanafiah (2014). "Comparison of cooling performance between high thermal conductivity steel (HTCS 150) and hot work tool steel (SKD 61) insert for experimental tool using finite element analysis." *Advanced Materials Research* **903**: 163-168.
- Montealegre, M., G. Castro, P. Rey, J. Arias, P. Vázquez and M. González (2010). "Surface treatments by laser technology." *Contemporary Materials*, I-1: 19-30.
- Mori, K., P. Bariani, B.-A. Behrens, A. Brosius, S. Bruschi, T. Maeno, M. Merklein and J. Yanagimoto (2017). "Hot stamping of ultra-high strength steel parts." *CIRP Annals* **66**(2): 755-777.
- Naderi, D. D. I. a. M. (2007). "Hot Stamping of Ultra High Strength Steels."
- Naderi, M., V. Uthaisangskuk, U. Prahll and W. Bleck (2008). "A numerical and experimental investigation into hot stamping of boron alloyed heat treated steels." *Steel Research International* **79**(2): 77.
- Nath, S., S. Pityana and J. D. Majumdar (2012). "Laser surface alloying of aluminium with WC+ Co+ NiCr for improved wear resistance." *Surface and Coatings Technology* **206**(15): 3333-3341.
- Norhafzan, B., S. Aqida, E. Chikarakara and D. Brabazon (2016). "Surface modification of AISI H13 tool steel by laser cladding with NiTi powder." *Applied Physics A* **122**(4): 1-6.
- Paczkowska, M. (2012). "Analysis of gray iron microstructure influence on potential laser heat treatment effects." *Archives of Mechanical Technology and Automation* **32**(1): 27-36.
- Papageorgiou, D., C. Medrea and N. Kyriakou (2013). "Failure analysis of H13 working die used in plastic injection moulding." *Engineering Failure Analysis* **35**: 355-359.
- Pavel, N., M. Tsunekane and T. Taira (2011). "Composite, all-ceramics, high-peak power Nd: YAG/Cr 4+: YAG monolithic micro-laser with multiple-beam output for engine ignition." *Optics express* **19**(10): 9378-9384.
- Peet, M., H. Hasan and H. Bhadeshia (2011). "Prediction of thermal conductivity of steel." *International Journal of Heat and Mass Transfer* **54**(11): 2602-2608.
- Petrovič, D. S. and R. Šturm (2014). "Fine-structured Morphology of Silicon Steel Sheet after Laser Surface Alloying of Sb Powder." *Strojniški vestnik-Journal of Mechanical Engineering* **60**(1): 5-11.

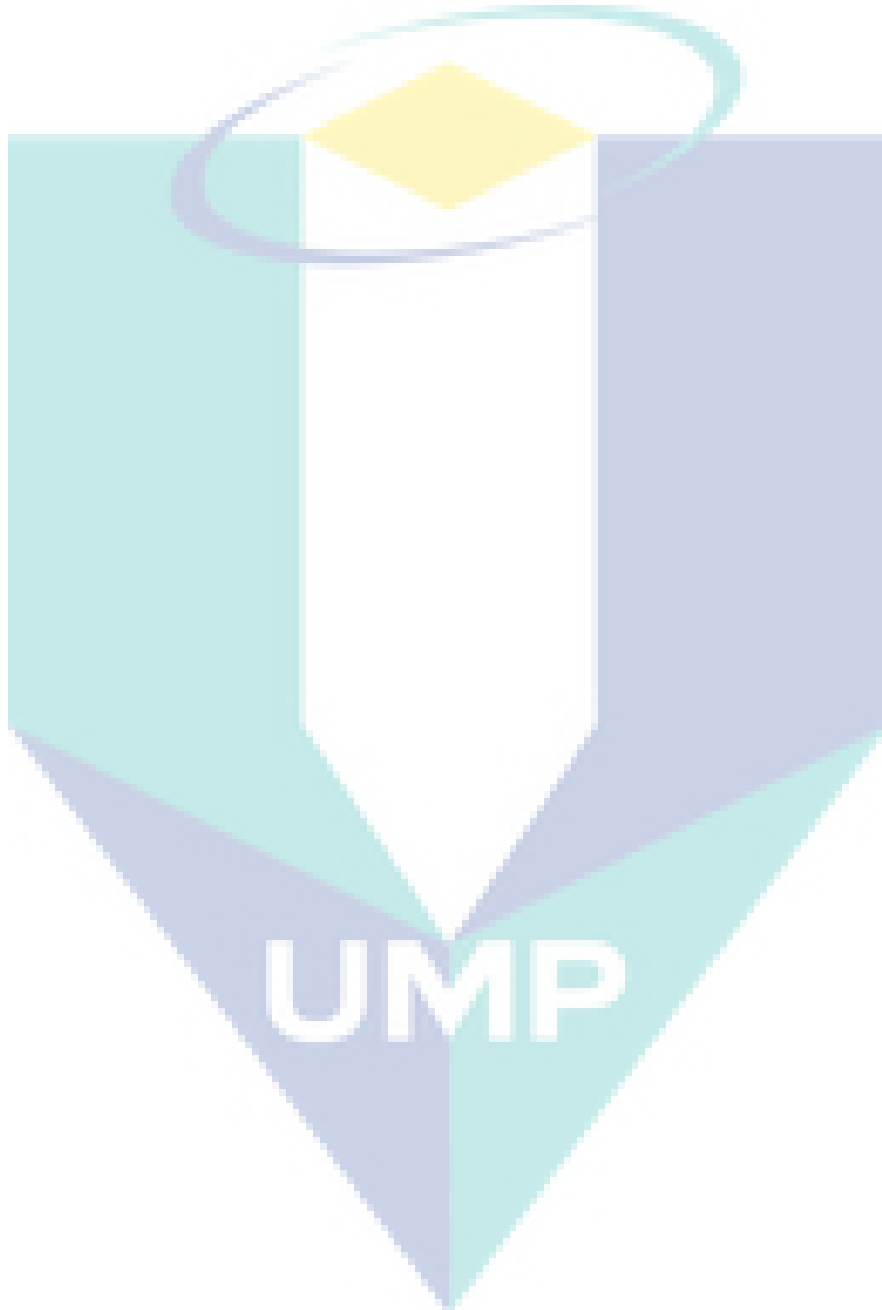
- Pinkerton, A. J. and L. Li (2003). "The effect of laser pulse width on multiple-layer 316L steel clad microstructure and surface finish." *Applied Surface Science* **208**: 411-416.
- Pleterski, M., J. Tušek, L. Kosec, M. Muhič and T. Muhič (2010). "Laser repair welding of molds with various pulse shapes." *Metalurgija* **49**(1): 41-44.
- Ren, X., H. Fu, J. Xing and Y. Yi (2019). "Effect of solidification rate on microstructure and toughness of Ca-Ti modified high boron high speed steel." *Materials Science and Engineering: A* **742**: 617-627.
- Rottwinkel, B., C. Nölke, S. Kaierle and V. Wesling (2014). "Crack repair of single crystal turbine blades using laser cladding technology." *Procedia CIRP* **22**: 263-267.
- Sabbaghzadeh, J., M. Azizi and M. J. Torkamany (2008). "Numerical and experimental investigation of seam welding with a pulsed laser." *Optics & Laser Technology* **40**(2): 289-296.
- Sadak, T. W. (2015). "Cyclic Heating Effect on Hardness of Aluminum." *International Journal of Engineering Research and Applications* **5**(7): 03-06.
- Sahoo, C. K. and M. Masanta (2015). "Effect of pulse laser parameters on TiC reinforced AISI 304 stainless steel composite coating by laser surface engineering process." *Optics and Lasers in Engineering* **67**: 36-48.
- Schneider, M. F. (1998). Laser cladding with powder, effect of some machining parameters on clad properties, Universiteit Twente.
- Shihomatsu, A., S. T. Button and I. B. d. Silva (2016). "Tribological behavior of laser textured hot stamping dies." *Advances in Tribology* **2016**.
- Shin, H. J. and Y. T. Yoo (2008). "Microstructural and hardness investigation of hot-work tool steels by laser surface treatment." *Journal of materials processing technology* **201**(1): 342-347.
- SN, A., S. LH, S. Naher and D. Brabazon (2014). "Rapid Solidification Processing and Bulk Metallic Glass Casting."
- Sohi, M. H., M. Ebrahimi, H. Ghasemi and A. Shahripour (2012). "Microstructural study of surface melted and chromium surface alloyed ductile iron." *Applied Surface Science* **258**(19): 7348-7353.
- Steen, W. and K. Watkins (1993). "Coating by laser surface treatment." *Le Journal de Physique IV* **3**(C9): C9-581-C589-590.
- Šturm, R., M. Štefanikova and D. S. Petrovič (2015). "Influence of pre-heating on the surface modification of powder-metallurgy processed cold-work tool steel during laser surface melting." *Applied Surface Science* **325**: 203-210.
- Suarez, A., A. M. Suarez and W. T. Preciado (2015). "Arc Welding Procedures on Steels for Molds and Dies." *Procedia Engineering* **100**: 584-591.

- Sun, Y., L. Fu, Z. Fu, A. Shan and E. J. Lavernia (2017). "Enhanced thermal stability and ductility in a nanostructured Ni-based alloy." *Scripta Materialia* **141**: 1-5.
- SUN, Y., S. HANAKI, H. UCHIDA, H. SUNADA and N. TSUJII (2004). Repair effect of hot work tool steel by laser-melting process. The Fourth International Conference on Physical and Numerical Simulation of Materials Processing (ICPNS'2004).
- Sun, Y. and M. Hao (2012). "Statistical analysis and optimization of process parameters in Ti6Al4V laser cladding using Nd: YAG laser." *Optics and Lasers in Engineering* **50**(7): 985-995.
- T. Wu (2013). *HTCS®-150*. **150**: 1–6.
- Tekkaya, A. E., H. Karbasian, W. Homberg and M. Kleiner (2007). "Thermo-mechanical coupled simulation of hot stamping components for process design." *Production Engineering* **1**(1): 85-89.
- Telasang, G., J. D. Majumdar, G. Padmanabham and I. Manna (2014). "Structure–property correlation in laser surface treated AISI H13 tool steel for improved mechanical properties." *Materials Science and Engineering: A* **599**: 255-267.
- Telasang, G., J. D. Majumdar, G. Padmanabham and I. Manna (2015). "Wear and corrosion behavior of laser surface engineered AISI H13 hot working tool steel." *Surface and Coatings Technology* **261**: 69-78.
- Telasang, G., J. D. Majumdar, G. Padmanabham, M. Tak and I. Manna (2014). "Effect of laser parameters on microstructure and hardness of laser clad and tempered AISI H13 tool steel." *Surface and Coatings Technology* **258**: 1108-1118.
- Treatment, L. S. (2014). "Surface Engineering Laser Surface Treatment 1 . Lasers in materials processing 3 . Advantages and Disadvantages of Laser Surface Treatment 4 . Classification of Laser Surface Treatment Processes." 2-7.
- Udalagama, C., X. Chen, A. Bettiol and F. Watt (2013). "An ion beam analysis software based on ImageJ." *Nuclear Instruments and Methods in Physics Research Section B: Beam Interactions with Materials and Atoms* **306**: 59-63.
- Valls, I., B. Casas, N. Rodríguez and U. Paar (2010). "Benefits from using high thermal conductivity tool steels in the hot forming of steels." *La Metallurgia Italiana*(11).
- Valls, I., A. Hamasaiid and A. Padré (2017). High Thermal Conductivity and High Wear Resistance Tool Steels for cost-effective Hot Stamping Tools. *Journal of Physics: Conference Series*, IOP Publishing.
- Ventura, A. P. (2017). "Microstructural Evolution and Mechanical Property Development of Selective Laser Melted Copper Alloys."
- Wang, L., J. Zhou, Y. Yu, C. Guo and J. Chen (2012). "Effect of powders refinement on the tribological behavior of Ni-based composite coatings by laser cladding." *Applied Surface Science* **258**(17): 6697-6704.

- Wang, Q.-Y., Y.-F. Zhang, S.-L. Bai and Z.-D. Liu (2013). "Microstructures, mechanical properties and corrosion resistance of Hastelloy C22 coating produced by laser cladding." *Journal of Alloys and Compounds* **553**: 253-258.
- Wang, Z., X. Lin, Y. Cao and W. Huang (2013). "Microstructure evolution in laser surface remelting of Ni–33wt.% Sn alloy." *Journal of Alloys and Compounds* **577**: 309-314.
- Wieland, M. and M. Merklein (2010). *Characterization of Heat Transfer Coefficients of Tool Materials and Tool Coatings for Hot Stamping of Boron-Manganese Steels*. Key Engineering Materials, Trans Tech Publ.
- Wu, Q., W. Li, N. Zhong, W. Gang and W. Haishan (2013). "Microstructure and wear behavior of laser cladding VC–Cr 7 C 3 ceramic coating on steel substrate." *Materials & Design* **49**: 10-18.
- Xu, M., J. Li, J. Jiang and B. Li (2015). "Influence of Powders and Process Parameters on Bonding Shear Strength and Micro Hardness in Laser Cladding Remanufacturing." *Procedia CIRP* **29**: 804-809.
- Zamri, M. F. and A. R. Yusoff (2015). "Heuristic optimisation of cooling channel design in the hot stamping die for hot stamping process." *Advances in Materials and Processing Technologies* **1**(1-2): 27-35.
- Zhang, Z., P. Lin, D. Cong, S. Kong, H. Zhou and L. Ren (2014). "The characteristics of treated zone processed by pulsed Nd-YAG laser surface remelting on hot work steel." *Optics & Laser Technology* **64**: 227-234.
- Zhang, Z., P. Lin, H. Zhou and L. Ren (2013). "Microstructure, hardness, and thermal fatigue behavior of H21 steel processed by laser surface remelting." *Applied Surface Science* **276**: 62-67.
- Zhang, Z., L. Ren, T. Zhou, Z. Han, H. Zhou, L. Chen and Y. Zhao (2010). "Optimization of laser processing parameters and their effect on penetration depth and surface roughness of biomimetic units on the surface of 3Cr2W8V steel." *Journal of Bionic Engineering* **7**: S67-S76.
- Zheng, L., J. Wu, S. Zhang, S. Sun, Z. Zhang, S. Liang, Z. Liu and L. Ren (2016). "Bionic Coupling of Hardness Gradient to Surface Texture for Improved Anti-wear Properties." *Journal of bionic engineering* **13**(3): 406-415.
- Zhu, Y.-Y., H.-B. Tang, Z. Li, C. Xu and B. He (2019). "Solidification behavior and grain morphology of laser additive manufacturing titanium alloys." *Journal of Alloys and Compounds* **777**: 712-716.
- Zimmermann, G., L. Sturz, B. Billia, N. Mangelinck-Noel, H. N. Thi, C.-A. Gandin, D. J. Browne and W. U. Mirihanage (2011). Investigation of columnar-to-equiaxed transition in solidification processing of AlSi alloys in microgravity–The CETSOL project. *Journal of Physics: Conference Series*, IOP Publishing.

Zulhishamuddin, A. and S. Aqida (2015). "An overview of high thermal conductive hot press forming die material development." *Journal of Mechanical Engineering and Sciences* 9(unknown): 1686-1694.

Zulhishamuddin, A., S. Aqida and E. Rahim (2016). Optimization of pulsed Nd: YAG laser melting of gray cast iron at different spot sizes for enhanced surface properties. *AIP Conference Proceedings*, AIP Publishing.



## APPENDIX A

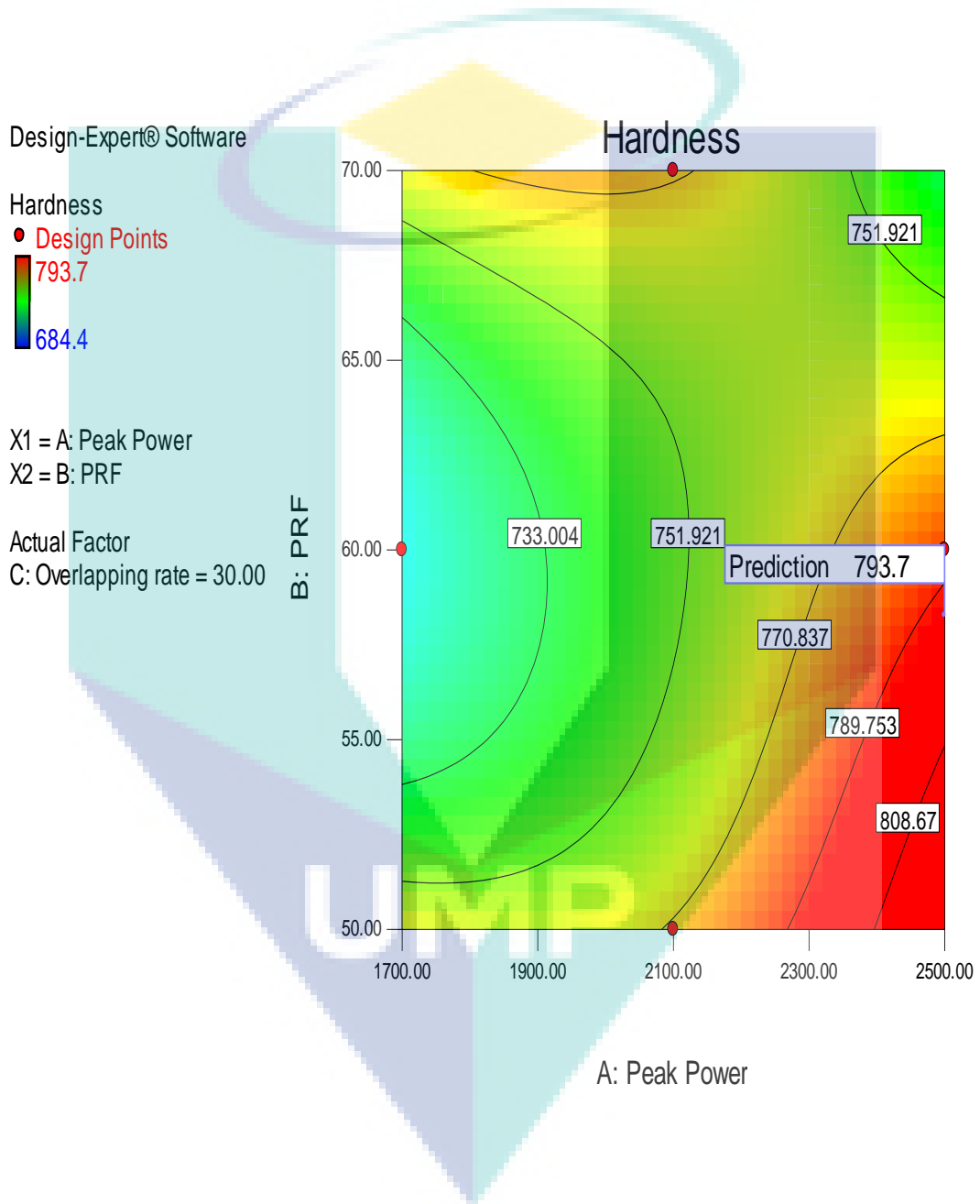
### LIST OF PUBLICATION

1. B. Norhafzan, S. Aqida, E. Chikarakara, and D. Brabazon, "Surface modification of AISI H13 tool steel by laser cladding with NiTi powder," *Applied Physics A*, vol. 122, pp. 1-6, 2016.
2. N. Bariman, S. N. Aqida, and F. Fauzun, "Laser Melting of High Thermal Conductivity Steel (HTCS) Surface," in *Materials Science Forum*, 2017.
3. F. Fauzun, S. N. Aqida, I. Ismail, and N. Bariman, "Micro-Bulges Investigation on Laser Modified Tool Steel Surface," in *MATEC Web of Conferences*, 2017, p. 02007.
4. B. Norhafzan, S. Aqida, F. Fazliana, M. Reza, I. Ismail, and C. Khairil, "Laser melting of groove defect repair on high thermal conductivity steel (HTCS-150)," *Applied Physics A*, vol. 124, p. 169, 2018.
5. B. Norhafzan, S. Aqida, F. Mifthal, A. Zulhishamuddin, and I. Ismail, "Effect of Heating Time on Hardness Properties of Laser Clad Gray Cast Iron Surface," in *IOP Conference Series: Materials Science and Engineering*, 2018, p. 012068.



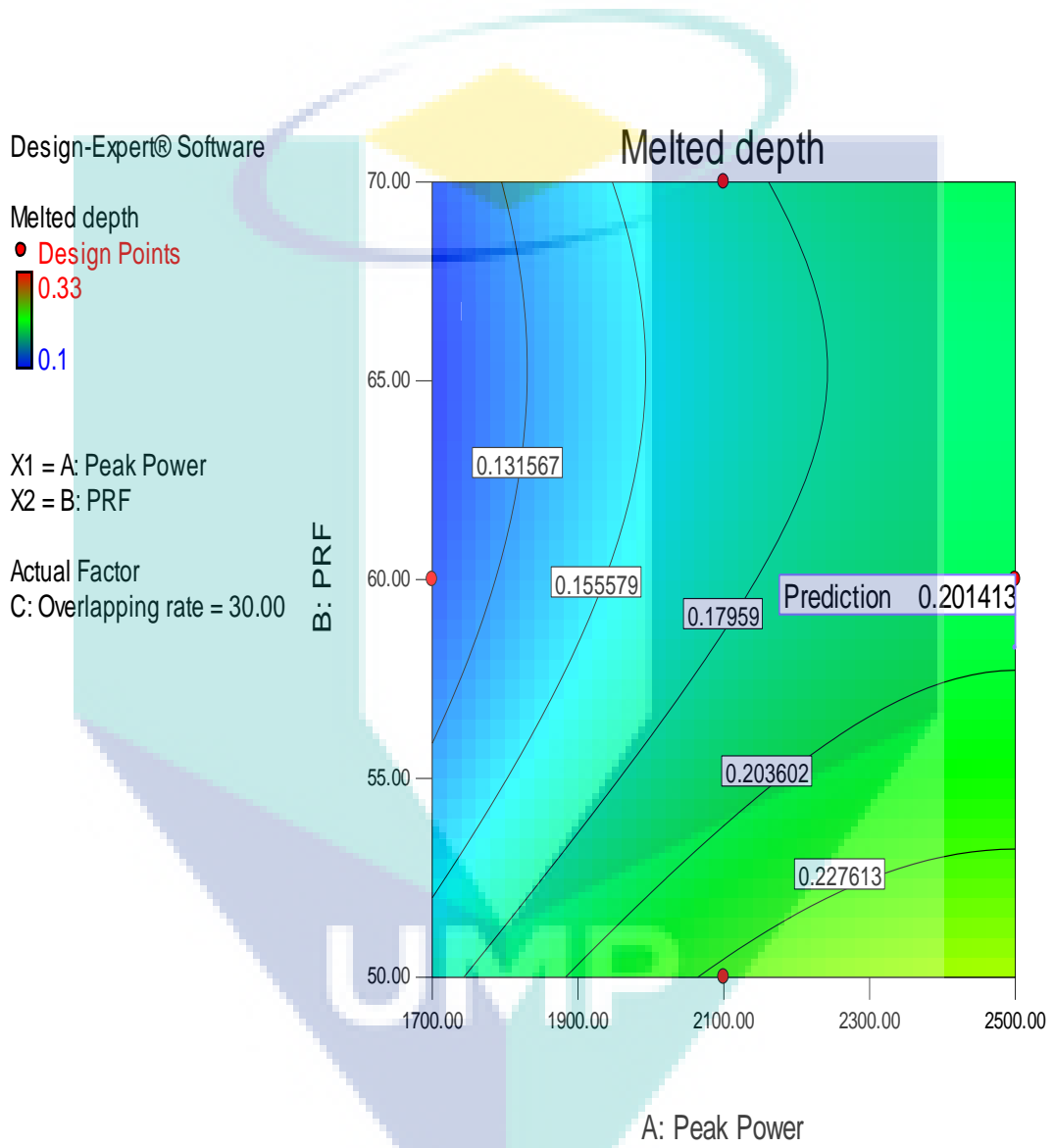
## APPENDIX B

### CONTOUR PLOT OF PRF, PEAK POWER AND HARDNESS AT 30% OVERLAPPING RATE.



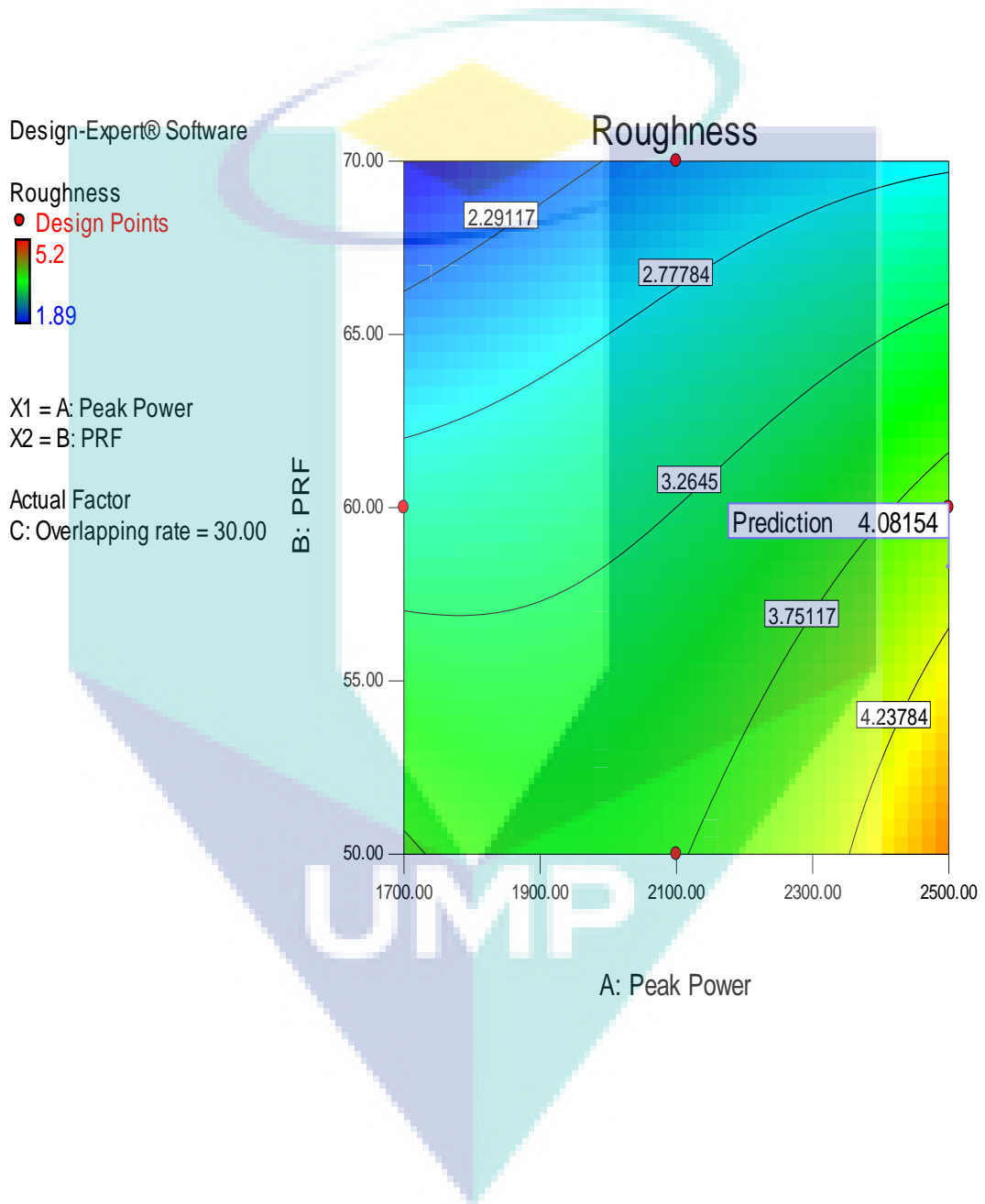
# APPENDIX C

## CONTOUR PLOT OF PRF, PEAK POWER AND MELT DEPTH AT 30% OVERLAPPING RATE.



APPENDIX D

CONTOUR PLOT OF PRF, PEAK POWER AND ROUGHNESS AT 30% OVERLAPPING RATE.



## APPENDIX E

### RELATIVE ERROR FOR HARDNESS

Parameter						DOE	Experiment	Relative error (%)
DOE			Experiment					
Peak power	PRF	Overlap rate	Peak power	PRF	Overlap rate	Hardness (HV <sub>0.1</sub> )		
2500	58.27	30.00	2500	60	30	793.7	793.7	0
2500	60.1	30.00	2500	60	30	785.2	793.7	1.1
2500	60.79	30.00	2500	60	30	781.9	793.7	1.5
2184	68.95	30.00	2100	70	30	765.2	749.4	2.1
1750	70	53.49	1700	70	50	752.0	749.9	0.3

UMP

## APPENDIX F

### RELATIVE ERROR FOR ROUGHNESS

Parameter						DOE	Experiment	Relative error (%)
DOE			Experiment			Roughness (μm)		
Peak power	PRF	Overlap rate	Peak power	PRF	Overlap rate			
2500	58.27	30.00	2500	60	30	4.08	3.89	4.7
2500	60.1	30.00	2500	60	30	3.91	3.89	0.5
2500	60.79	30.00	2500	60	30	3.83	3.89	1.6
2184	68.95	30.00	2100	70	30	2.63	2.43	7.6
1750	70.00	53.49	1700	70	50	2.17	2.10	3.2



UMP

## APPENDIX G

### LASER PROCESSING PARAMETER

#### Pulse Energy, E

Pulse energy is the amount of heat resulting from a given peak power and pulse width, measured in Joule (J). The pulse energy is calculated using Equation 3.

$$E = \frac{\text{Average Power}}{\text{Pulsed Repetition Frequency}}$$
$$= \frac{P_A}{PRF}$$

#### Duty Cycle, DC

Duty cycle is the division of time when the laser system is in 'active' or 'on' condition measured in percentage (%) during a laser pulse period.

$$DC = \frac{\text{Pulse width}}{\text{Length}}$$
$$= \frac{\tau}{L}$$

#### Pulse Width, $\tau$

Pulse width refers to the time duration when the pulse was in 'active' or 'on' state.

$$\tau = \frac{\text{Pulse energy}}{\text{Peak power}}$$
$$= \frac{E}{P_p}$$



### Residence Time, TR

Residence time is the materials-beam interaction time measured in millisecond (ms).

$$T_R = \frac{(Pulse\ width)(spot\ size)(PRF)}{Processing\ speed}$$
$$= \frac{(\tau)(d)(PRF)}{v}$$

### Laser Irradiance, I

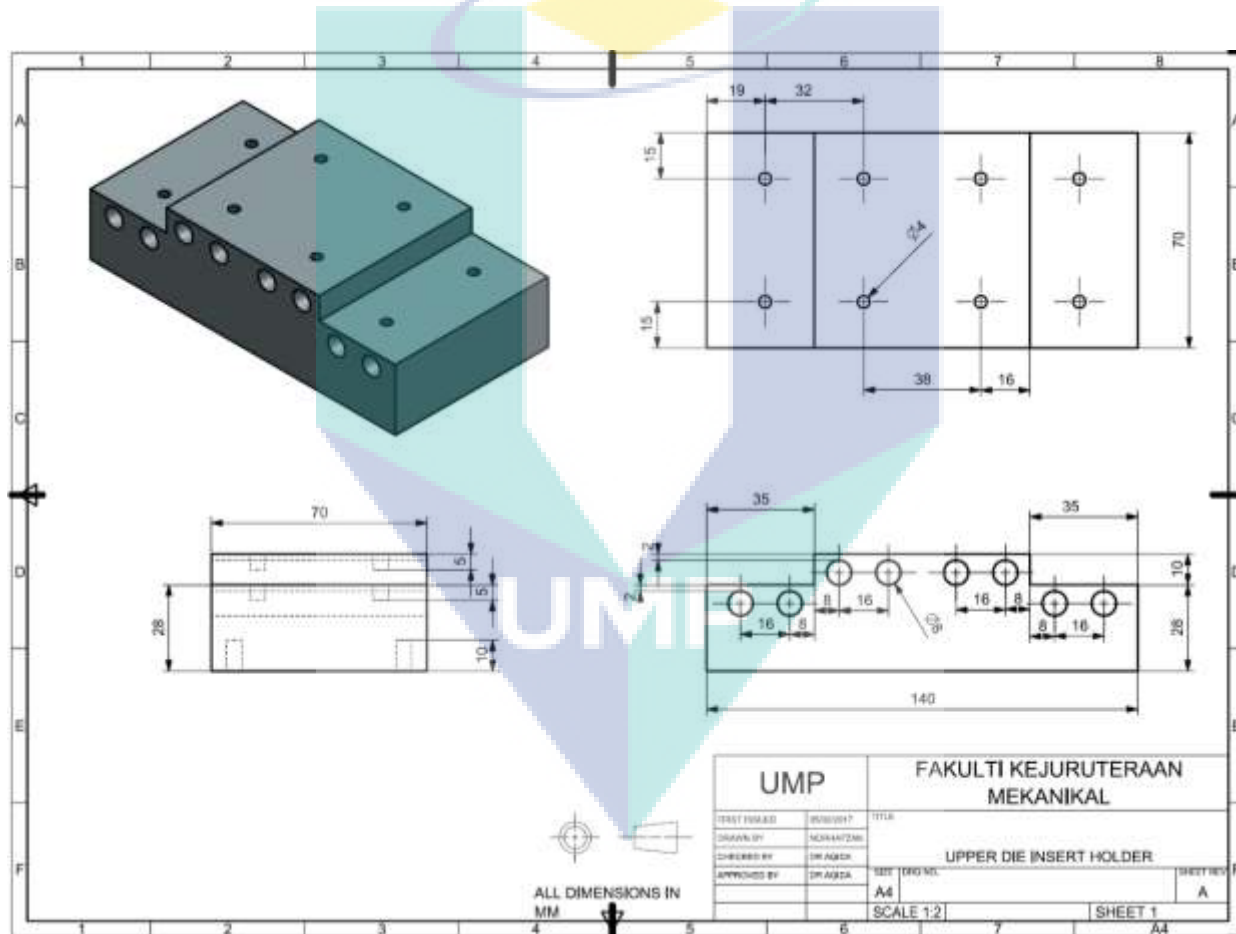
Laser irradiance is the laser power density measured in Watts per beam area (W/mm<sup>2</sup>).

$$I = \frac{(Energy\ Density)}{Residence\ Time} \times Duty\ Cycle$$
$$= \frac{(F)}{TR} \times DC$$

UMP

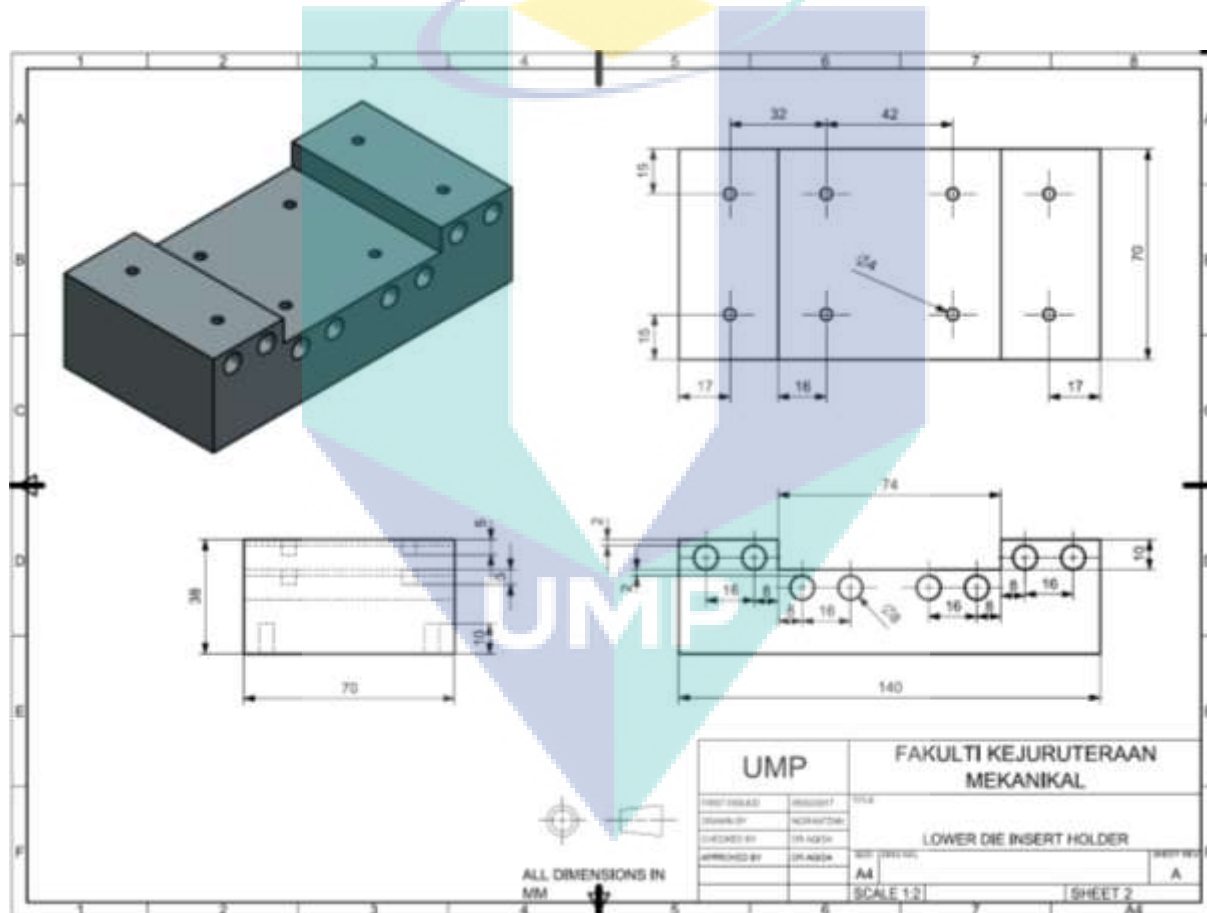
## APPENDIX H

### UPPER DIE INSERT HOLDER DRAWING



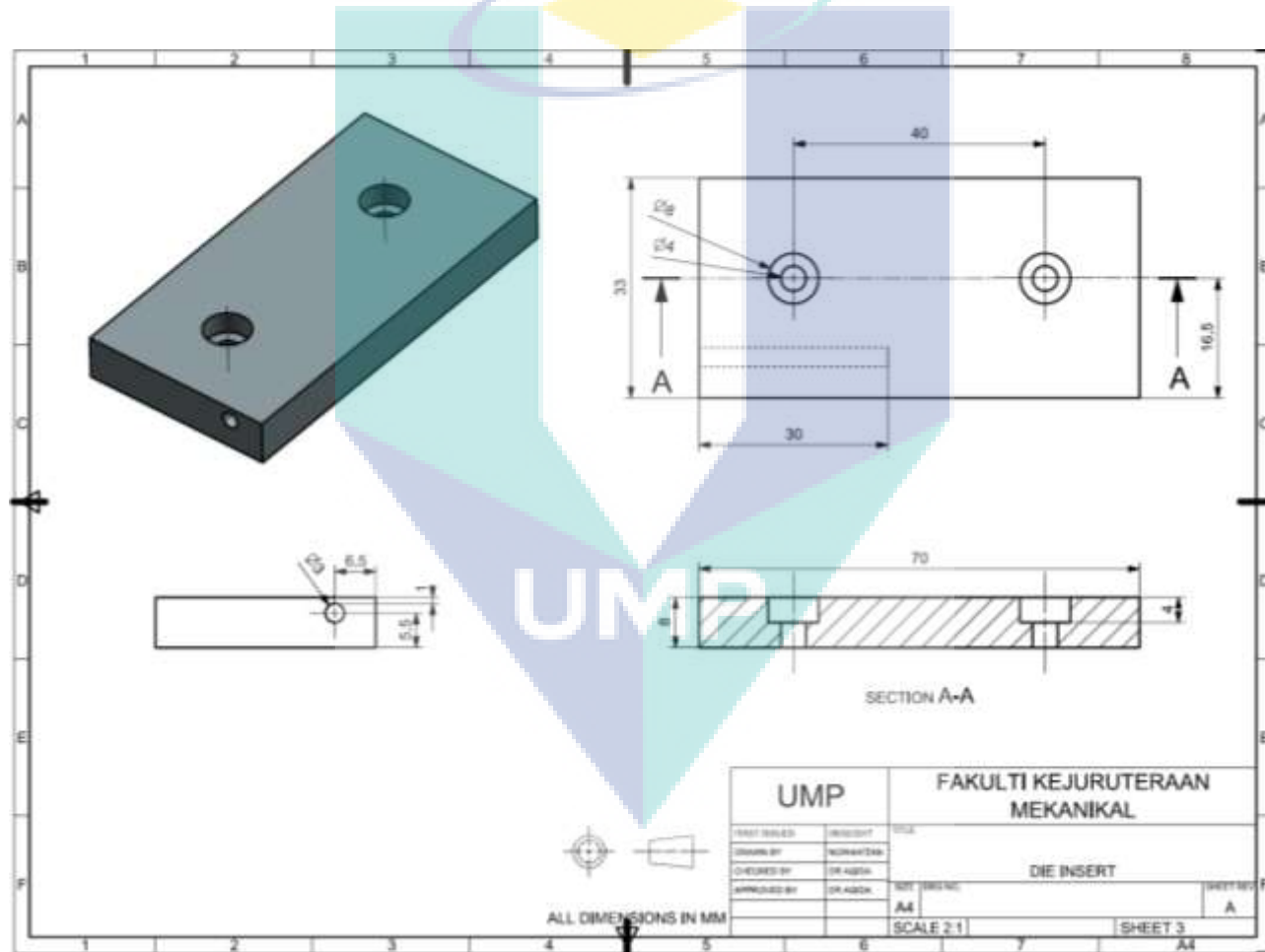
# APPENDIX I

## LOWER DIE INSERT DRAWING



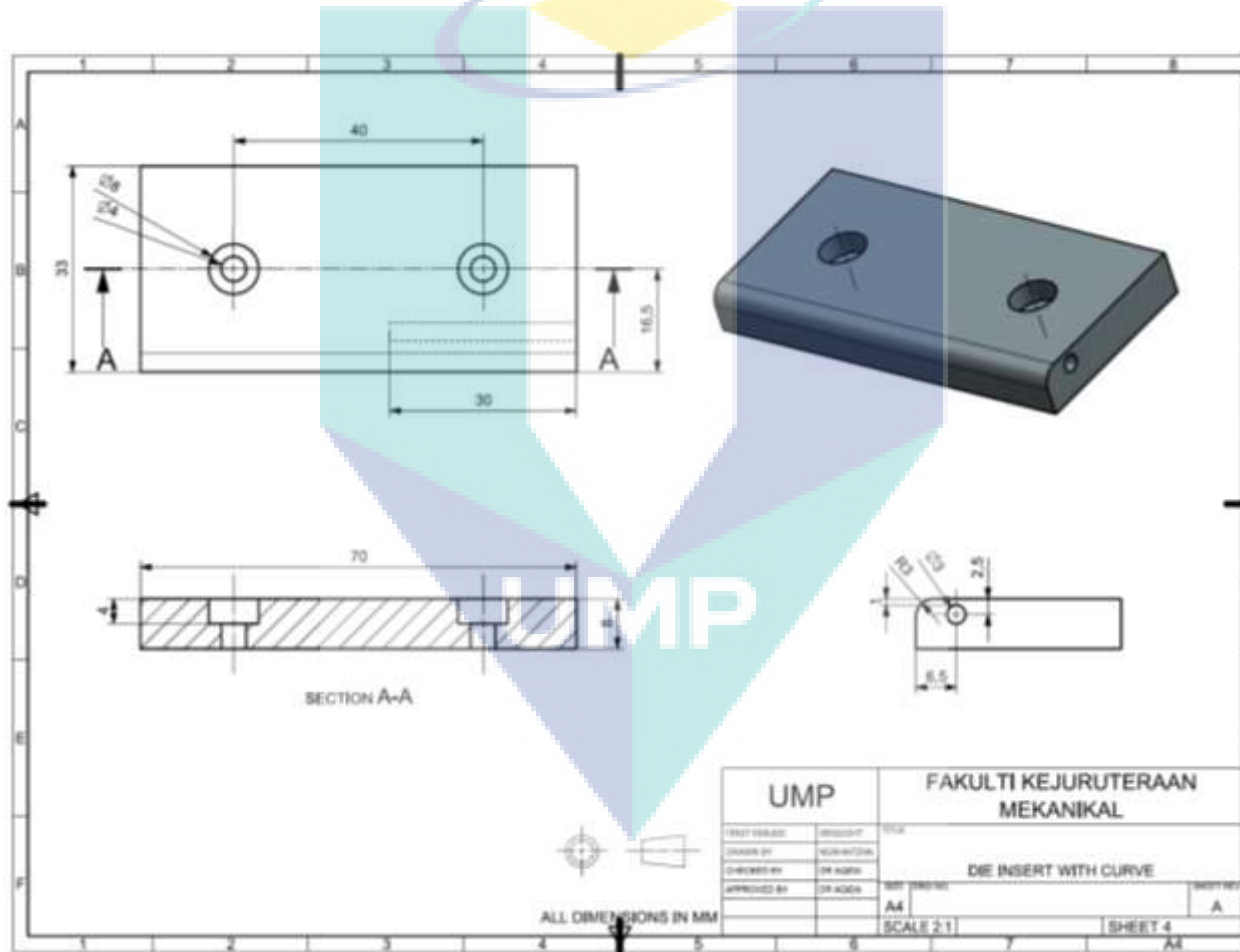
## APPENDIX J

### DIE INSERT DRAWING



## APPENDIX K

### DIE INSERT WITH CURVE DRAWING



## APPENDIX L

**DIE INSERT WITH CURVE DRAWING: DIE INSERT WITH CURVE DRAWING (A) MICROGRAPH OF LASER MELTED LAYER OF SAMPLE 9, AND THE CORRESPONDING EDXS MAPPING OF, (B) SILICON, (C) SULFUR, (D) TITANIUM, (E) VANADIUM, (F) CHROMIUM, (G) MANGANESE, (H) IRON, (I) NICKEL, (J) MOLYBDENUM AND (K) CARBON DISTRIBUTION.**

